UNIVERSITÀ DEGLI STUDI DELL'AQUILA

Department of Engineering and Information Science and Mathematics

Ph.D in Mathematics and Models
XXXVII cycle

Thesis title

A forward model in electricity price with fractional dynamics

SSD SECS-S/06

Ph.D Student
Marco Mastrogiovanni

Tutor
Prof. Marco Castellani

Coordinatore del Corso
Debora Amadori

Supervisor
Prof. Fabio Antonelli

Anno Accademico 2023-2024

A tutti i miei studenti

Abstract

In the last decade, a new generation of stochastic models has emerged in finance, built upon the fractional Brownian motion originally introduced by Mandelbrot in 1948. This revolution started with the groundbreaking article by Gatheral, Jaisson and Rosenbaum *"Volatility is rough"*, where the authors improve the forecasts of an asset realized volatility by employing a rough fractional (stochastic volatility) model. In our work, we aim to extend the use of fractional dynamics to energy markets, with the goal of capturing their distinctive structural and stochastic features.

In these kinds of market, the spot price is not tradeable, because in general there are very limited storage possibilities, which implies a strong seasonality in the underlying price. In addition, basic tradeable assets in electricity markets can typically be described as futures and forward contracts with electricity delivery over a period of time. The owner of the contract with delivery over the time interval $[T_1, T_2]$ receives a constant flow of the commodity over the period, against a fixed payment per unit. Typical delivery periods are days, weeks, months, quarters, or years. We develop a consistent model to describe a forward market avoiding arbitrage, to ensure that we work within the Heath-Jarrow-Morton paradigm.

The model we are going to propose for the evolution of forward prices in the energy market is additive and mean-reverting, and it is obtained by modifying the Lucia-Schwartz model with the introduction of fractional dynamics. In line with the existing literature, forward prices are regulated by two factors, X_1 and X_2, hidden in the dynamics. As in the Lucia-Schwartz model, the first one is stationary and mean-reverting to represent the short-term movements of the price curve. It is also responsible for the Samuelson effect; in fact, as time to maturity decreases, volatility increases. The novelty in our model lies in the second factor that includes a fractional martingale as introduced by Norros, Valkeila and Virtamo. The idea behind this choice is that forward's fractional dynamics is due to the non-Markovian behavior of energy spot prices. Also we mean to keep the price's seasonality features hoping to achieve it by a simpler description since it often requires a high number of parameters to be properly described (as in Vargiolu et al. 2018). The choice of a fractional martingale in the spot price allows keeping the martingale property of the instantaneous forwards also in this extended model. By introducing a fractional process, capturing the non-Markovian nature of the price, we aim at reducing the number of parameters when calibrating the model on actual market data. Clearly we will have to calibrate also the Hurst parameter H on the time series, exploiting the quadratic variation/covariation of the martingale components.

Summarizing, the goal is to obtain a model that does not allow arbitrage and which recovers some known results in energy markets by reducing the number of parameters to be estimated. Calibration will be conducted within a one-year temporal interval, utilizing data from the time series of Phelix Base forward prices in the Italian market. Within this temporal window, multiple forwards covering the same time period are observed, including monthly, quarterly, and calendar year contracts. In this context, our model aims to mitigate arbitrage possibilities, ensuring its robustness in capturing the dynamics of the energy market. We limit our analysis to the one-dimensional case. A natural

extension of this work would involve generalizing the model to multiple dimensions and exploring its application in describing co-movements among commodities.

Keywords: Fractional Brownian motion, Hurst exponent, energy markets, Spot price, Forward price, Long memory processes.

Contents

List of Figures

List of Tables

Introduction

In recent years, electricity markets, and more broadly energy markets, have received considerable attention from both academics and practitioners. This interest has been fueled by the progressive deregulation of the energy sector in many countries and by the growing concern for environmental sustainability and climate change. Electricity, together with emission trading permits, is now treated as a tradable commodity and is exchanged both on power exchanges and over-the-counter (OTC) platforms.

These markets are evolving rapidly and pose significant challenges from a modeling and analytical perspective, attracting the interest of both practitioners and researchers. Among the various segments, the forward market is typically the most active and liquid, with forward contracts representing the primary instruments for trading and hedging. As a result, the analysis, modeling, and forecasting of energy prices have become central tools for the development of trading strategies and for effective risk management. This has spurred a growing body of research that combines economic theory with quantitative finance, leading to a wide range of models tailored to capture the specific features of energy markets.

Several papers have tried to explain the economic features and implications of market structures and mechanisms, of bidding systems, and of strategies to improve competition. Others have focused on financial aspects such as price modeling, forecasting, risk management, and derivative pricing.

The purpose of this thesis is to investigate the role of fractional dynamics in energy markets from both a probabilistic and a financial perspective. On the one hand, we study statistical and estimation problems related to fractional stochastic processes, with particular emphasis on the normalized integrated fractional Brownian motion and the estimation of its Hurst parameter. On the other hand, we develop a modeling framework for electricity forward prices that incorporates fractional effects.

In the literature, several approaches have been proposed for modeling and pricing forward contracts in energy markets; see, for instance [10] and [27]. A common methodology consists in specifying a stochastic model for the spot price and for the factors influencing its dynamics, and then deriving forward prices from this representation. This approach has proved particularly effective in identifying and interpreting the various sources of uncertainty that contribute to forward price formation.

Within this framework, a natural question is how to incorporate the long-memory and persis-

tence effects often observed in energy prices. The present work addresses this issue by combining recent developments in the theory of fractional processes with the modeling requirements arising in energy finance.

For instance, in [71] the model for the spot price includes several stochastic factors such as stochastic convenience yield and stochastic interest rates, while in [48], using data from the Nordic market, the authors suggest and test single and two-factor models under stochastic volatility and various specifications of seasonal deterministic components. Finally, in [45], the authors extend the two-factor model proposed in [48] by introducing a seasonal component in the volatility.

Motivated by the empirical evidence of long-range dependence and persistence in energy prices, we investigate the introduction of fractional dynamics into the modeling framework. These features naturally lead to the consideration of fractional Brownian motion and related fractional processes. However, this choice presents significant theoretical challenges, since fractional Brownian motion is not a semimartingale whenever $H \neq 1/2$. As a consequence, many of the classical tools of arbitrage-free pricing theory are no longer directly applicable, making the construction of financially consistent models considerably more difficult.

This thesis is organized into several chapters, each devoted to a specific aspect of the proposed modeling framework. The first chapter provides an overview of energy markets, with particular emphasis on spot prices and forward contracts, describing their main empirical features and reviewing the most relevant models proposed in the literature.

The second chapter introduces the basic tools of stochastic analysis needed in the sequel and recalls some fundamental results that will be used throughout the thesis. In the third chapter, we focus on estimation methods for the Hurst parameter, motivating from both a theoretical and an empirical perspective the introduction of fractional dynamics in the model.

In the fourth chapter, the fractional Brownian motion and its main properties are presented, with special attention to the fundamental martingale introduced in [60]. The fifth chapter is devoted to the analysis of the normalized integrated fractional Brownian motion, defined as the time integral of a fractional Brownian motion, relevant to model the fractional components in the electricity prices, and we study the related parameter estimation problem. Although this part may appear only loosely connected to the rest of the thesis at first glance but we provide a clear motivation for its relevance in the modeling of electricity prices.

The final chapters are devoted to applications. First, we introduce an original model for spot prices and, consequently, for forward pricing, in which the fundamental martingale plays a central role. Finally, the framework is extended to the pricing of options written on electricity forward contracts, and the thesis concludes with a discussion of the results and possible directions for future research.

Chapter 1

Energy markets

The liberalization of electricity and gas markets began in the early 1990s, initially in a few pioneering countries and subsequently expanding across many regions worldwide. This structural transformation aimed to eliminate monopolies, promote competition, and improve market efficiency. As a result, new market segments emerged, including organized exchanges for spot transactions and a growing variety of derivative products. These changes were supported by regulatory reforms introduced at both national and supranational levels, particularly within the European Union, where successive legislative packages established common rules for market access and the creation of independent regulatory authorities.

The development of financial instruments related to energy commodities, such as futures, options, and swaps, has further enhanced market liquidity and transparency. In parallel, the development of financial instruments linked to external risk factors such as weather conditions, transportation costs, and greenhouse gas emissions (e.g., via the EU Emissions Trading System) has contributed to greater flexibility in risk management for both producers and consumers. These developments have transformed energy markets into dynamic and complex environments, requiring sophisticated models for price formation, risk assessment, and regulatory compliance.

Our main focus will be the electricity market, the assets traded in this markets differ significantly in nature and structure from those found in more traditional commodity markets such as metals, coal, oil or agricultural products.

One of the most distinctive features of electricity is its limited storability. While producers can indirectly store energy, by accumulating water in reservoirs for hydroelectric generation or by holding fuels like gas, oil, or coal for thermal production, electricity itself cannot be economically stored by consumers. In contrast, classical commodity markets rely on the cost-of-carry relationship, which links spot and forward prices through the costs of storage, financing, and the convenience yield. This relationship assumes that the commodity is storable, enabling arbitrage opportunities through the physical holding of inventory.

Electricity cannot be stockpiled or carried over time in a cost-effective manner. Unlike oil or grains, large-scale storage solutions, as batteries or pumped hydro—remain limited in scale and often economically unfeasible. The lack of storability has further implications for market behavior.

In particular, it contributes to the pronounced seasonality and the occurrence of price spikes, both of which are well-known stylized facts of electricity markets. Spot prices can exhibit extreme short-term volatility, often in response to sudden supply shocks, such as the unexpected shutdown of a nuclear power plant or changes in demand, like a sharp drop in temperature. In such cases, prices can surge dramatically for short periods before quickly returning to more typical levels.

The limited storage possibility also means that electricity market are regional, supply and demand must be balanced locally and in real time. This results in a strong dependence on the geographic configuration of the transmission network, local generation capacity, consumption patterns, and grid constraints. Consequently, price formation is highly localized, and significant price differences can persist across regions, even within the same country or interconnected area. A difference in the price of electricity between different zones does not imply an arbitrage opportunity. An arbitrageur cannot buy for storage and transportation, and therefore the spot asset cannot be used to set up dynamic hedging strategies exploiting price differentials. The tradable assets in such markets are typically average-based forward contracts, that deliver electricity over a specified time period. This is why electricity has been called a flow commodity. Deregulated power markets have market mechanisms to balance supply and demand, where electricity is traded in an auction system for standardized contracts. All contracts guarantee the delivery of a given amount of power for a specified future time period.

Electricity markets operate through a combination of physical and financial contracts, each serving different purposes and market participants.

Physical contracts involve the actual delivery of electricity and are typically arranged through organized markets or bilateral agreements. These include transactions in the day-ahead (DA) market and the real-time or intraday market, where electricity is traded for physical delivery in specific hourly intervals. The Transmission System Operator (TSO) plays a crucial role in this context by ensuring the real-time balance between supply and demand, maintaining frequency stability, and managing grid congestion, an example of TSO in Italy is *Terna*. The day-ahead market, often organized by a power exchange (e.g. EPEX SPOT), determines hourly clearing prices. In Italy, this function is performed by the Mercato del Giorno Prima (MGP), operated by GME, which sets zonal prices for each hour of the next day based on the aggregation of supply and demand bids submitted by market participants, one day before delivery. In contrast, the real-time market adjusts for deviations that occur due to forecast errors or unexpected events, with prices often more volatile and driven by short-term imbalances.

Financial contracts, on the other hand, do not involve the physical delivery of electricity. Instead, they are settled in cash against a reference price, typically the day-ahead system price. These contracts include futures, forwards, options, and are widely used by producers, retailers, and speculators to hedge price risk or take speculative positions. Unlike physical contracts, financial contracts can be traded by entities that do not produce or consume electricity. They allow participants to lock in a fixed price and hedge against adverse price movements.

In this context, it is important to note that the day-ahead market serves as the main reference

for spot pricing in most European electricity markets. Participants submit bids for each hour of the following day, and market-clearing prices are determined through the intersection of aggregated supply and demand curves. These hourly prices, published on a daily basis, are commonly referred to as **spot prices**. Although financial electricity contracts do not entail physical delivery, they are economically linked to the physical market through their settlement mechanism, which is typically based on the day-ahead spot price. This linkage enables financial instruments to function as effective hedging tools, allowing producers, retailers, and other stakeholders to manage price risk arising from their exposure in the physical electricity market. A Comprehensive treatment of electricity price modeling, financial and physical contracts, and market structure can be found in [10] while for an excellent introduction to power market design, cost-of-carry, spot vs forward prices, and TSO roles can be consulted [72].

1.1 Spot price

Usually, in a spot market, the seller delivers the goods immediately and the buyer pays for them "on the spot". No conditions are attached to the delivery. This means that neither party can back out of the deal. A fruit and vegetable market is a good example of a spot market: you inspect the quality of the produce and tell the vendor how many cucumbers you want, she hands them to you, you pay the price indicated and the transaction is complete. If later on you decide that you would rather eat lettuce, you probably would not even think of trying to return the cucumbers and getting your money back. A spot market has the advantage of immediacy. As a producer, I can sell exactly the amount that I have available. As a consumer, I can purchase exactly the amount I need. Unfortunately, prices in a spot market tend to change quickly.

The spot price in electricity markets refers to the real-time or near-term price at which electricity are bought and sold for immediate delivery. Unlike forward or futures contracts, the spot price in electricity can be influenced by different factors: the current supply and demand conditions, the cost of energy used to produce electricity as fuel, oil or coal that can vary, the weather conditions, the availability of power plants in particular renewable energy sources are intermittent and whether depended, and geopolitical events as happened recently with Russian-Ukrainian war.

The spot electricity prices are established in a day-ahead market through an auction process for blocks of electricity that will be delivered the following day. Buyers—market participants looking to purchase electricity—must submit their bids between 8:00 a.m. and 12:00 noon on the day before delivery. These bids cover hourly blocks, meaning each buyer submits 24 separate offers, each with a different price and quantity for each hour of the following day. These are all submitted simultaneously. On the other side, sellers also submit their offers, specifying how much electricity they are willing to supply and at what price. The market price for each hour is determined by the intersection of the aggregate demand and supply curves. Once the market price is established for a given hour, all electricity traded during that hour is settled at this single market price, regardless of the individual bids and offers.

In the figure 1.1 is presented a plot of Italian electricity prices PUN (prezzo unico nazionale) from the beginning of 2016 to January 2024. Two significant periods stand out. First, during the COVID-19 pandemic, we observe a sharp decline in prices, driven largely by reduced demand. Second, during the Russia–Ukraine war, electricity prices show a chaotic behavior due to energy supply shocks and market uncertainty.

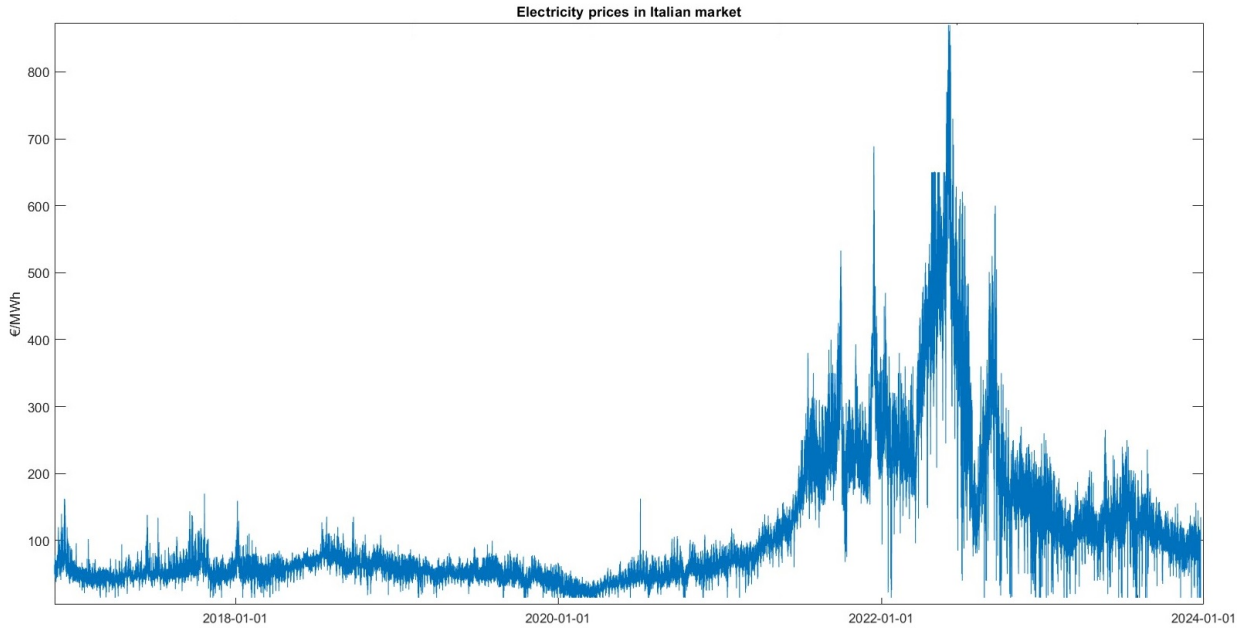

Figure 1.1: The path of the spot price electricity in the Italian market from 2016 until 2024.

A dynamics for the spot price evolution is desirable for several reasons. Models describing the uncertainty in the spot price is of interest for traders operating in these markets. However, they are also used as the reference point for settlement of forward and futures contracts, and thus is a basic input in understanding the dynamics of these derivatives. In this work the spot dynamics will be based on Ornstein-Uhlenbeck (OU) processes, which model mean reversion in a natural way, furthermore since the demand of electricity vary with temperatures that can drastically change over the year it is a common choice include in the model a seasonality function.

1.2 Forward prices

Forwards are contracts between two parties: a seller and a buyer to exchange a certain asset at a future time at an agreed price, established at the initial time of the contract. Hence, the contract must specify:

- the asset to be traded (the underlying);
- a date T, called maturity, when the trade takes place;
- a delivery price F_0, at which the asset is traded at time T.

The traded asset may be a good, such as wheat or gold, or a financial one, such as a currency, an index, or a stock. The parties agree on the delivery price, taking into account also S_0, the initial asset value. Both parties are bound to honor the contract at time T, therefore a risk is enticed for both: if $S_T > F_0$, the seller will be forced to undersell the asset at F_0, while in the other case the buyer will overpay the asset. Such forward contracts are widely used in financial and commodity markets because they provide a valuable tool for risk management. From the seller's perspective, a forward contract ensures the future sale of a predetermined quantity of the product at a fixed price, allowing her to lock in revenue and gain certainty over future cash flows, which is essential for covering planned operational costs, investment repayments, or other financial obligations.

From the buyer's perspective, the main advantage lies in hedging against future price uncertainty. Since the spot price of the commodity may fluctuate significantly over time, entering into a forward contract allows the buyer to protect against the risk of price increases, ensuring cost predictability and budget stability. This mutual benefit, price certainty for both parties, is one of the primary reasons why forward contracts are so prevalent in energy, agricultural, and financial markets.

In the context of electricity markets, forward contracts similarly play a crucial role, but they have been slightly modified to consider the asset's feature to be a non-storable commodity, delivering over a time interval rather than at a fixed maturity.

The forward price encapsulates market expectations about future spot price dynamics and is influenced by factors such as demand forecasts, fuel costs, regulatory frameworks, renewable generation, and geopolitical risks. These contracts are typically financially settled against a reference price (usually, the day-ahead market spot price), to provide stability and predictability for energy producers, utilities, and large consumers to manage risk by securing energy costs in advance, reducing exposure to volatility. These contracts can be customized over-the-counter (OTC) or standardized on Exchange Boards, such as the Intercontinental Exchange (ICE) and Chicago Mercantile Exchange (CME) or EEX (European Energy Exchange). The owner of a forward contract with delivery over a time interval would receive a constant flow of the commodity over this period, against a fixed payment per unit. This structure reflects the nature of electricity consumption and production, which occur continuously over time. The buyer agrees to pay a predefined fixed unitary price, while the seller commits to delivering the agreed quantity at a uniform rate, typically expressed in megawatts (MW) over each hour of the delivery interval.

1.3 Energy Markets models

Given the specific characteristics of electricity markets, there is strong interplay between spot and forward markets and accurate and flexible modeling frameworks are essential for understanding price dynamics and supporting decision-making processes. In particular, the forward price is not simply determined by arbitrage arguments, as in classical financial markets, but reflects expectations over future spot prices. Therefore, a model describing forward prices must be realistic and

consistent with the representation of the spot market.

A natural way to establish this connection is through the Heath–Jarrow–Morton (HJM) approach (see [34]), originally developed for interest rate modeling and later adapted to energy markets (see [11]). Rather than deriving forward prices from a specified spot dynamics under a risk-neutral measure, the HJM methodology starts by postulating a dynamics for the forward itself. This dynamics can be formulated either under the historical probability measure $\mathbb{P}$ or under an equivalent martingale measure $\mathbb{Q}$.

Another distinctive feature of electricity markets is that contracts with overlapping delivery periods may be traded on the same dates, for instance two contracts might have respective delivery periods given by the first four months of the year and the first quarter.In an arbitrage-free market, delivery-period forward contracts must satisfy a consistency condition: assuming as delivery period $[T_1, T_2]$, we denote the price of the energy forwards contracts traded on the market by $F(t, T_1, T_2)$ ($t < T_1 < T_2$), which are liquid instruments and must be priced to avoid arbitrage opportunities (see [34]). Since contracts with overlapping delivery periods may be traded at the same time, given a sequence of times $\{T_i\}_{i=1}^n$, which represent the endpoints of the delivery periods, to ensure the absence of arbitrage opportunities, forward prices must satisfy the following relation

$$(T_n - T_1)F(t, T_1, T_n) = \sum_{i=1}^{n-1}(T_{i+1} - T_i)F(t, T_i, T_{i+1}), \tag{1.1}$$

which states that the value of a forward contract for a period $[T_1, T_n]$ must be the weighted sum of the values of the forwards having delivery periods partitioning $[T_1, T_n]$. Thus, it is necessary to have a representation of forward prices that implies equation (1.1) to be satisfied under some risk-neutral probability.

We are now going to provide our general framework, let $[0, \mathbb{T}]$ with $\mathbb{T} < \infty$ be a finite time interval, and $(\Omega, \mathcal{F}, \{\mathcal{F}_t\}_{t\in[0,\mathbb{T}]}, \mathbb{P})$ a complete filtered probability space, satisfying the standard hypotheses (right-continuity and completeness) and with $\mathbb{P}$ denoting the historical (real-world) probability. We assume that a riskless asset with constant return rate r is traded and we denote by $\{S(t)\}_{\{t\in[0,\mathbb{T}]\}}$ the energy spot price. Following the HJM methodology, as adapted to the energy context in [11], we assume the existence of theoretical instantaneous forwards, $f(t, T)$ with $t \in [0, \mathbb{T}]$, delivering an electricity at maturity T, not necessarily actually traded in the market[1], whose price evolution under the real-world probability $\mathbb{P}$ is given by

$$df(t, T) = \mu(t, T)dt + \sum_{i=1}^{d}\sigma_i(t, T)dB_i(t), \qquad t < T \leq \mathbb{T},$$

where $\mathbf{B} = (B_0, ..., B_d)$ is a d-dimensional standard Brownian motion and μ and $\sigma_i,\ i = 1, ..., d$ are real-valued continuous function on $S^{\mathbb{T}} = \{(t, T) \in [0, \mathbb{T}]^2 : t \leq T\}$.

The contract does not require any initial cash settlement, therefore the net payoff at maturity

[1] In some literature, these are referred to simply as “forwards", while $F(t, T_1, T_2)$ is referred to as a “swaps".

will be $S(T) - f(t,T)$. Under appropriate integrability conditions on the coefficients, the absence of arbitrage in the market is equivalent to the existence of a martingale measure $\mathbb{Q} \sim \mathbb{P}$ such that the discounted price of the contract is a martingale (see e.g. [58]), that is to say

$$\mathrm{e}^{-r(T-t)}\mathbb{E}^{\mathbb{Q}}[S(T) - f(t,T)|\mathcal{F}_t] = 0,$$

which implies ,

$$f(t,T) = \mathbb{E}^{\mathbb{Q}}[S(T)|\mathcal{F}_t]. \tag{1.2}$$

Under standard square-integrability assumptions and assuming that the filtration is generated by the Brownian motion $\mathbf{B}$, the martingale representation theorem implies that, under $\mathbb{Q}$,

$$df(t,T) = \sum_{i=1}^{d} \sigma_i(t,T) dB_i^{\mathbb{Q}}(t), \tag{1.3}$$

with a $\mathbb{Q}-$Brownian motion $\mathbf{B}^{\mathbb{Q}} = (B_1^{\mathbb{Q}}, \ldots, B_d^{\mathbb{Q}})$ satisfying $d\mathbf{B}^{\mathbb{Q}}(t) = d\mathbf{B}(t) + \mathbf{\Lambda}(t,T)dt$ for some adapted process $\mathbf{\Lambda}(t,T)$ representing the market price of risk. In this framework, spot prices can be viewed as instantaneous-delivery forwards with zero time to maturity, which implies $S(t) = f(t,t)$, that is, an arbitrage-free pricing dynamics for the energy price under $\mathbb{Q}$. We emphasize that the volatility structure is preserved under the change of measure, consistently with the classical HJM framework, while only the drift component is modified through the market price of risk.

As the mesh of the partition in equation (1.1) tends to zero, for all intermediate times we have $\Delta_i T = T_{i+1} - T_i \to 0$ and the values of the forward contracts $F(t, T_i, T_{i+1})$ collapse to the price of the instantaneous forwards, so the no-arbitrage condition becomes

$$F(t,T_1,T_2) = \frac{1}{T_2 - T_1} \int_{T_1}^{T_2} f(t,T)dT,^{2} \tag{1.4}$$

which indicates that the forward price with delivery period is an integral average of the prices of instantaneous forward contracts over the same interval, in other words, forward contracts with delivery over a period can be viewed as an infinite combination of instantaneous forward contracts. The formula (1.4) is the continuous-time version of (1.1) it was presented for the first time in [11]. At this stage, it is important to stress once again that $\mathbb{Q}$ denotes the risk–neutral probability measure. In this framework, we can define the *risk premium* RP, as the difference between the instantaneous forward price and the expected spot price at delivery under the historical measure $\mathbb{P}$:

$$RP(t,T) = f(t,T) - \mathbb{E}^{\mathbb{P}}[S(T) \mid \mathcal{F}_t],$$

[2] Actually, the definition used in the literature is $F(t,T_1,T_2) = \int_{T_1}^{T_2} \omega(t,T_1,T_2) f(t,T)dT$, where $\omega(t,T_1,T_2)$ is a weighted function that takes value 1 if the settlement takes place at the end of the delivery period while $\omega(t,T_1,T_2) = \mathrm{e}^{-rt}$ if the contract is settled continuously over the delivery period.

which plays a fundamental role, as it represents a key quantity in commodity markets (see [29]). From a modeling perspective, the risk premium naturally arises from the change of probability measure from $\mathbb{P}$ to $\mathbb{Q}$ and is characterized by the market price of risk $\Lambda(t,T)$ through its impact on the spot price drift. Unlike storable commodities such as oil or gas, electricity cannot be economically stored. This invalidates the classical cost–of–carry arbitrage relations and implies that forward prices must incorporate a risk premium reflecting the market participants' risk preferences and hedging needs. Typically, producers are risk–averse to falling prices and thus hedge by selling forwards, while retailers are risk–averse to rising prices and therefore hedge by buying forwards. The balance of these opposite hedging pressures determines the sign of the risk premium, which is often negative in electricity markets, but may turn positive in periods of high demand risk.

The fundamental link between spot prices $S(t)$, which carry market risk, and delivery-period forward contracts $F(t,T_1,T_2)$, used as hedging instruments, is given by the *forward curve*, defined as the set of all unit futures prices $f(t,T)$ for $T \geq t$. For this reason, most models in the literature aim to describe, either directly or indirectly, the forward curve, which is regarded as the cornerstone of electricity price modeling. Several works, such as Björk and Landén [18] and Benth and Krühner [9], investigate the valuation principles of derivative products based on the forward curve. They define a general valuation framework and discuss the choice of a risk-neutral probability measure. However, since electricity markets are incomplete, due to the presence of price spikes, and dependence on exogenous variables that cannot be hedged, many models acknowledge the impossibility of ensuring the uniqueness of the risk-neutral measure. While some authors explicitly address this issue, others simply assume the existence of a suitable pricing measure. This motivates the development of a realistic model for the spot price process $(S(t))$ under the historical probability measure, from which a consistent forward pricing framework can subsequently be derived.

Historically, two main categories have been used to model electricity spot prices. In the arithmetic case, the stochastic component enters the model additively, typically represented as $S(t) = \mu(t) + X(t)$, where $\mu(t)$ is a deterministic function capturing trend or seasonality, and $X(t)$ denotes a stochastic process (or a combination of processes). In contrast, the geometric models assumes a multiplicative structure of the form $S(t) = \mu(t)\,\mathrm{e}^{X(t)}$, which ensures strictly positive prices. In recent years, arithmetic models have become more prevalent, particularly because many electricity markets allow for negative spot prices.

A classical framework for modeling commodity spot prices is provided by the Schwartz model [71]. This geometric factor model incorporates mean-reverting features through a stochastic convenience yield and has had a significant influence on the development of energy price models. One of its main advantages is that it allows for the derivation of explicit forward pricing formulas within an arbitrage-free setting for markets.

An important predecessor of this approach is the two-factor model proposed by Gibson and Schwartz in [30], where the spot price and the convenience yield are modeled as correlated stochastic factors. This framework proved particularly successful in the modeling of crude oil markets and

inspired a large body of subsequent research on commodity and energy price dynamics.

Later, in [48], the authors, neglecting the notion of convenience yield, adapted this class of models for the first time to electricity prices. They introduced also a seasonality function, recognizing the distinct features of power markets. This model, which will be described in detail in the following section, constitutes the foundation of our framework. It represents a milestone in electricity price modeling and has inspired several subsequent developments. For instance, in [45] it serves as the baseline model upon which a seasonality structure is introduced also in the volatility component. Finally we point out this class of models do not take in account the spikes typical of energy markets, that usually correspond to periods of high tension in the system, followed by a quick return to equilibrium. There are both upward and downward price spikes, especially for regions with a high proportion of renewable generation. To represent this phenomenon, many research papers replace the Brownian motion(s) with more general Lévy processes that can represent jumps in a price series. Several authors studied models for electricity spot and futures prices, for example in [20] the authors include a Poisson process in a mean reverting Lucia-Schwartz model for the spot price, a comprehensive overview on model with jumps is provided in [25], and further examples discussed in [11].

In our work, we do not delve into models incorporating jumps, as our framework does not account for discontinuities. Instead, we concentrate on representing the main and most commonly used dynamics in the literature, excluding more specialized cases such as jump-diffusion models. To this aim, we explore the integration of fractional dynamics into electricity price modeling. After the publication of [28] by Gatheral et al., which demonstrated improved volatility forecasting through a rough fractional volatility model, the interest in fractional dynamics spread from the financial community. Those dealing with commodities and electricity markets, where fractional dynamics offer a better answer to several empirical features, such as correlation between increments, memory, self-similarity, extreme variability of prices when compared to traditional financial time series or storable commodities. Several authors have shown that incorporating fractional dynamics in modeling electricity spot prices is appropriate and effective. Many papers tried to test empirically the presence of fractional dynamics, in [74], fractional behavior in spot electricity time series from NordPool (one of the oldest and most important electricity markets in Europe) was observed and the same conclusion applied to electricity prices in the California market as argue in [78]. Although the roughness of price series in several energy markets is now well documented, only a few studies have translated this empirical observation into actual models for spot price dynamics. A notable exception is [70], where the authors compare a rough model based on a multifractal random walk with a classical (non-rough) Ornstein–Uhlenbeck-type model, concluding that the latter provides a better fit for Nord Pool spot prices over the period from May 1992 to August 2011. Furthermore, [8] proposed a mean-reverting multifractal process that includes both a jump component and a rough component, offering a more flexible framework to capture the complex structure of electricity spot prices. In their analysis, the authors remove seasonal and spiky components from the raw market data and estimate the degree of roughness in electricity spot

price dynamics. Another noteworthy contribution in the field is found in [54], where the authors introduce a non-Markovian model in which the spot price is driven by a combination of Gaussian Volterra processes—such as fractional Brownian motions (fBms), Riemann-Liouville processes, or Gaussian-Volterra driven Ornstein–Uhlenbeck processes. However, the paper does not provide empirical validation of the proposed models using market data.

Along with the same of the discussed (see, for example, [12], [45]), we use an arithmetic model for the spot price, because of its analytical tractability and flexibility to allow for negative prices, a feature that is potentially important especially in light of the recent global crises, which led to increasingly frequent occurrences of negative spot prices.

The spot price dynamics will be based on Ornstein–Uhlenbeck (OU) processes, which naturally model a mean-reverting behavior. Moreover, since electricity demand is highly influenced by temperature fluctuations over the year, we include also a seasonality function and, to capture the observed roughness in electricity prices, we introduce a fractional component, through a combination of fundamental martingales.

Chapter 2

Basic Definitions and Analytical Tools for Stochastic Processes

Before delving into the proposed model, it is essential to clarify some fundamental definitions related to stochastic processes. This chapter does not aim to provide a comprehensive introduction to the theory of stochastic processes; rather, our goal is to present only the basic tools that will be used throughout this work. For a more detailed and rigorous treatment of these topics, we refer the reader to [39]. In particular, only the definitions and fundamental theorems necessary to deal with stochastic processes are presented here, while some specific theorems whose proofs are reported in the Appendix. Readers already familiar with these topics may skip this chapter and proceed directly to the next one.

Definition 2.1. ***(Stochastic process)***
*Let $(\Omega, \mathcal{F}, \mathbb{P})$ be a probability space. A **stochastic process** is a collection of random variables $\{X_t : t \in T\}$ defined on $(\Omega, \mathcal{F}, \mathbb{P})$, where:*

- *T is an index set (typically representing time), which may be discrete (e.g., $T = \mathbb{N}$) or continuous (e.g., $T = [0, \infty)$),*
- *for each fixed $t \in T$, the mapping $\omega \mapsto X_t(\omega)$ is a random variable.*

In other words, a stochastic process is a family of random variables that can represent the evolution of a system.

One way to think of a stochastic process is through its law. The law of a stochastic process is characterized by its finite-dimensional distributions (fdd, in short); that is, the probability distributions

$$\mathbb{P}(X(t_1) \leq \omega_1, \cdots, X(t_n) \leq \omega_n), \quad t_i \in T, \omega_i \in \mathbb{R}, n \geq 1$$

Definition 2.2. ***(Covariance Function of a Stochastic Process)***
*Let $\{X_t\}_{t \in T}$ be a stochastic process defined on a probability space $(\Omega, \mathcal{F}, \mathbb{P})$. The **covariance***

function *(or autocovariance function) of the process is defined by*

$$\gamma(s,t) = \mathrm{Cov}(X_s, X_t) = \mathbb{E}[(X_s - \mathbb{E}[X_s])(X_t - \mathbb{E}[X_t])], \quad \textit{for all } s,t \in T.$$

This function measures the linear dependence between the values of the process at two time points.

Definition 2.3. ***(Correlation Function of a Stochastic Process)***
Let $\{X_t\}_{t\in T}$ be a stochastic process with finite second moments. The ***correlation function*** *(or autocorrelation function) is the normalized covariance function, defined by*

$$\rho(s,t) = \frac{\mathrm{Cov}(X_s, X_t)}{\sqrt{\mathrm{Var}(X_s)\,\mathrm{Var}(X_t)}}, \quad \textit{for all } s,t \in T.$$

Definition 2.4. ***(Gaussian Process)***
Let $(X_t)_{t\in T}$ be a stochastic process indexed by a set $T \subseteq \mathbb{R}$. The process is called a Gaussian process *if for every finite set of time points $t_1, t_2, \ldots, t_n \in T$, the random vector*

$$(X_{t_1}, X_{t_2}, \ldots, X_{t_n})$$

has a multivariate normal (Gaussian) distribution. That is, there exists a mean vector $\mu = (\mu_1, \ldots, \mu_n)$ and a covariance matrix Σ such that

$$(X_{t_1}, X_{t_2}, \ldots, X_{t_n}) \sim \mathcal{N}(\mu, \Sigma).$$

Definition 2.5. ***(Strictly stationary Process)***
A stochastic process $\{X_t\}_{t\in T}$ is said to be ***strictly stationary*** *if, for any $n \in \mathbb{N}$, any time points $t_1, \ldots, t_n \in T$, and any shift $k \in T$, the joint distribution of $(X_{t_1}, \ldots, X_{t_n})$ is the same as that of $(X_{t_1+k}, \ldots, X_{t_n+k})$.*

Definition 2.6. ***(Weakly Stationary Process)*** *A process is called* ***weakly stationary*** *(or* second-order stationary*) if:*

- $\mathbb{E}[X_t] = \mu$ *for all* $t \in T$,
- $\mathrm{Var}(X_t) = \sigma^2 < \infty$ *for all* $t \in T$,
- $\mathrm{Cov}(X_t, X_{t+k}) = \gamma(k)$, *i.e., the autocovariance depends only on the lag k, not on the specific time t.*

For Gaussian processes, weak stationarity is the same as strong stationarity (and is referred simply as *stationarity*). It is important to note that not all stochastic processes are stationary. However, in some applications, it is sufficient to require that the *increments* of the process be stationary, even if the process itself is not.

A stochastic process $\{X(t)\}_{t\in T}$ is said to have stationary increments if $T = \mathbb{R}$, $\mathbb{Z}$, $\mathbb{R}_+$, or $\mathbb{Z}_+$, and for any $h \in T$,

$$\{X(t+h) - X(h)\}_{t\in T} \stackrel{d}{=} \{X(t) - X(0)\}_{t\in T}.$$

An example of such a process is the standard Brownian motion, which is not strictly stationary but possesses stationary increments. This property is particularly relevant in modeling contexts where the emphasis is not on the specific time point, but rather on the evolution of the process over time intervals.

Definition 2.7. ***(Standard Brownian Motion)***
The Brownian motion $\{B(t)\}_{t\geq 0}$ is a stochastic centered normal distributed process with variance t and covariance

$$Cov(B_t, B_s) = \min(t, s)$$

it is also called Wiener process and it satisfies the following properties:

1. $B(0) = 0$ *almost surely,*
2. *The process has* independent increments*, i.e., for any $0 \leq t_0 < t_1 < \cdots < t_n$, the random variables $B(t_1) - B(t_0), B(t_2) - B(t_1), \ldots, B(t_n) - B(t_{n-1})$ are independent,*
3. *The increments are* stationary and normally distributed*: for all $s < t$, the increment $B(t) - B(s) \sim \mathcal{N}(0, t-s)$,*
4. *The sample paths of $B(t)$ are almost surely continuous functions of t.*

Here we introduce some useful definition in the frequency domain, while, in time domain, the dependence structure of a process is characterized by the autocovariance function, in frequency domain (after Fourier transformation) it is characterized by the spectral density function. The following notion are fundamental to define long and short memory processes.

Definition 2.8. ***(Spectral density)***
For a stationary process (X_t) with autocovariance function γ, the spectral density *is (formally) defined as the Fourier transform of the autocovariance function:*

$$f_X(\lambda) := \frac{1}{2\pi} \sum_{k=-\infty}^{\infty} \gamma(k) e^{-ik\lambda}, \quad \lambda \in [-\pi, \pi]. \tag{2.1}$$

Conversely, the (formally defined) Fourier transform of the spectral density f is the autocovariance function γ given by

$$\gamma(k) = \frac{1}{2\pi} \int_{-\pi}^{\pi} f_X(\nu) e^{ik\nu}\, d\nu, \quad k \in \mathbb{Z}. \tag{2.2}$$

For an overview of spectral analysis of time series, see [66]. In the spectral domain, attention is focused on the function $f_X(\lambda)$. The variable λ is restricted to the domain $(-\pi, \pi)$ since the spectral

density $f_X(\lambda)$ is 2π-periodic; that is,

$$f_X(\lambda + 2\pi k) = f_X(\lambda), \quad \text{for all } k \in \mathbb{Z}.$$

Note also that the spectral density f_X is well-defined pointwise whenever $\gamma \in \ell^1(\mathbb{Z})$ (the space of absolutely summable sequences in $\mathbb{Z}$). The frequency variable λ enters $f_X(\lambda)$ through the complex exponential $e^{-ih\lambda}$, involving sine and cosine terms. When λ is close to 0, we refer to *low frequencies* (corresponding to *long waves*); conversely, when λ is close to π, we refer to *high frequencies* (corresponding to *short waves*).

Theorem 2.0.1. ***Martingale Representation Theorem***
Let $(\Omega, \mathcal{F}, (\mathcal{F}_t)_{t\geq 0}, \mathbb{P})$ be a filtered probability space satisfying the usual conditions, and let $(W_t)_{t\geq 0}$ be a standard Brownian motion adapted to $(\mathcal{F}_t)_{t\geq 0}$.

Then, for any square-integrable $(\mathcal{F}_t)$-martingale $(M_t)_{t\geq 0}$ with $M_0 = 0$, there exists a unique progressively measurable process $(\phi_t)_{t\geq 0}$ such that

$$\mathbb{E}\left[\int_0^T \phi_t^2 \, dt\right] < \infty$$

and

$$M_t = \int_0^t \phi_s \, dW_s, \qquad t \geq 0.$$

The martingale representation theorem implies that any square-integrable martingale adapted to the Brownian filtration can be expressed as a stochastic integral with respect to Brownian motion. *The martingale representation theorem may be extended to several dimensions and to local martingale.*

Definition 2.9. ***(Hölder continuity)***
Let $(X_t)_{t\in T}$ be a stochastic process. We say that a sample path $t \mapsto X_t(\omega)$ is Hölder continuous of order $\alpha \in (0, 1]$ if there exists a finite constant $C(\omega)$ such that

$$|X_t(\omega) - X_s(\omega)| \leq C(\omega)\,|t - s|^\alpha, \quad \forall\, s, t \in T.$$

The process X_t is said to be Hölder continuous of order α if almost all of its sample paths satisfy the above property.

Definition 2.10. ***(p-variation)***
Let $(X_t)_{t\in[0,T]}$ be a real-valued stochastic process and let $p \geq 1$. For a partition $\Pi = \{0 = t_0 < t_1 < \cdots < t_n = T\}$ of the interval $[0, T]$, define the p-variation of the path $t \mapsto X_t(\omega)$ over Π as

$$V_p\big(X(\omega), \Pi\big) := \sum_{i=1}^{n} \big|X_{t_i}(\omega) - X_{t_{i-1}}(\omega)\big|^p.$$

If $p = 2$ we call $V_2\big(X(\omega), \Pi\big)$ quadratic variation.
The (total) p-variation of the path $X(\omega)$ over $[0, T]$ is then

$$V_p\big(X(\omega), [0, T]\big) := \sup_{\Pi} V_p\big(X(\omega), \Pi\big),$$

where the supremum is taken over all finite partitions Π of $[0, T]$. We say that the process X has finite p-variation on $[0, T]$ if $V_p\big(X(\omega), [0, T]\big) < \infty$ for almost all $\omega \in \Omega$.

Definition 2.11. ***(Quadratic covariation)***
Let $(X_t)_{t\in[0,T]}$ and $(Y_t)_{t\in[0,T]}$ be real-valued stochastic processes. For a partition $\Pi = \{0 = t_0 < t_1 < \cdots < t_n = T\}$ of the interval $[0, T]$, define the quadratic covariation of the paths $t \mapsto X_t(\omega)$ and $t \mapsto Y_t(\omega)$ over Π as

$$V_2\big(X(\omega), Y(\omega); \Pi\big) := \sum_{i=1}^{n} \big(X_{t_i}(\omega) - X_{t_{i-1}}(\omega)\big)\big(Y_{t_i}(\omega) - Y_{t_{i-1}}(\omega)\big).$$

If the limit

$$[X, Y]_t(\omega) := \lim_{|\Pi|\to 0} V_2\big(X(\omega), Y(\omega); \Pi\big)$$

exists, we call it the quadratic covariation process of X and Y on $[0, T]$. In particular, $[X, X]_T$ coincides with the quadratic variation of X.

The following theorem is fundamental to construct estimators in our prestige (in chapter 5), it connects time average with space average. [Theorem 5, Section 8 [31]].

Theorem 2.0.2. *(Ergodic theorem)*
Let $(Y_k)_{k\in\mathbb{Z}}$ be a strictly stationary and ergodic sequence[1] *of real-valued random variables. Then, for any measurable function $Q : \mathbb{R} \to \mathbb{R}$ such that $\mathbb{E}|Q(Y_0)| < \infty$, we have*

$$\frac{1}{N}\sum_{k=0}^{N-1} Q(Y_k) \xrightarrow[N\to\infty]{a.s.} \mathbb{E}\big[Q(Y_0)\big].$$

Theorem 2.0.3. *(Girsanov's Theorem)*
Let $(\Omega, \mathcal{F}, \{\mathcal{F}_t\}_{t\geq 0}, \mathbb{P})$ be a filtered probability space supporting an n-dimensional Brownian motion $W(t) = (W_1(t), \ldots, W_n(t))$ under $\mathbb{P}$. Let $\theta(t) = (\theta_1(t), \ldots, \theta_n(t))$ be an adapted process satisfying Novikov's condition

$$\mathbb{E}_{\mathbb{P}}\left[\exp\left(\tfrac{1}{2}\int_0^T \|\theta(s)\|^2\, ds\right)\right] < \infty, \quad \forall T > 0.$$

[1] A strictly stationary sequence $(Y_k)_{k\in\mathbb{Z})}$ is said to be *ergodic* if its long-run time averages coincide with the corresponding ensemble averages.The statistical properties of the sequence can be recovered from a single sufficiently long realization.

Define the stochastic exponential

$$Z_T = \exp\left(- \int_0^T \theta(s)^\top dW(s) - \tfrac{1}{2} \int_0^T \|\theta(s)\|^2 ds \right).$$

Then $(Z_t)_{t\geq 0}$ *is a* $\mathbb{P}$*-martingale with* $\mathbb{E}_{\mathbb{P}}[Z_T] = 1$*. We may define a new probability measure* $\mathbb{Q}$ *on* $(\Omega, \mathcal{F}_T)$ *by*

$$\frac{d\mathbb{Q}}{d\mathbb{P}}\Big|_{\mathcal{F}_T} = Z_T.$$

Under $\mathbb{Q}$*, the process*

$$W^{\mathbb{Q}}(t) := W(t) + \int_0^t \theta(s)\, ds$$

is an n*-dimensional Brownian motion.*

The process $\theta(t)$ in the financial applications is identified as *market price of risk*. It quantifies the excess drift under the real-world measure $\mathbb{P}$ relative to the risk-neutral measure $\mathbb{Q}$. In particular, when pricing financial assets, the change of measure removes this excess drift, ensuring that discounted asset prices are $\mathbb{Q}$-martingales.

Chapter 3

Estimation of the Hurst exponent

In this chapter, we explain our modeling choice and provide empirical evidence validating the use of fractional dynamics to describe the characteristics of electricity markets.

We look at the electricity prices in the Italian market and we want to estimate the Hurst exponent of the price time series. This parameter was introduced in the seminal paper [35] by Harold E. Hurst, a British hydrologist who studied the long-term storage capacity of water reservoirs, observing a long-range dependence in the water levels of the Nile River. In doing so, he developed the empirical rescaled range methodology to measure long-range dependence. The Hurst exponent, used since then, was named after him.

This exponent becomes a key parameter in modeling memory effects and roughness in time series, in finance, cardiology, geophysics, and commodities markets.

In general, the Hurst exponent provides a measure for long-term memory of a time series, in detail it is a scalar value that helps to identifying whether a series is mean reverting, random walking or trending. The value of the Hurst exponent varies in the interval $[0, 1]$ and based on its value, a time series can be classified in one of these three categories. If $H = 0.5$ the time series is random, if $H < 0.5$ indicates anti-persistence which means an up value is more likely to be followed by a down value, and vice versa, if $H > 0.5$ the series is said to be persistent, it means that the direction of the next movement is more likely to be the same as the current variation.

In the literature, various methods have been proposed to estimate the Hurst parameter in time series. In the following, we analyze the rescaled range (R/S) analysis, a classical technique already used in [67] to estimate the Hurst parameter in Dow-Jones daily returns. Additionally, we explore the variance time plot estimate, which was applied in real network traffic analysis [80] and in energy market [78]. This method exploits on the asymptotic behavior of the autocovariance function.

Empirical evidence and an estimate of the Hurst exponent in electricity markets are provided in [74], where the author analyzes time series data from the Nord Pool market. By applying rescaled range (R/S) analysis and the average wavelet coefficient (AWC) method at a daily time scale, they obtain Hurst exponent values that confirm the antipersistent behavior of electricity prices in Norway. The findings in [26] further support this antipersistence, but also highlight a crucial limitation:

relying on a single Hurst exponent is not sufficient, as its value exhibits significant variations over time. In [59] it is used a multifractal detrended fluctuation analysis (MF-DFA) to numerically investigate correlation, persistence, multifractal properties and scaling behavior of the hourly spot prices for the Spain electricity exchange, finding an evidence for a Hurst exponent smaller than 0.5. Additional support for antipersistence is found in [78], where rescaled range (R/S) analysis is applied to the time series from the California Power Exchange (CalPX). This study is extended in [77], where the analysis is broadened to include a wider set of electricity markets—such as Nord Pool, several regional U.S. markets, and the U.K. Telerate day-ahead electricity prices. In addition to R/S analysis, two further estimation techniques were employed: Detrended Fluctuation Analysis (DFA) and Periodogram Regression. The combined results reinforce the presence of long-range dependence and antipersistent behavior across diverse electricity market datasets.

Other estimation procedures are based on the assumption that the observed time series follows a fractional Brownian motion (fBm). This process will be discussed in detail in the next chapter, where we examine the construction of consistent estimators, such as those proposed in [43]. We will also explore their application to real-world datasets, as in [32], where these methods are employed to estimate the Hurst parameter from daily time series in the Italian electricity market.

In this chapter, we begin by introducing the concepts of long memory and self-similarity. We then present and compare several methods for estimating the Hurst parameter H, highlighting their theoretical foundations and empirical performance. These techniques are subsequently applied to electricity spot price time series, allowing us to compare our findings with those reported in the literature and to assess the appropriateness of fractional models in this context. In particular, a significant deviation of the estimated H from the benchmark value of $1/2$ would provide strong support for employing models with fractional dynamics to describe spot price behavior. Finally, we compare the H estimates obtained from spot price data with those inferred from the calibration of our model on forward contract series, in order to explore potential relationships between the two.

3.1 Long memory and Self-similar property

Before addressing the estimation methods, we introduce some important concepts: the mathematical definition of long-range memory and the self-similarity. Long-range dependence is a measure of the decay of statistical dependence, represented by the series autocorrelation function on large lags of time. Here we report, notions and definitions from [14] and [65]. Following the approach in [14], we define the slowly varying functions, as introduced in two slightly different manners respectively by Karamata and Zygmund .

Definition 3.1. *(Slowly Varying Function) A function $L : (c, \infty) \to \mathbb{R}$ $(c \geq 0)$ is called slowly*

varying at infinity in Karamata sense *if it is positive (and measurable) for x large enough and,*

$$\lim_{x\to\infty}\frac{L(ux)}{L(x)}=1, \qquad \textit{for every } u>0.$$

A function $L(x)$, defined and positive for $x \geq A$, for some $A > 0$, is said to belong to the Zygmund class of slowly varying functions *if, for a fixed but arbitrary $\delta > 0$ and any $\lambda > 0$, the inequalities*

$$x^{\delta}L(x) \leq (x+\lambda)^{\delta}L(x+\lambda) \quad \textit{and} \quad x^{-\delta}L(x) \geq (x+\lambda)^{-\delta}L(x+\lambda) \tag{3.1}$$

hold for all $x \geq x_0(\delta)$. That is, $x^{\delta}L(x)$ is eventually monotonically increasing and $x^{-\delta}L(x)$ is eventually monotonically decreasing, for every fixed $\delta > 0$. Besides, L is called slowly varying at the origin if $\widetilde{L}(x) = L(x^{-1})$ is slowly varying at infinity.

Propotion 3.1.1. *Every Zygmund slowly varying function is slowly varying in the sense of Karamata.*

Proof. Let $L(x)$ be a Zygmund slowly varying function. Fixed $\delta > 0$, by definition, there exists an $x_0 > 0$ such that for all $x \geq x_0$ the function $x^{\delta}L(x)$ is non-decreasing and $x^{-\delta}L(x)$ is non-increasing. Therefore, chosen $\lambda > 0$ and setting $x + \lambda = ux$ with $u > 1$ for all $x \geq x_0$ we have,

$$(ux)^{\delta}L(ux) \geq x^{\delta}L(x) \quad \text{and} \quad (ux)^{-\delta}L(ux) \leq x^{-\delta}L(x).$$

Dividing the first inequality by $x^{\delta}L(x)$ and the second one by $x^{-\delta}L(x)$, we obtain

$$u^{-\delta} \leq \frac{L(ux)}{L(x)} \leq u^{\delta}, \qquad x \geq x_0.$$

Taking $\liminf_{x\to\infty}$ and $\limsup_{x\to\infty}$ yields

$$u^{-\delta} \leq \liminf_{x\to\infty}\frac{L(ux)}{L(x)} \leq \limsup_{x\to\infty}\frac{L(ux)}{L(x)} \leq u^{\delta}.$$

Since $\delta > 0$ is arbitrary and $u^{\pm\delta} \to 1$ as $\delta \downarrow 0$, it follows that

$$\lim_{x\to\infty}\frac{L(ux)}{L(x)}=1.$$

Hence L is slowly varying in the sense of Karamata. □

Based on the previous definition, we can define different types of (*linear*) dependence.

Definition 3.2. *(Memories) Let $(X_t)_{t\geq 0}$ a weakly stationary process* (2.6)*, with autocovariance function $\gamma(k)$ with $k \in \mathbb{Z}$ and spectral density $f_X(\lambda)$* (2.8) *with $\lambda \in [-\pi, \pi]$*

$$f_X(\lambda) = L_f(\lambda)|\lambda|^{-2d}, \tag{3.2}$$

where $L_f(\lambda) \geq 0$ *is a symmetric function, slowly varying at zero in Zygmund sense and* $d = \left(-\frac{1}{2}, \frac{1}{2}\right)$ *then* X_t *is said to have:*

- "Long range dependence", *if* $d \in (0, 1/2)$*;*
- "Intermediate dependence", *if* $d = 0$ *and* $\lim_{\lambda \to 0} L_f(\lambda) = \infty$*;*
- "Short range dependence", *if* $d = 0$ *and* $\lim_{\lambda \to 0} L_f(\lambda) = c_f \in (0, \infty)$*;*
- "Antipersistence", *if* $d \in (-1/2, 0)$.

This parameter d is the so-called memory parameter. The following results (for the proofs we refer to ([14])) show the relationship between the behavior of the spectral density at the origin and the asymptotic decay of the autocovariance function.

Theorem 3.1.1. *Let* $(X_t)_{t \geq 0}$ *be a stationary process with autocovariance function* $\gamma(k)$*with* $k \in \mathbb{Z}$ *and spectral density* $f_X(\lambda)$ *with* $\lambda \in [-\pi, \pi]$*, and let* L_γ *and* L_f *be slowly varying functions in Zygmunds' sense.*

(i) If L_γ *is slowly varying at infinity and*

$$\gamma(k) = L_\gamma(k)|k|^{2d-1},$$

for $d \in \left(0, \frac{1}{2}\right)$ *or* $d \in \left(-\frac{1}{2}, 0\right)$*, and* $\sum_{k \in \mathbb{Z}} \gamma(k) = 0$*, then*

$$f_X(\lambda) \sim L_f(\lambda)|\lambda|^{-2d}, \quad (\lambda \to 0)$$

with

$$L_f(\lambda) = L_\gamma(\lambda^{-1})\pi^{-1}\Gamma(2d)\sin\left(\frac{\pi}{2} - \pi d\right). \tag{1.7}$$

(ii) If L_f *is slowly varying at the origin and of bounded variation on* (a, π) *for all* $a > 0$ *such that for* $0 < \lambda < \pi$*, we have*

$$f_X(\lambda) = L_f(\lambda)|\lambda|^{-2d},$$

where $d \in \left(-\frac{1}{2}, 0\right) \cup \left(0, \frac{1}{2}\right)$*, then*

$$\gamma(k) \sim L_\gamma(k)|k|^{2d-1}, \quad (k \to \infty)$$

with

$$L_\gamma(k) = 2L_f(k^{-1})\Gamma(1 - 2d)\sin(\pi d). \tag{1.9}$$

The Theorem 3.1.1 formalizes the precise asymptotic link between the time and frequency domains. Statement (i) shows that, if the autocovariance function decays polynomially with exponent $2d - 1$ then the spectral density necessarily behaves like $|\lambda|^{-2d}$ near the origin. Conversely,

statement (ii) proves that a power-law behavior of the spectral density at zero implies the same polynomial decay for the autocovariance function at infinity. Therefore, the memory parameter d uniquely determines both the strength of the singularity of the spectral density at the origin and the asymptotic decay rate of the autocovariance function. This dual characterization justifies the classification of dependence structures introduced above. Taking into account the relationship between the behavior of the spectral density at the origin and the summability of the autocovariance, we obtain a further statement that gives the complete scenario about the detection of the kind of memory a stochastic process follows:

Corollary 3.1.1. *Under the same assumptions of the previous theorem, we have:*

(i) long range dependence: for $d \in \left(0, \frac{1}{2}\right)$,

$$\sum_{k\in\mathbb{Z}} \gamma(k) = 2\pi \lim_{\lambda\to 0} f(\lambda) = \infty;$$

(ii) intermediate dependence: for $d = 0$ *and* $\lim_{\lambda\to 0} L_f(\lambda) = \infty$,

$$\sum_{k\in\mathbb{Z}} \gamma(k) = 2\pi f(0) = \lim_{\lambda\to 0} f(\lambda) = \infty;$$

(iii) short range dependence: for $d = 0$ *and* $\lim_{\lambda\to 0} L_f(\lambda) = c_f \in (0, \infty)$,

$$\sum_{k\in\mathbb{Z}} \gamma(k) = 2\pi f(0) = 2\pi c_f \in (0, \infty);$$

(iv) antipersistence: for $d \in \left(-\frac{1}{2}, 0\right)$,

$$\sum_{k\in\mathbb{Z}} \gamma(k) = 2\pi f(0) = 0.$$

Based on this corollary, one can shortly summarize the conditions on the memory parameter d for the three main dependence types (i), (iii) and (iv). For more details on different models exhibiting this special dependence type of *intermediate dependence*, see, e.g., [33].

(i) (X_t) exhibits long range dependence if $d \in \left(0, \frac{1}{2}\right)$, which means that the spectral density f has a hyperbolic pole at the origin or that (X_t) has slowly (hyperbolically) decaying correlations. (X_t) is short-range dependent if $d = 0$ and the correlations are summable, and antipersistent if $d \in \left(-\frac{1}{2}, 0\right)$.

(ii) The different parameter ranges can be interpreted as follows: A value $d \in \left(0, \frac{1}{2}\right)$ means that high values of the process will be followed by high values for a long time; a value $d \in \left(-\frac{1}{2}, 0\right)$ indicates a tendency of switching between high and low values; and for $d = 0$

we have a random process with neither a tendency to switching nor a tendency of maintaining the same behavior.

Another classical way of studying long memory and antipersistence is based on the relationship between dependence and self-similarity. Self-similar processes were introduced [41], is a stochastic process that looks the same at different time scales. Formally is defined in terms of the distribution of the process:

Definition 3.3. *A stochastic process $\{Y_t\}_{t\geq 0}$ is called self-similar with self-similar parameter $H \in (0,1)$ if for all $c > 0$,*

$$Y_{ct} \overset{d}{=} c^H Y_t \quad \forall t \in \mathbb{R}.$$

Where $\overset{\mathrm{d}}{=}$ denotes equality in distribution. It is not the path of Y_t but its distribution which scales, one should say "statistical self-similarity" or better, "statistical self-affinity." We will continue to use "self-similarity" because this term is now widely used. Intuitively, self-similarity means that a stochastic process scaled in time looks statistically the same as the original process when properly rescaled in space. Physically, expanding the time scale (large c) should require an expansion of the space scale, that is, a large factor c^H and hence the self-similarity parameter H cannot be negative.

The importance of self-similarity arises with the Lamperti theorem (1962) that says that whenever a process is the limit of normalized partial sums of random variables, it is self-similar.

Theorem 3.1.2. *(Lamperti [44])*

i) Suppose that $(Y_t)_{t\geq 0}$ is a stochastic process which is the limit in distribution of the sequence of normalized partial sums:

$$\frac{S_{nt}}{a_n} = \frac{1}{a_n}\sum_{i=1}^{[nt]} X_i, \quad n \in \mathbb{N}$$

where $[nt]$ denotes the integer part of nt, $\{X_i\}_{i\in\mathbb{N}}$ is a stationary sequence of random variables, and $a_1, a_2, \cdots$ is a sequence of positive normalizing constants such that $log(a_n) \to \infty$. Then there exists a $H > 0$ such that for any $u > 0$,

$$\lim_{n\to\infty} \frac{a_{nu}}{a_n} = u^H,$$

and Y_t is self-similar with self-similarity parameter H, and has strong stationary increments.

ii) All self-similar processes with stationary increments and $H > 0$ can be obtained by partial sums as given in i).

The normalizing constants (a_n) rescale the growth of the partial sums to produce a non-degenerate limit, and their asymptotic behavior determines the self-similarity parameter of the limiting process.

Intuitively, one can verify that the scaling property, which is characteristic of self-similar processes, implies the presence of memory in the process.
Taking a H-self similar and with stationary increments process (usually in literature is identified as a H-SSSI process) $\{Y_t\}_{t>0}$, with $Y_0 = 0$, using the property of self-similarity and stationarity the covariance function $\gamma_Y(t,s) = \mathbb{C}ov(Y_t, Y_s)$ can be computed. Assuming that the second moment exists by stationarity $\mathbb{E}[(Y_t - Y_{t-1})^2] = \mathbb{E}[Y_1^2] = \sigma^2$ since we take $\mathbb{E}[Y_t] = 0$. Then for $s < t$ using the stationarity and the similarity

$$\mathbb{E}[(Y_t - Y_s)^2] = \mathbb{E}[(Y_{t-s} - Y_0)^2] = \mathbb{E}[((t-s)^H Y_1)^2] = \sigma^2 (t-s)^{2H}.$$

On the other hand

$$\begin{aligned}\mathbb{E}[(Y_t - Y_s)^2] =& \mathbb{E}[Y_t^2] + \mathbb{E}[Y_s^2] - 2\mathbb{E}[Y_t Y_s] \\ =& \sigma t^{2H} + \sigma s^{2H} - 2\gamma_Y(t,s).\end{aligned}$$

Hence,

$$\gamma_Y(t,s) = \frac{1}{2}\sigma^2[t^{2H} - (t-s)^{2H} + s^{2H}].$$

Denoting by $X_i = Y_i - Y_{i-1}$ the increments sequence $(i = 1, 2, 3, \cdots)$, using the stationarity and the self-similarity, the covariance function between X_i and X_{i+k} with $k > 0$ can be computed as well

$$\begin{aligned}\gamma_X(k) &= \mathbb{C}ov(X_i, X_{i+k}) = \mathbb{C}ov(X_1, X_{k+1}) = \mathbb{C}ov(Y_1 - Y_0, Y_{k+1} - Y_k) \\ &= \mathbb{C}ov(Y_{k+1}, Y_1) - \mathbb{C}ov(Y_k, Y_1) - \mathbb{C}ov(Y_{k+1}, Y_0) + \mathbb{C}ov(Y_k, Y_0) \\ &= \frac{\sigma^2}{2}\Big[\big((k+1)^{2H} - k^{2H} - 1\big) - \big(k^{2H} - (k-1)^{2H} - 1\big)\Big] \\ &= \frac{\sigma^2}{2}[(k+1)^{2H} + (k-1)^{2H} - 2k^{2H}].\end{aligned}$$

Let us observe that the covariance of the increment sequence does not depend on t, and it is an even function, $\gamma_X(k) = \gamma_X(-k)$ with $k \in \mathbb{N}$. The correlation parameter is given by

$$\rho(k) = \frac{1}{2}[(k+1)^{2H} + (k-1)^{2H} - 2k^{2H}]. \tag{3.3}$$

We can see that for $H = 1$ the correlations are equal to 1 for any lag k, while for $H > 1$ diverges to infinity. In Figure 3.1 we plot the correlation as a function of k for three different values of the parameter H. For $H = 0.5$ the correlation is identically zero, for $H = 0.7$ is observed positive correlations with slow decay as k increases. Conversely, for $H = 0.2$ the correlations are negative and decay more rapidly.

Furthermore the asymptotic behavior of the autocovariance $\gamma_X(k)$ follows by Taylor expansion. Indeed, taking $g(x) = (1+x)^{2H} - 2 + (1-x)^{2H}$, the correlation function of the increments can be rewritten as: $\gamma_X(k) = \sigma^2 k^{2H} g(k^{-1})$ with $H \in (0,1), H \neq 0.5$, and by Taylor expansion at the

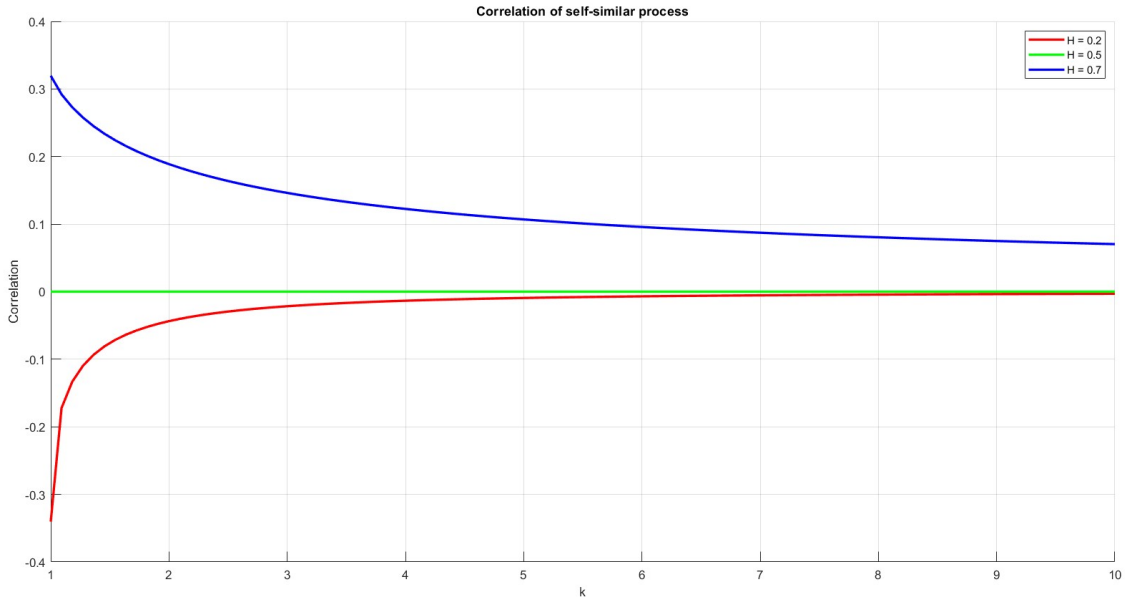

Figure 3.1: The Correlation (3.3) of a self-similar process for three different values of H, namely $H = 0.2$ in red, $H = 0.5$ in green and $H = 0.7$ in blue.

origin of $g(x)$

$$\begin{aligned} g(x) =& g(0) + g'(0)(x-0) + \frac{1}{2}g''(0)(x-0)^2 + \cdots \\ =& \cancel{2Hx} - \cancel{2Hx} + \frac{1}{2}[H(2H-1) + H(2H-1)]x^2 + \cdots \\ =& H(2H-1)x^2 + \cdots, \end{aligned}$$

therefore as k tends to infinity, $\gamma_X(k)$ is asymptotically equivalent to $\sigma^2 H(2H-1)k^{2H-2}$

$$\gamma_X(k) \sim \sigma^2 2H(2H-1)k^{2H-2}.$$

Accordingly with the Theorem 3.1.1, we can identify the slowly varying function $L_\gamma = \sigma^2 2H(2H-1)$ and the memory parameter $d = H - \frac{1}{2}$. For $H \in (\frac{1}{2}, 1)$ covariance decay to zero so slowly that

$$\sum_{k=-\infty}^{+\infty} \gamma_X(k) = \infty,$$

hence that the process X_t has long memory if $\frac{1}{2} < H < 1$.
For $H = \frac{1}{2}$, all values of $\gamma_X(k)$ are zero except when $k = 0$, so that $(X_t)_{t\in\mathbb{Z}}$ is an uncorrelated sequence.
For $H \in \left(0; \frac{1}{2}\right)$, the exponent $2H - 2 > 1$ then $\gamma_X(k)$ is summable, the sum can be split into three

terms, changing the indices $k-1$ and $k+1$ with k the first two sums are identical to the third,

$$\sum_{k=-\infty}^{\infty} \left[|k-1|^{2H} + |k+1|^{2H} - 2|k|^{2H}\right]$$

$$= \sum_{k=-\infty}^{\infty} |k-1|^{2H} + \sum_{k=-\infty}^{\infty} |k+1|^{2H} - 2\sum_{k=-\infty}^{\infty} |k|^{2H}$$

$$= \sum_{k=-\infty}^{\infty} |k|^{2H} + \sum_{k=-\infty}^{\infty} |k|^{2H} - 2\sum_{k=-\infty}^{\infty} |k|^{2H} = 0.$$

The condition *(iv)* of the Corollary 3.1.1 is satisfied, in other words $H \in \left(0, \frac{1}{2}\right)$ implies antipersistence.
It results that the sample mean of the increments $\tilde{X} = \frac{1}{n}\sum_{i=1}^{n} X_i$, because of the self-similarity property, is equivalent in distribution to $n^{H-1}(Y_1 - Y_0)$, and consequently its variance is

$$Var(\tilde{X}) = \sigma^2 n^{2H-2}.$$

For $H = \frac{1}{2}$, we get the classical result $Var(\tilde{X}) = \sigma^2 n^{-1}$.
The parameter H is known as *Hurst* exponent, and it is a measure of the long range dependence in a time series, since for H-SSSI processes, the memory parameter is given by $d = H - \frac{1}{2}$.
The dependence structure can be summarized as follows:

- $0.5 < H < 1$ indicates a high persistence or long range dependence.
- $H = 0.5$ absence of past dependence (short range dependence).
- $0 < H < 0.5$ indicates antipersistence.

A well-known representative of self-similar processes is the fractional Brownian motion, which is a generalization of the Brownian motion (2.7). This process will be introduced in the next chapter. In the remainder of this chapter, we address the estimation methods for the Hurst exponent in order to characterize the long range dependence of the analyzed time series. Specifically, these methods are applied to the spot price time series.

3.2 Estimation methods

In this section, we provide an overview of the most commonly used methods for estimating the Hurst coefficient. We begin with the R/S analysis, followed by the variance plot estimation, and conclude with a more in-depth discussion of advanced estimation techniques.

3.2.1 R/S analysis

The R/S analysis was originally created by the British hydrologist Harold Edwin Hurst [35] while he was studying the problem of water storage on the Nile River. Later, it was popularized by Benoit Mandelbrot especially in the area of long term dependence analysis of the stock market. The method involves calculating the rescaled range (R/S) as the ratio between the range and the standard deviation within a window of data. This is done across various window sizes to assess the scaling behavior of the time series. The range is the difference between the maximum and minimum values observed within the considered window, while the standard deviation quantifies the variability of the data points. The R/S ratio is indicative of the long term dependence, based on the scaling behavior of the rescaled range statistic for stochastic processes with stationary increments $(X_n)_{n\in\mathbb{N}}$. In particular, for processes exhibiting long-range dependence, the ratio between the centered cumulative range $R(k)$ and the standard deviation $S(k)$, for large n, in a window of length k, grows asymptotically with the time horizon according to a power law:

$$\frac{R(k)}{S(k)} \sim Ck^H, \qquad k \to \infty, \tag{3.4}$$

where H is the Hurst exponent and C is a positive constant not depending on k. Let us analyze this technique in detail; let $X_1, \cdots, X_N$ be a realization of the process of the increments. For a fixed block of size k, we divide the time series into $M = \lfloor \frac{N}{k} \rfloor$ non overlapping sub-series indexed by $m = 1, \cdots, M$ each of length k. Denote by $X_{m,i} = 1, ..., k$, the observations in the m-th block. For each block we compute the mean $\bar{X}_m$ and the standard deviation S_m;

$$\bar{X}_m = \frac{1}{k}\sum_{i=1}^{k} X_{m,i}, \quad S_m = \sqrt{\frac{1}{k}\sum_{i=1}^{k}\left(X_{m,i} - \bar{X}_m\right)^2}$$

compute the mean adjusted series, by subtracting the sample mean from the data.

$$Y_{m,i} = X_{m,i} - \bar{X}_m, \quad i = 1, \cdots, k \quad m = 1, \cdots, M$$

Calculate cumulative deviate series.

$$Z_{m,i} = \sum_{j=1}^{i} Y_{m,j} \quad i = 1, \cdots, k$$

Calculate the range series

$$R_m = \max_{1\le i\le k} Z_{m,i} \; - \; \min_{1\le i\le k} Z_{m,i}.$$

Finally, the rescaled range series R_m/S_m and its mean across all sub-series of length k, is given by

$$(R/S)_k = \left\lfloor \frac{k}{N} \right\rfloor \sum_{m=1}^{\lfloor \frac{N}{k} \rfloor} \frac{R_m}{S_m}.$$

In practice, to use all data for calculation, the value of N should preferably be divisible by k. We can plot the $(R/S)_k$ statistic against k in log-log scale.

$$\log(R/S)_k = c + H \log k$$

where the slope of the regression line provides an estimate of the Hurst exponent. If the process is a white noise then the plot is roughly a straight line with slope 0.5. If the process is persistent then the slope is greater than 0.5; if it is antipersistent the slope is less than 0.5. For $k < 10$, $(R/S)_k$ is not accurate, thus the block size k should be at least 10 for reliable estimation. For further details on the R/S methodology, the interested reader is referred to [13, 65].

3.2.2 Variance-time plots

Estimating the Hurst parameter H using variance-time plots is a method based on the behavior of the variance of aggregated time series data, this procedure is also known as aggregated variance method. While the R/S analysis focuses on the scaling behavior of the range of cumulative deviations, the variance-time method exploits the power-law decay of the variance of aggregated observations. Both approaches ultimately rely on the self-similarity property of long-memory processes and yield consistent estimators of the Hurst parameter. In details given a stochastic process $(X_n)_{n\in\mathbb{N}}$ that follows the assumptions of self-similarity and stationarity, we saw that the variance of its sample mean is given by

$$Var(\tilde{X}) = \sigma^2 n^{2H-2} \tag{3.5}$$

where $\tilde{X} = \frac{1}{n}\sum_{i=1}^{n} X_i$ is the sample mean over n observations and σ^2 the variance of X_i. These considerations on the power law decay on the variance of the aggregated series allow to introduce the following procedure to estimate H. Given a sample $X_1, \cdots X_N$ the aggregation process involves dividing it into non-overlapping blocks and calculating the average value within each block, as before we divide the sample of dimension N into m_k different blocks of length k, with $2 \leq k \leq \lfloor \frac{N}{2} \rfloor$, we compute the sample mean for each block

$$\tilde{X}_j(k) = \frac{1}{k}\sum_{i=1}^{k} X_{j,i}, \qquad j = 1, \ldots, m_k.$$

and their overall mean

$$\bar{X}(k) = \frac{1}{m_k}\sum_{j=1}^{m_k} \tilde{X}_j(k)$$

For each k, compute the sample variance of the sample means $\tilde{X}_1(k), \ldots, \tilde{X}_{m_k}(k)$

$$s^2(k) = \frac{1}{m_k - 1} \sum_{j=1}^{m_k} \left(\tilde{X}_j(k) - \bar{X}(k) \right)^2 .$$

Plotting $\log s^2(k)$ against $\log(k)$, in what is called a *variance plot*, and fitting a simple least squares line through the resulting points in the plane, we expect to observe the points scattered around a straight line with a negative slope $S = 2H - 2$ for large values of k. Consequently, the Hurst parameter can be estimated as

$$\hat{H} = 1 + \frac{1}{2} S.$$

In the case of uncorrelated observations (e.g. white noise), the slope is equal to -1 corresponding to $H = \frac{1}{2}$. The variance plot estimator is straightforward to implement and performs well when applied to large datasets, providing reliable estimates of the Hurst exponent. However, it shares some of the limitations of the R/S analysis. In particular, there is no formal criterion for selecting the aggregation sizes k, which are often chosen heuristically. Moreover, the method requires the original process to be stationary. For short series (e.g., a few hundred observations), the variance plot tends to produce biased estimates, to obtain ones reliable ones generally requires several thousand observations; otherwise, bias-correction techniques should be employed.

From a practical viewpoint, the variance–time method is computationally simpler and numerically more stable, but it requires the underlying process to be stationary and typically performs well only for sufficiently large datasets. Conversely, the R/S analysis can be applied more broadly, but it lacks robustness with respect to short-range dependence and deterministic trends, often leading to spurious detection of long-range dependence. For these reasons, both methods are often used together, and their results are compared to assess the reliability of the estimated Hurst parameter.

A more detailed discussion of these two methods can be found in [14], while a comparative analysis between them and other estimators of the Hurst exponent, such as the Whittle method, which is not discussed here, is provided in [75].

3.2.3 Detrended Fluctuation Analysis

The rescaled range (R/S) analysis and the variance plot are classical techniques for the investigation of scaling properties and long-range dependence in time series. However, both methods are intrinsically formulated under stationarity assumptions and are known to be highly sensitive to the presence of deterministic trends or low-frequency nonstationarities. When such components are present, these approaches may lead to biased or even spurious estimates of the scaling exponent, making their interpretation problematic in empirical applications.

In order to address these limitations, we introduce the *Detrended Fluctuation Analysis* (DFA), a method proposed by Peng et al. [64] and later systematically developed in [40]. DFA was specifically designed to investigate the scaling properties of time series that may exhibit nonstationary behavior due to deterministic components, while preserving the statistical structure of the under-

lying stochastic fluctuations.

Furthermore DFA provides a natural framework for assessing the validity of monofractal scaling assumptions[1] . In a monofractal setting, the scaling properties of a time series are governed by a single exponent that remains valid across a wide range of temporal scales. The emergence of scale-dependent behavior or multiple scaling regimes signals a breakdown of this assumption and suggests that a single global scaling parameter is insufficient to describe the underlying dynamics.

In the following, we present the DFA algorithm and introduce the quantities required for the estimation of the associated scaling exponent.

Let $\{X_t\}_{t=1}^N$ denote a real-valued time series with finite mean

$$\bar{X} = \frac{1}{N}\sum_{t=1}^{N} X_t.$$

we define the integrated profile

$$Y(k) = \sum_{t=1}^{k} \big(X_t - \bar{X}\big), \qquad k = 1, \dots, N. \tag{3.6}$$

then we fix a scale (window length) $s \in \mathbb{N},\ s < N$ and partition the profile $\{Y(k)\}$ into

$$N_s = \left\lfloor \frac{N}{s} \right\rfloor$$

non-overlapping segments of equal length s. For each segment $\nu = 1, \dots, N_s$, fit a polynomial trend of order m to the data in that segment,

$$Y_\nu(k) \approx P_\nu^{(m)}(k), \qquad k = 1, \dots, s,$$

where $P_\nu^{(m)}$ denotes the least-squares polynomial approximation. The detrended profile in segment ν is then given by

$$\widetilde{Y}_\nu(k) = Y\big((\nu-1)s + k\big) - P_\nu^{(m)}(k).$$

Define the fluctuation function at scale s as

$$F(s) = \left(\frac{1}{N_s} \sum_{\nu=1}^{N_s} \frac{1}{s} \sum_{k=1}^{s} \widetilde{Y}_\nu(k)^2 \right)^{1/2}. \tag{3.7}$$

The scaling behavior of the series is assessed by analyzing the dependence of $F(s)$ on the scale s. If a power-law relationship holds,

$$F(s) \sim s^\alpha, \qquad s \to \infty, \tag{3.8}$$

[1] Monofractal scaling assumption means that the process is governed by a single Hurst exponent H that determines its scaling behavior.

then the exponent α is referred to as the *DFA scaling exponent*.

In empirical applications, however, the log–log plot of $F(s)$ against s often deviates from a single linear behavior over the entire range of scales. The presence of multiple linear regimes, or the absence of scaling at short and intermediate scales, indicates that different dynamical mechanisms dominate at different time horizons. In such cases, the interpretation of α as a unique global parameter becomes questionable, and the analysis must explicitly account for scale-dependent behavior.

In the following, DFA is applied to the deseasonalized electricity price series. Particular attention is devoted to the identification of stable scaling regimes and to the comparison of the resulting estimates with those obtained via R/S analysis and the variance plot.

3.3 Spot electricity time series in Italian market

We analyze data from the Italian electricity market, where spot prices are quoted on an hourly basis, whereas forward contracts can be traded continuously over the trading period. This differs from other commodity markets, where liquid trading is typically observed in both the underlying and derivative instruments. Our goal is to apply the methods introduced in the previous sections in order to assess the nature of the memory properties exhibited by electricity market time series.

Several challenges arise in this context. First, different studies adopt different data granularity: some estimate long-memory parameters from hourly time series (the finest available resolution for Italian markets)[2], while others use aggregated series, such as daily averages. The choice of the granularity is not neutral, it depends on the research objective. In particular, the estimation methods considered, excluding DFA, require the assumption that the analyzed time series is both stationary and self-similar, which is a fundamental prerequisite for obtaining a meaningful estimate of the self-similarity parameter H. This raises the question of whether long memory should be investigated in the hourly series, the daily series, or both.

A second issue concerns seasonality, discussed in Section 1.1, the presence of deterministic, time-dependent components in the series can distort long-memory estimation. Since the functional form of this seasonal component is unknown, it is not possible to completely rule out its influence on the results.

Finally, the memory parameter may not be constant over time: certain periods may exhibit markedly different persistence or antipersistence properties compared to others.

In the first part of this section, we present and implement several approaches to mitigate seasonality. We then perform the estimation of the long-memory parameters and compare our results with those reported in the literature.

[2]Starting from October 1, 2025, prices in the Italian day-ahead electricity market (MGP) have been quoted on a 15-minute basis, in line with the transition of the European Single Day-Ahead Coupling (SDAC) to 15-minute Market Time Units (MTUs).

3.3.1 Treatment of Seasonality and peaks

A well-documented stylized fact of electricity market time series is the presence of strong seasonal patterns. These seasonalities can be regarded as deterministic, time-dependent components of the process and may arise at multiple frequencies, such as annual, monthly, weekly, or daily cycles. In the literature, several approaches have been proposed to address seasonality and to isolate the stochastic component of the series.

A first approach relies on the use of *dummy variables*, as applied in [32]. The idea is to estimate and subsequently remove a recurring seasonal pattern by means of fixed-effect indicators.

In the case of weekly seasonality in an hourly time series spanning several years, the procedure consists in computing, over the entire dataset, the average value associated with each hour of the week. Specifically, each seasonal effect is estimated by averaging all observations corresponding to the same hour and weekday across different weeks. For instance, the first seasonal coefficient is obtained by averaging all observations corresponding to the first hour of Sunday in the sample. Repeating this procedure for all hours yields a seasonal profile consisting of 168 values, which represents the typical weekly pattern of the series.

The original series is then deseasonalized by subtracting, from each observation, the corresponding value of the estimated seasonal profile and adding back the overall mean of the series. This adjustment ensures that the mean level of the data is preserved after deseasonalization. In this way, the weekly seasonal component is effectively removed from the time series.

Figure 3.2 shows the weekly seasonality pattern computed for Italian electricity market using a dataset spanning from January 2014 to December 2023. The weekly path starts on Sunday. During weekdays the pattern is similar across days, in particular the price typically peaks around noon, coinciding with higher electricity demand, then shows a small dip shortly after, possibly because many people take a lunch break. A second peak occurs around 8:00 P.M., when electricity demand increases again; this is partly due to the fact that solar power generation drops to zero after sunset, reducing overall supply. In contrast, weekends follow a different pattern: most companies are closed, and a large portion of the population is not working, leading to a different demand structure compared to weekdays. Nevertheless, even during weekends, a noticeable peak is observed around 8:00 P.M., again coinciding with the end of photovoltaic production for the day.

This method is straightforward to implement and does not require specifying a functional form for the seasonal pattern, making it flexible in applications. However, it also has limitations. It requires a sufficiently large sample covering multiple complete seasonal cycles, as the estimation of seasonal means from only a few cycles may be unreliable. Moreover, it implicitly assumes that the seasonal pattern remains constant over time, an assumption that may be violated in electricity markets, where structural changes or evolving demand–supply conditions can alter seasonal effects. In such cases, the dummy-variable approach may fail to fully remove the seasonal component.

Another common approach to remove seasonality in time series is *harmonic regression*, as described in [19] that we use for the yearly seasonality. The method is based on the idea that a seasonal pattern can be expressed as a finite sum of sinusoidal components at specific frequencies.

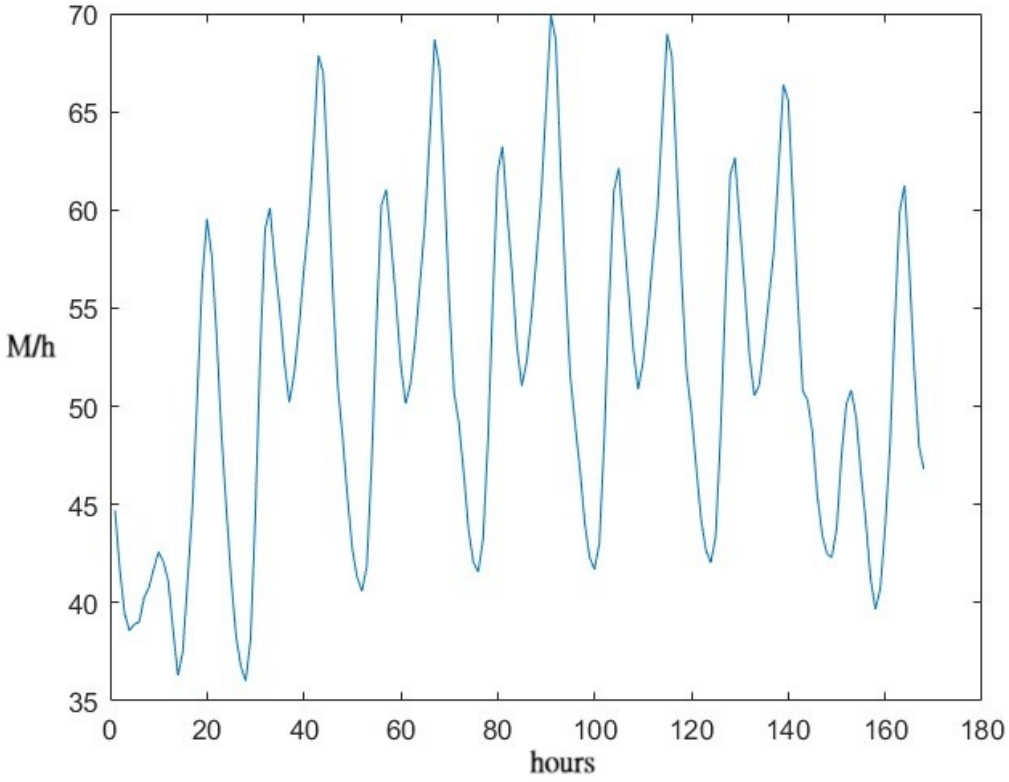

Figure 3.2: Weekly seasonality pattern.

In practice, the procedure consists in identifying the significant frequencies of the observed process, sampled at discrete times $(X(t_i))_{i=1,\dots,l}$, and representing the seasonal component as a linear combination of cosine and sine terms, plus a residual noise term.

Let f_k, $k = 1, \dots, n$, denote the significant frequencies for the dataset. The seasonal component can then be approximated as

$$S(t_i) = \sum_{k=1}^{n} A_k \cos(2\pi f_k t_i) + B_k \sin(2\pi f_k t_i) + \epsilon(t_i),$$

where A_k and B_k are the amplitudes associated with the cosine and sine waves at frequency f_k, respectively, and $\epsilon(t_i)$ is a residual term capturing the stochastic component of the process.

Once the coefficients A_k and B_k are estimated—typically via least squares—the fitted seasonal component

$$\hat{S}(t_i) = \sum_{k=1}^{n} \hat{A}_k \cos(2\pi f_k t_i) + \hat{B}_k \sin(2\pi f_k t_i), \tag{3.9}$$

is subtracted from the original series to obtain a deseasonalized version. This approach is particularly effective when the seasonal pattern is periodic and can be well approximated by a number of harmonics. In our case, we identify the significant frequencies as the yearly ones and apply this method using four harmonic functions in the sum (3.9). Figure 3.3 shows both the original data pattern and the fitted harmonic functions for the dataset. The harmonic components exhibit a sea-

sonal profile consistent with electricity prices: the maximum occurs in the winter period, while the minimum lies between spring and summer, reflecting the seasonal variation in demand and supply. A peculiar deviation appears at the beginning of 2020, corresponding to the onset of the COVID-19 pandemic. In many studies, harmonic analysis is employed to capture the different components of seasonality. However, the main challenge lies in identifying all significant frequencies, which is not always feasible.

Another important issue in electricity price series is the occurrence of spikes, often due to unexpected power plant outages or some political events (such as the outbreak of wars, increases in duties, and similar shocks). If we aim to estimate the Hurst exponent, it is crucial that the time series is approximately Gaussian, which requires removing such extreme values. Moreover, in the model introduced later in Section 6, we do not explicitly incorporate price spikes. For models that account for spikes, we refer to [15], where the authors introduce a Poisson-distributed jump component with time-dependent intensity to capture sudden price changes, to [32], who use Hawkes processes combined with fractional dynamics, and to [20], who model electricity prices with mean reversion, seasonality, and jump components calibrated to the UK market.

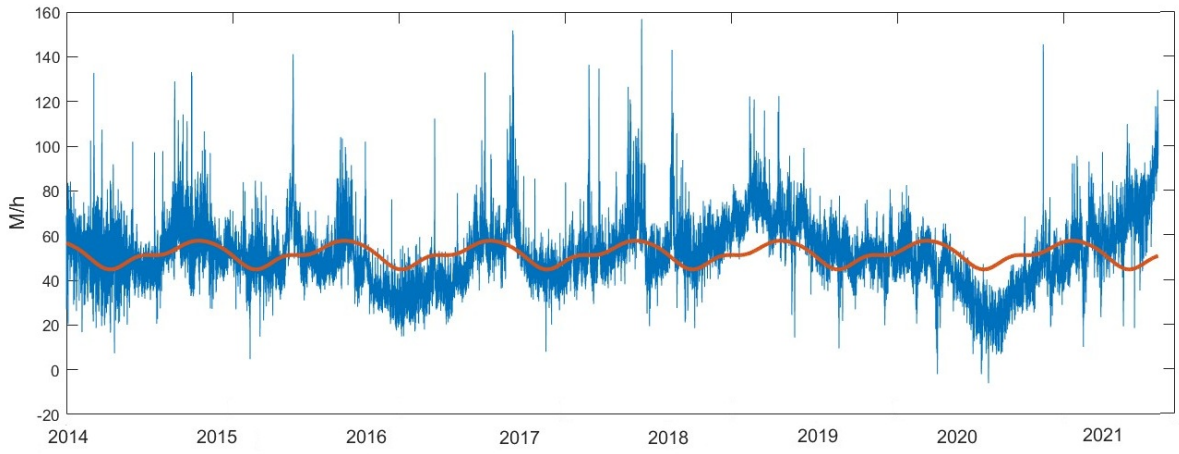

Figure 3.3: Yearly seasonality computed by harmonic function

To eliminate peaks, we adopt the following procedure: a spike is identified when its value deviates by more than three standard deviations from the mean. In such cases, the spike is replaced with the average between the two immediately neighboring values (the preceding and the following).

Figure 3.4 shows the electricity price data after the deseasonalization procedure and spike removal. In particular, peaks are eliminated as described above, followed by the application of weekly and yearly deseasonalization, as previously explained, and subsequent rescaling of the data by subtracting the mean. This results in a dataset centered around the origin. Our time window spans from early 2014 to the end of June 2021, and this processed dataset will be used for the subsequent analysis, in particular our aim will be understand the long term behavior of this time series.

Other methods presented in the literature to deseasonalized data include the Fast Fourier Trans-

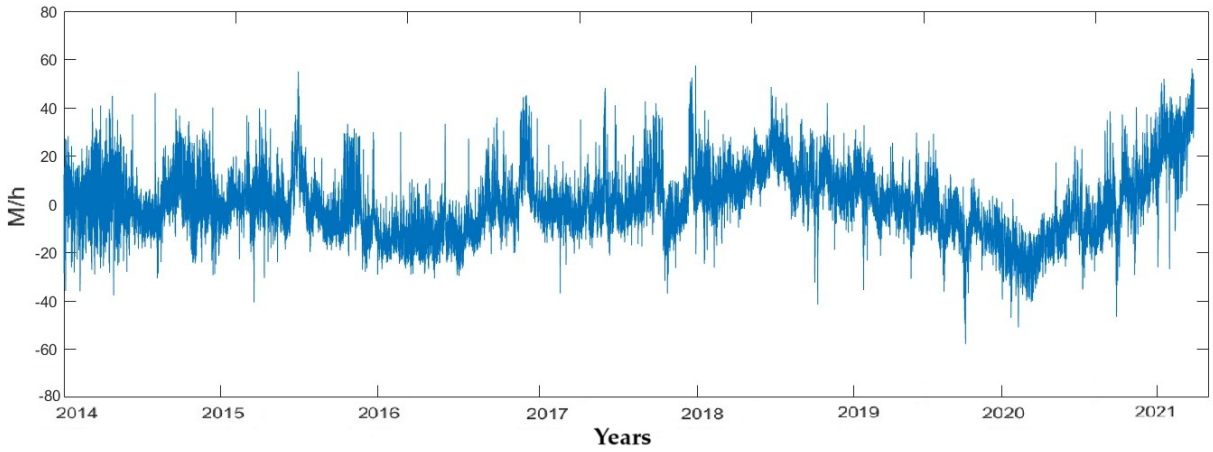

Figure 3.4: Deseasonalized Italian electricity prices

form (FFT). This technique automatically reveals, in the frequency domain, the periodic components of the series, which can then be removed by reconstructing the seasonal signal from the significant frequencies and subtracting it from the original data. For a detailed discussion, see [19], or [23], where this approach is implemented within the Iterative Filtering framework.

Lastly, many authors prefer to work with daily data. To obtain such data, it is necessary to compute the average over the 24 hourly values within each day. Figure 3.5 illustrates the daily pattern of the dataset under consideration. This daily averaging is performed after applying the aforementioned procedures for removing seasonal components and spikes. Compared to the hourly data, the daily series appears significantly smoother, as the intraday fluctuations have been averaged out. In this dataset, the number of daily observations is 2738, corresponding to the total number of days included.

A natural question that arises is whether estimation methods based on the self-similarity properties of the process remain valid when applied to the time-averaged series. In Section 5.1, we address this issue by analyzing the properties of a stochastic process defined as the time-averaged version of a self-similar process, specifically the fractional Brownian motion (fBm).

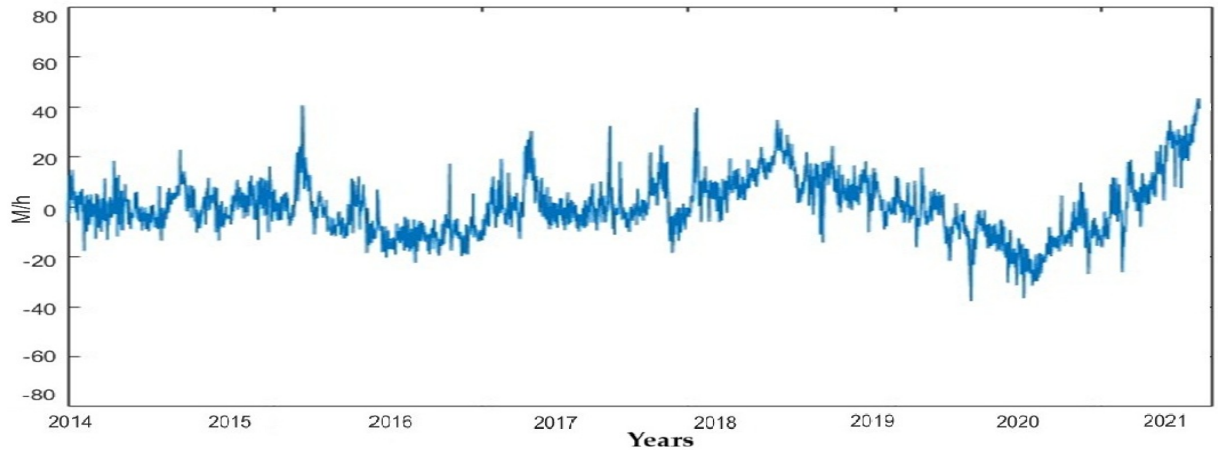

Figure 3.5: Daily path of electricity prices

3.3.2 Hurst exponent in electricity prices

Our aim is to assess whether it is appropriate to describe the stochastic component of the Italian electricity spot price by processes that exhibit some dependence form the past. In particular, we focus on estimating the Hurst exponent in the analyzed time series in order to develop a model that incorporates fractional dynamics for describing the spot price, and consequently, the forward prices.

In this section we present the results obtained through rescaled range R/S analysis and the variance plot method applied to the considered dataset. The dataset consists of 65712 different hourly spot prices, covering the period from the first of January 2014 to the 30th of June 2021 (a total of 2738 days), and was retrieved from the official website of the electricity market operator GEM (Gestore dei Mercati Elettrici S.p.A.).

After preprocessing the data by removing spikes and the deterministic seasonal component, as described above, our first tool for assessing the presence of long-range dependence is the empirical autocorrelation function. In particular, we seek to verify whether it exhibits the decay behavior predicted by the theoretical relation (3.3) for a fixed Hurst parameter H. Given the time series $\{X_i\}_{i=1}^n$, we used the following estimator (as found in [19]) to compute the autocorrelation function at lag k, with $k \leq n-2$:

$$\bar{\rho}(k) = \frac{1}{n\bar{s}} \sum_{i=1}^{n-k} (X_i - \bar{X})(X_{i+k} - \bar{X}), \tag{3.10}$$

where n is the sample size, $\bar{X} = \frac{1}{n}\sum_{i=1}^n X_i$ the sample mean, and

$$\bar{s} = \frac{1}{n-1} \sum_{i=1}^{n} (X_i - \bar{X})^2$$

is the sample variance. This estimator provides a first insight into the memory structure of the process and serves as a preliminary diagnostic before applying more sophisticated Hurst estimation techniques. Figure 3.6 shows the autocorrelation function as a function of the lag. From the graph, it is difficult to draw any definitive conclusion about the behavior of the time series. Initially, a slow decay is observed, which might suggest persistence in the series, but later there is a shift to negative correlation, providing an indication of antipersistence.

These observations suggest that a single Hurst exponent may be inadequate to fully characterize the dynamics of the time series. These empirical results suggest that multiple fractional processes, with Hurst parameters both below and above one half, are needed to adequately describe price dynamics. We now employ different estimation techniques to validate and reinforce our analysis.

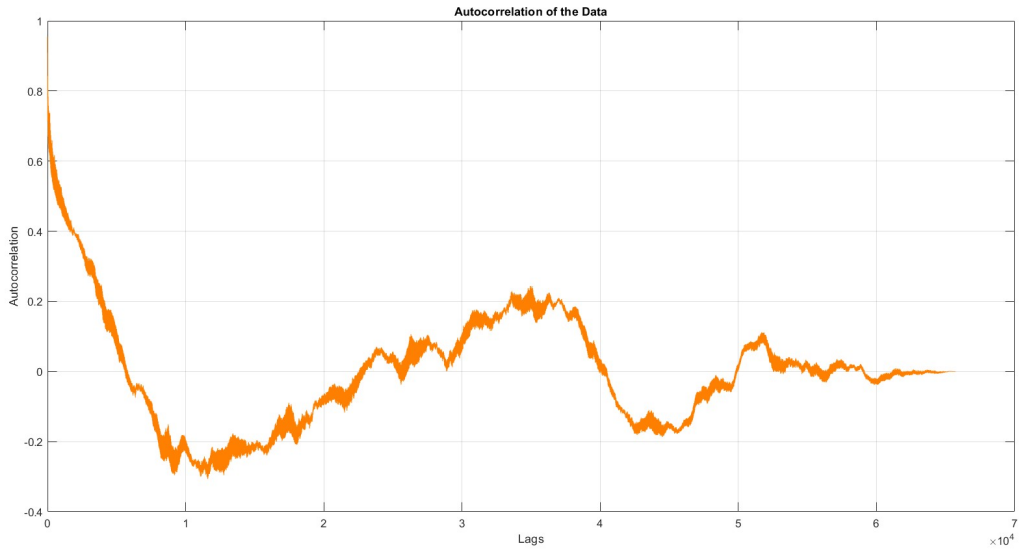

Figure 3.6: Autocorrelation of the hourly spot prices

3.3.3 Results in the estimation techniques

In this section, we apply the previously described methods to the hourly deseasonalized time series. All numerical implementations are carried out in MATLAB, and the correctness of the codes has been carefully verified by testing them on time series with known behavior, namely white noise ($H = 1/2$), antipersistent processes ($H < 1/2$), and persistent processes ($H > 1/2$). In all cases, the estimators successfully recover the input value of the Hurst exponent.

The local R/S analysis performed over different scale intervals yields Hurst exponent estimates predominantly below 0.5, indicating antipersistent behavior across a wide range of temporal scales. However, the estimated exponents exhibit a clear dependence on the scale, varying significantly from one scale interval to another and failing to stabilize around a common value. The results are reported in the Table 3.1, we can note that also if there is antipersistent behavior in all the scales, the estimate for H does not remain constant.

values of k	H_{RS}
230	0.28
304	0.29
376	0.32
497	0.28
658	0.29
811	0.34
1001	0.28

Table 3.1: Scale-dependent R/S estimates computed on the deseasonalized price increments.

The pronounced scale dependence of the estimated exponents is incompatible with a description based on a single Hurst exponent characterizing the diffusion structure of the time series. To further substantiate this conclusion, we also apply the variance plot estimator to the deseasonalized price

series in order to investigate the temporal scaling of the variance, as described by (3.5). Since the variance plot is theoretically justified under stationarity assumptions, the analysis is performed on the increments of the deseasonalized series[3]. To assess whether the scaling behavior remains invariant over time, we fix the aggregation scale to $k = 1000$ and divide the dataset into three non-overlapping subperiods of equal length. Table 3.2 reports the corresponding estimates of the Hurst exponent $\hat{H}$ in each subperiod.

Subperiod	1	2	3
$\hat{H}$	0.11	0.82	0.43

Table 3.2: Variance plot estimates of H computed on three non-overlapping subperiods.

The resulting estimates exhibit substantial variability across time windows, with markedly different values of H obtained for the three parts of the examined dataset. Such a dispersion cannot be reconciled with a time-invariant monofractal description, which would require a single scaling exponent governing the dependence structure independently of the observation window. Rather, these results indicate that the scaling properties are not temporally stable even when the aggregation scale is kept fixed.

In order to provide further evidence that the analyzed time series may not be fully described by a single Hurst parameter, we now apply the Detrended Fluctuation Analysis (DFA). Applying DFA to the deseasonalized price series reveals a pronounced scale-dependent behavior. When the analysis is performed over short and intermediate temporal scales, the estimated scaling exponent is found to be $\alpha \approx 0.0742$, a value close to zero. This indicates that, on these scales, a clear power-law behavior cannot be identified. Such a result suggests that the dynamics at shorter horizons are dominated by non-scaling components, such as residual deterministic effects that prevent the emergence of long-range correlations.

In contrast, restricting the DFA to sufficiently large temporal scales yields a markedly different estimate, namely $\alpha \approx 0.4891$. This value is close to $\alpha = 1/2$, corresponding to short-memory or weakly correlated dynamics. The discrepancy between these estimates points to the presence of distinct scaling regimes across time horizons. This evidence further supports the view that the scaling behavior of the series cannot be characterized by a single exponent.

Taken together, the classical scaling estimators do not support the existence of a unique Hurst exponent valid across temporal scales. The dependence of the estimates on both the method and the regression range indicates that the monofractal assumption is not satisfied. Rather, the empirical evidence suggests heterogeneous scaling properties, motivating the adoption of models with multiple stochastic components.

Before concluding this chapter, we point out an additional feature of these time series. When the estimation methods are applied to daily averaged prices instead of hourly data, significantly different Hurst exponent estimates are obtained. This behavior is not surprising, as the averaging

[3]The deseasonalized process itself is generally non-stationary, its increments are expected to form a stationary sequence, consistently with the properties of fractional Gaussian noise associated with fractional Brownian motion.

procedure alters the covariance structure of the process, making the direct application of the original estimation techniques inappropriate. In the next chapters, we introduce fractional Brownian motion, a process exhibiting long-range dependence, and discuss how the covariance structure and the corresponding estimation methods differ from those of its normalized integrated average.

Chapter 4

Fractional Brownian motion

Fractional Brownian motion (fBm) is a stochastic process that significantly differs from standard Brownian motion, semimartingales, and other classical processes commonly used in probability theory. As a centered Gaussian process, fBm is characterized by stationary increments and exhibits either long-range or antipersistent features that stand in sharp contrast to the memoryless properties of martingales and Markov processes.

The process was first introduced by Kolmogorov in 1940 [41] who was studying spiral curves in Hilbert space, under the name Wiener Helix. The term fractional Brownian motion was later coined by Mandelbrot and Van Ness who recognized the relevance of this random process and, in his seminal work [50] derived many important properties. A distinctive feature of fractional Brownian motion is that the interdependence between its increments extends over arbitrarily long time spans. In contrast, much of the classical theory of stochastic processes has focused on sequences of independent random variables, on Markov processes, and on other random functions with the property that samples taken sufficiently far apart are independent or nearly independent. Empirical evidence from various random phenomena, however, often reveals a strong dependence even between observations that are widely separated in time. Why the name "fractional Brownian motion"? This is because the process can be represented as an integral with respect to Brownian motion. In fact Mandelbrot and Van Ness also provided a stochastic integral representation of fBm in terms of standard Brownian motion. See [49] for a summary of their work.

Under the usual assumptions of finite variance and independent and identically distributed observations, the R/S statistic should grow like $n^{\frac{1}{2}}$, where n is the sample size. The Nile data, however, indicated a growth of n^H, where $1/2 < H < 1$. The growth $n^{\frac{1}{2}}$ is typically associated with random walk, so n^H, and $H \neq \frac{1}{2}$ must correspond to something else. This is why Mandelbrot suspected that a process like fractional Brownian motion B_t^H may perhaps be relevant in this framework since, while the standard deviation of Brownian motion (2.7) at time t is $t^{1/2}$, that of fractional Brownian motion at time t is t^H, where $0 < H < 1$. The parameter H, known as the Hurst parameter in honor of hydrologist Hurst and adopted by Mandelbrot, has since become standard in this context.

Fractional Brownian motion has attracted considerable attention due to its ability to model both

short-range and long-range dependent phenomena, making it relevant in various applied fields such as physics, biology, and finance. The aim of this chapter is to provide an introduction to fBm and to present some of its key theoretical properties. For a comprehensive treatment of this topic, we refer the reader to [16], [51], [62], and [4].

In the final section of the chapter, we introduce the fundamental martingale constructed by Norros, Valkeila, and Virtamo [60], which will play a central role in our model for the electricity market.

4.1 Fractional Brownian motion

The fractional Brownian motion (fBm) $B = \{B_t, t \in [0,T]\}$ is an extension of the Brownian motion, in which the increments may be correlated. From the mathematical point of view, it differs from classical Brownian motion because it is neither Markovian nor a semimartingale.

Definition 4.1. *(Fractional Brownian motion)*
The fractional Brownian motion (fBm) with Hurst parameter H is defined as a centered Gaussian process $B^H = \{B_t^H, t \in [0,T]\}$ with stationary increments and covariance function given by:

$$\mathbb{E}(B_t^H B_s^H) = \frac{1}{2}(t^{2H} + s^{2H} - |t-s|^{2H}) \tag{4.1}$$

for some $H \in (0,1)$ called the Hurst parameter, and when $H = \frac{1}{2}$, fBm reduces to standard Brownian motion.

From the previous definition it is possible to derive several basic properties of fBm. For example, if we compute the correlation between two increments, it is different from zero. Consider $t > s \geq u > r$

$$\begin{aligned} Cov[(B_t^H - B_s^H)(B_u^H - B_r^H)] &= E[(B_t^H - B_s^H)(B_u^H - B_r^H)] \\ &= E(B_t^H B_u^H) - E(B_t^H B_r^H) - E(B_s^H B_u^H) + E(B_s^H B_r^H) \\ &= \frac{1}{2}(-(t-u)^{2H} + (t-r)^{2H} + (s-u)^{2H} - (s-r)^{2H}). \end{aligned}$$

If $H = \frac{1}{2}$, the above quantity is equal to zero, which is consistent with the fact that the Brownian motion has independent increments. If $H \neq \frac{1}{2}$, we may write

$$E[(B_t^H - B_s^H)(B_u^H - B_r^H)] = H(2H-1)\int_r^u \left(\int_s^t (\epsilon - \theta)^{2H-2} d\epsilon \right) d\theta.$$

Considering the increments over equally spaced intervals of length $h > 0$,

$$X_n = B_{nh}^H - B_{(n-1)h}^H, \quad n \geq 1,$$

and using the covariance function above, the covariance between two increments X_n and X_{n+k} is

$$\mathrm{Cov}(X_n, X_{n+k}) = \frac{h^{2H}}{2}\left[|k+1|^{2H} - 2|k|^{2H} + |k-1|^{2H}\right], \quad k \in \mathbb{Z}.$$

The correlation function is then obtained by normalizing with the variance $Var(X_n) = h^{2H}$ and we obtain the same correlation structure $\rho(k)$ as (3.3). This implies that the properties already established for self-similar processes with stationary increments also apply to fBm. For $H = 1/2$, it corresponds to the standard Brownian motion and $\rho(k) = 0$ for all $k \neq 0$, reflecting the independence of increments. For $H > 1/2$, the correlation is positive and decays hyperbolically as $n \to \infty$, giving rise to long-range dependence, whereas for $H < 1/2$ the correlation is negative, a phenomenon commonly referred to as antipersistence. Another property of the fBm is the Hölder continuity.

Theorem 4.1.1. *Let $H \in (0,1)$ and let $\{B_t^H\}_{t\in[0,T]}$ be a fractional Brownian motion with Hurst parameter H. Then B^H admits a modification whose sample paths are almost surely Hölder continuous of any order $\alpha < H$.*

Proof. Since B^H is Gaussian, all moments of the increments can be computed explicitly. In particular, for any $p > 0$,

$$\mathbb{E}\left[|B_t^H - B_s^H|^p\right] = \mathbb{E}\left[|B_1^H (t-s)^H|^p\right] = \mathbb{E}\left[|B_1^H|^p\right]|(t-s)|^{pH},$$

Let $p > 0$ be such that $pH > 1$; for instance, take $p > \frac{1}{H}$. By the Kolmogorov–Centsov continuity theorem [39].

$$\mathbb{E}\left[|B_t^H - B_s^H|^p\right] \leq K_p\,|t-s|^{1+\beta p},$$

with $\beta = H - \frac{1}{p} > 0$ and $K_p = \mathbb{E}[|Z|^p]$ with $Z \sim \mathcal{N}(0,1)$.

There exists a modification of B^H whose sample paths are almost surely Hölder continuous of any order

$$\alpha < \frac{pH-1}{p}.$$

Since p can be taken arbitrarily large, we can make $\frac{1}{p}$ arbitrarily close to zero, hence obtaining Hölder continuity for every $\alpha < H$. □

It is well known that the fBm is not a semimartingale. This result appears early in the literature (see [47]). This property can be studied from the p-variation (2.10) of the fBm. Using the stationarity and ergodicity of the increment, in [62] is proved that for $H > \frac{1}{2}$ the fBm has zero quadratic variation but infinite total variation, whereas for $H < \frac{1}{2}$ it has infinite quadratic variation and infinite total variation. Since a semimartingale must have finite quadratic variation, and if its quadratic variation is zero it must be of bounded variation, the fBm cannot be a semimartingale for any $H \neq \frac{1}{2}$.

As mentioned in the introduction of this chapter, the name fractional Brownian motion arises

from the fact that it can be expressed in terms of a standard Brownian motion. In the literature, several representation formulas are available. The following formula was introduced by Mandelbrot and Van Ness in [50]:

$$\tilde{B}_t^H = \frac{1}{\Gamma(H+\frac{1}{2})}\left(\int_{-\infty}^{0}((t-s)^{H-\frac{1}{2}}-(-s)^{H-\frac{1}{2}})dB_s + \int_0^t (t-s)^{H-\frac{1}{2}}dB_s\right). \tag{4.2}$$

for all $t > 0$, where B_s denotes a two-sided Brownian motion (i.e., a Brownian motion defined for all real times $t \in \mathbb{R}$) and Γ represents the gamma function. This formula shows that fBm can be represented as a Wiener integral with respect to a Brownian motion. In particular, the process $\tilde{B}_t^H$ has the same variance and covariance structure as the process defined in Definition 4.1 (see [16] for explicit computations of the covariance and variance starting from this representation).
Another useful representation is the Molchan-Golosov [57] that provides a representation of fBm over a finite interval,

$$B_t^H := \int_0^t K_H(t,s)dB_s, \;\; t \geq 0, \tag{4.3}$$

where B_s is a standard Brownian motion and the kernel K_H has two different forms depending on the value of H in particular if $H > \frac{1}{2}$

$$K_H(t,s) = c_H s^{\frac{1}{2}-H}\int_s^t |u-s|^{H-\frac{3}{2}}u^{H-\frac{1}{2}}du \tag{4.4}$$

where $c_H = \left[\frac{H(2H-1)}{\beta\left(2-2H,H-\frac{1}{2}\right)}\right]^{\frac{1}{2}}$, $s < t$, with β Beta function ,
while for $H < \frac{1}{2}$,

$$K_H(t,s) = b_H\left[\left(\frac{t}{s}\right)^{\frac{1}{2}-H}(t-s)^{H-\frac{1}{2}} - \left(H-\frac{1}{2}\right)s^{\frac{1}{2}-H}\int_t^s (u-s)^{H-\frac{1}{2}}u^{H-\frac{3}{2}}du\right], \tag{4.5}$$

with $b_H = \left[\frac{2H}{(1-2H)\beta(1-2H,H+\frac{1}{2})}\right]^{\frac{1}{2}}$, in this representation, the filtration generated by B^H and by the standard Brownian motion coincide. The process in the equation 4.3 is Gaussian with zero mean. Furthermore it can be proven that the covariance of this process coincides with the covariance of the fractional Brownian motion (the computation is provided in [16] and [37]). Moreover, [38] provides an analytical connection between the generalized Molchan–Golosov and Mandelbrot–Van Ness integral transforms of fBm. These two formulas are examples of a more general class of Gaussian processes known as *Volterra processes*, The definition is the following.

Definition 4.2. *Volterra process*
Let $(W_t)_{t\geq 0}$ be a standard Brownian motion defined on a probability space $(\Omega, \mathcal{F}, \mathbb{P})$. A process

$(X_t)_{t\in[0,T]}$ *is said to be* Volterra process *if it admits the representation*

$$X_t = \int_0^t K(t,s)\, dW_s, \quad t \in [0,T], \tag{4.6}$$

where the kernel $K : [0,T] \times [0,T] \to \mathbb{R}$ *satisfies:*

1. $K(t,s) = 0$ *for* $s > t$ *(causality condition),*
2. $K(t,\cdot) \in L^2([0,t])$ *for each* $t \in [0,T]$.

The Molchan-Golosov representation is an example of a Volterra process, if the kernel K is square integrable on $[0,t]$, the stochastic integral is well-defined in the Itô sense. The importance of such representations lies in the fact that they provide explicit constructions of fBm from standard Brownian motion, making them fundamental tools for both theory and applications. In particular, they enable efficient simulation, allow the development of stochastic integration with respect to fBm via the underlying Wiener process, and serve as a bridge to the general framework of Volterra processes.

In general, Volterra processes are neither Markovian nor martingales. Indeed, let $\mathcal{F}_s$ denote the natural filtration generated by the Brownian motion W. For $s < t$, the conditional expectation of (4.6) satisfies

$$\mathbb{E}[X_t \mid \mathcal{F}_s] = \int_0^s K(t,u)\, \mathrm{d}W_u,$$

which coincides with

$$X_s = \int_0^s K(s,u)\, \mathrm{d}W_u$$

only if the kernel $K(t,u)$ does not depend on the upper time variable t. In this special case, the Volterra process reduces to an Itô stochastic integral and therefore defines a martingale. An explicit example of a Volterra process which is a martingale is discussed in Section 4.2.

Moreover, Volterra processes generally fail to satisfy the Markov property. Indeed, the conditional law of X_t given $\mathcal{F}_s$ depends on the full past trajectory through the term $\int_0^s K(t,u)\, \mathrm{d}W_u$, which cannot, in general, be expressed as a function of the current state X_s alone. For a detailed treatment of fractional Brownian motion and its properties, we refer the reader to [51].

4.1.1 Simulation of fractional Brownian motion

In this section we introduce simulation methods for fractional Brownian motion (fBm). Since fBm has dependent increments, simulation is not straightforward. Broadly, methods fall into two classes: *exact* methods, which simulate a discretised fBm as a Gaussian vector with the exact covariance, and *approximate* methods, which approximate fBm by other processes or expansions. We adopt the following framework: simulate a standard fBm of length N at times $t_i = i/N$, $i = 0, \ldots, N-1$.

Mandelbrot–Van Ness (MVN) discretisation. Starting from the MVN representation, one can discretise the integral (4.2) by (truncated) Riemann sums with a lower bound $-a_N < 0$. For $t = 1, \dots, N-1$,

$$\widetilde{B}_H\left(\frac{t}{N}\right) = \frac{V_H^{1/2}}{\Gamma\left(H+\frac{1}{2}\right)} \frac{1}{N^H} \left\{ \sum_{k=-a_N}^{0} \left[(t-k)^{H-\frac{1}{2}} - (-k)^{H-\frac{1}{2}} \right] B_1(k) + \sum_{k=0}^{t} (t-k)^{H-\frac{1}{2}} B_2(k) \right\},$$

where V_H is a normalising constant, and $B_1 = \{B_1(k)\}_{k=-a_N}^{0}$ and $B_2 = \{B_2(k)\}_{k=0}^{N-1}$ are independent families of i.i.d. standard normal variables. The truncation parameter a_N balances accuracy (larger a_N reduces truncation error) and computational cost. This historical approach involves several approximations and is generally not recommended for high-quality or large-scale simulation. A similar method can be implemented used instead of MVN discretisation the Molchan-Golosov one.

Wavelet (Abry–Sellan). Since fBm can be obtained by fractional integration of Gaussian white noise, one may build it via a multiresolution analysis (MRA) and a wavelet expansion (Abry–Sellan [1]). Going into the details of this method is beyond the scope of this work; for further information, see [24]. We mention it here because MATLAB provides an implementation, `wfbm(H,N,T)`, which generates N samples of an fBm with Hurst parameter H over the time horizon T based on this algorithm. Figures 4.1 and 4.2 show the simulated paths with this procedure for two different values of H.

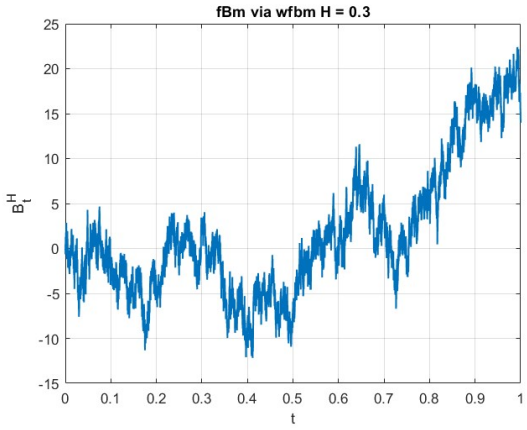

Figure 4.1: Simulated path of an fBm by the Abry–Sellan algorithm with $H = 0.3$.

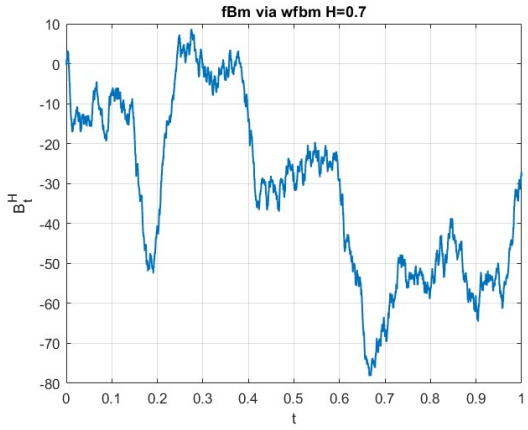

Figure 4.2: Simulated path of an fBm by the Abry–Sellan algorithm with $H = 0.7$.

Cholesky decomposition. This method is based on the structure of the covariance of an fBm. Let Γ be the covariance matrix of a standard fBm, discretized at times i/N, for $i = 0, \dots, N-1$. From (4.1),

$$(\Gamma)_{i,j} = \Gamma\left(\frac{i}{N}, \frac{j}{N}\right), \quad \text{for } i, j = 0, \dots, N-1.$$

Define Γ' as the matrix Γ with its first row and first column removed, since the fBm starts from 0. Since Γ' is a symmetric positive definite matrix, it admits a Cholesky decomposition

$$\Gamma' = LL^t,$$

where L is a lower triangular matrix and the symbol ^{t} denotes the transpose of the matrix. Thus, simulating a sample of an fBm at times i/N for $i = 1, \dots, N-1$ is equivalent to generating a vector Z of $(N-1)$ independent standard Gaussian variables and computing the product LZ. Indeed, LZ is a centered Gaussian vector and

$$\mathbb{E}\big((LZ)(LZ)^t\big) = \Gamma'.$$

Define $\widetilde{B} = \big(0, (LZ)^t\big)$; $\widetilde{B}$ is then a sample of an fBm at times i/N for $i = 0, \dots, N-1$. This method is exact in theory, but due to its computational complexity $\mathcal{O}(N^3)$ and the fact that Γ' can be extremely ill-conditioned, it is often preferable to use methods that are less computationally demanding.

Method of Wood-Chan The Wood–Chan method is an efficient algorithm for simulating fractional Brownian motion (fBm). The key idea is to exploit the fact that the increments of fBm, form a stationary Gaussian sequence with a Toeplitz covariance matrix. The method embeds this Toeplitz matrix into a larger circulant matrix whose eigenvalues can be computed via the Fast Fourier Transform (FFT). By generating Gaussian random vectors with the appropriate spectral density and applying the inverse FFT, one obtains a realization of fGn. The sample path of fBm is then recovered by taking cumulative sums of these increments. This method is applied in [42] to simulate a fbm trough appropriate MatLab function. Other simulation techniques for fBm paths are available; for a comprehensive summary, see [24] and [16] and the references therein.

4.1.2 Estimation of H for fractional Brownian motion

For the estimation of the Hurst parameter of a fBm we refer to [43], in this book many estimation techniques are presented. The one we present can be used to estimate the Hurst coefficient only by assuming that the observed path belongs to a fractional Brownian motion without any drift. This estimator for the Hurst parameter H is based on the second-order increment of a stochastic process X, which is defined as:

$$\Delta^{(2)}_{n,k} X = X\left(\frac{k+1}{n}T\right) - 2X\left(\frac{k}{n}T\right) + X\left(\frac{k-1}{n}T\right).$$

Using these increments, the Hurst parameter H is estimated by:

$$\hat{H}_n = \frac{1}{2} - \frac{1}{2\log 2} \log \left(\frac{\sum_{k=1}^{2n-1} \left(\Delta_{2n,k}^{(2)} X \right)^2}{\sum_{k=1}^{n-1} \left(\Delta_{n,k}^{(2)} X \right)^2} \right). \tag{4.7}$$

Knowing that the increments are Gaussian and asymptotically non-correlated, this estimator is obtained applying ergodic theorem (2.0.2), then it is strongly consistent for H, which means:

$$\lim_{n\to\infty} \hat{H}_n = H, \quad \text{almost surely.}$$

The estimator quantifies the self-similarity of the noise term. The second-order increment $\Delta_n^{(2)} X$ captures variations at finer scales, the ratio of the two sums in the logarithm compares variations at two different resolutions, n and $2n$, exploiting the scaling properties of fBm.

If we assume that the preprocessed hourly series (after spike removal and deseasonalization) is well described by a fractional Brownian motion, we can compute the Hurst parameter H on the increments. In detail, we apply this estimator on our dataset in the period 2017-2020. To analyze seasonal variations, the dataset was divided into periods corresponding to different seasons. The results show that the Hurst parameter varies across seasons. Figure (4.3) presents the seasonal variations in H, revealing a periodic behavior. Most values are above 0.5, with the exception of autumn 2020, which suggests some degree of persistence in the series. Moreover, we can observe periodicity: in fact, the value of H generally decreases before increasing again within the yearly cycle. The table (4.1) summarizes the seasonal estimates of H. These findings are in contrast with what we found in the previous chapter where the time series of electricity market seems to be antipersistent.

Season / Year	**2017**	**2018**	**2019**	**2020**
Winter	0.70	0.66	0.70	0.73
Spring	0.67	0.79	0.69	0.82
Summer	0.66	0.69	0.52	0.78
Autumn	0.61	0.59	0.69	0.47

Table 4.1: Values of H across different seasons and years.

Following the seasonal analysis discussed above, we further investigate the behavior of the Hurst exponent by examining its convergence as the sample size increases. In this analysis, using the same part of the dataset we compute the Hurst exponent iteratively adding ten observations from the data series and applying the estimator (4.7). The results are shown in Figure 4.4 which illustrates the convergence of H to the value 0.67 as the number of data points considered for estimation increases. The hourly time series shows persistence, using this estimator, as indicated by the Hurst parameter, which suggests that the series tends to maintain its trend over time. Based on the previous analysis, we conclude that the use of fractional dynamics in energy markets and particularly within the framework of electricity markets is appropriate. Furthermore, as observed

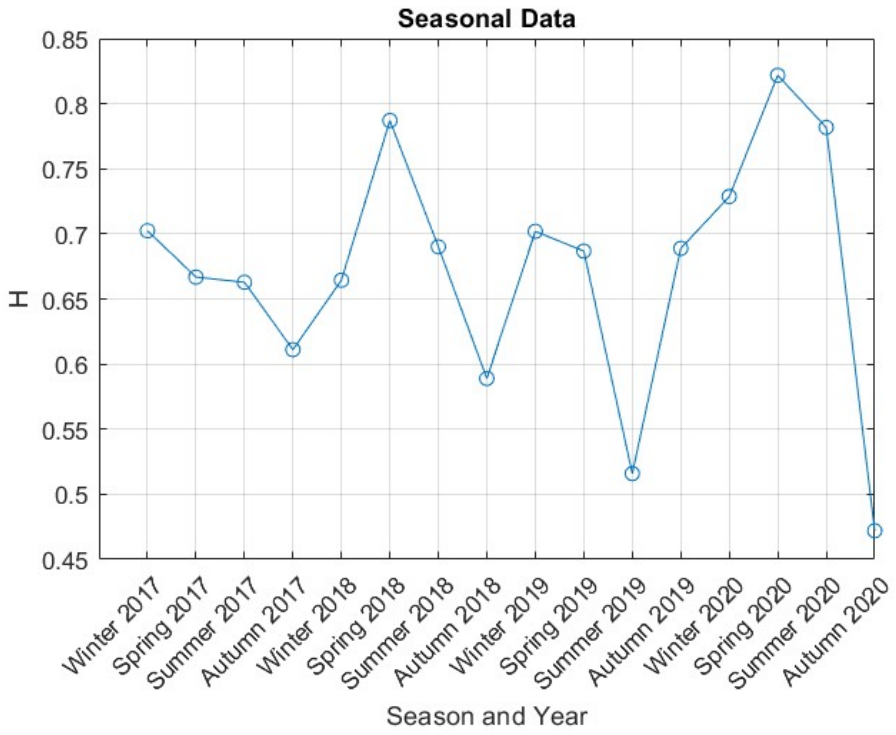

Figure 4.3: The seasonal variation of the Hurst parameter H over the years

in Figure (4.3) and Table (4.1), the Hurst exponent varies over time. This observation, align with what we found in Chapter 3.3 suggests that a single Hurst exponent in spot price models may be insufficient to fully capture the dynamics, and the variability of the Hurst exponent should be taken into account.

In light of these findings, it becomes natural to explore alternative stochastic structures capable of accommodating the observed variability in H and avoiding the possibility of arbitrage opportunities (which is extensively discussed in the fractional Brownian motion models presented in [69] and [21].).

In the next section, we introduce a class of processes that are martingales with respect to fractional Brownian motion. We then consider a linear combination of these martingales, each corresponding to a different Hurst parameter, to overcome the limitations of single–Hurst models and to better reproduce the empirical characteristics of electricity price dynamics. Moreover, this approach enables us to maintain the martingale property of the spot price under the risk–neutral probability measure and, as a consequence, of the corresponding forward prices.

4.2 The fundamental martingale

We know that the fractional Brownian motion is not a semimartingale, but in [60] the authors proved that this centered Gaussian process defined by an integral w.r.t. a fractional Brownian

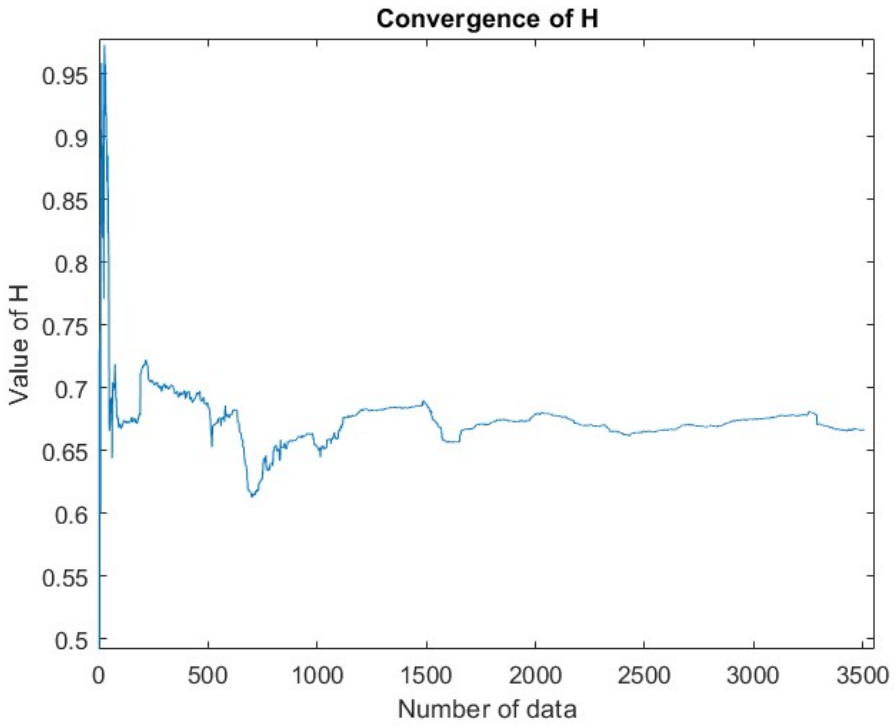

Figure 4.4: Convergence of estimation of H in the time series.

motion is a martingale:

$$M_t = c_1 \int_0^t s^{\frac{1}{2}-H}(t-s)^{\frac{1}{2}-H} dB_s^H, \tag{4.8}$$

where B_t^H is a fractional Brownian motion, $c_1 = \frac{1}{2H}(\beta(\frac{3}{2}-H, H+\frac{1}{2}))^{-1}$ and the Hurst parameter $H \in [(0;\frac{1}{2}) \cup (\frac{1}{2};1)]$. Since fractional Brownian motion is not a semimartingale for $(H \neq \frac{1}{2})$, the stochastic integral appearing below is not understood in the Itô sense, it is defined as a Wiener integral with respect to fractional Brownian motion within the framework of Gaussian process integration. Since the kernel

$$s \mapsto c_1 s^{\frac{1}{2}-H}(t-s)^{\frac{1}{2}-H}\mathbf{1}_{[0,t]}(s)$$

is deterministic, the integral is well defined as a centered Gaussian random variable. In [**?**] the authors also prove that this process has uncorrelated and thus independent increments, with variance:

$$\mathbb{E}[M_t^2] = c_2^2 t^{2-2H},$$

where $c_2 = \frac{c_H}{2H(2-2H)^{\frac{1}{2}}}$ and $c_H = \left(\frac{2H\Gamma(\frac{3}{2}-H)}{\Gamma(H+\frac{1}{2})\Gamma(2-2H)}\right)^{\frac{1}{2}}$.
We can find a function $f(t)$ such that by martingale representation theorem allows us to write the

process M_t as an integral w.r.t. a standard Brownian motion W_t:

$$M_t = \int_0^t f(s) dW_s,$$

and

$$< M_t, M_t >= \int_0^t f^2(s) ds = c_2^2 t^{2-2H}$$

Which implies $f(s) = \frac{c_H}{2H} s^{\frac{1}{2}-H}$ and

$$M_t = \frac{c_H}{2H} \int_0^t s^{\frac{1}{2}-H} dW_s, \tag{4.9}$$

These means that there exist different representations of the process M_t, one through an integral with respect to a fBm and another as a Wiener. In particular this process provides an example of Gaussian Volterra process whose kernel does not depend on the time variable t, and therefore defines a martingale. In our model, we include a combination of fundamental martingales, preserving the martingale property of forward prices while accounting for the empirical evidence that fractional dynamics provide a more realistic description of energy markets.

It is worth stressing that the introduction of the fundamental martingale is primarily a technical device aimed at overcoming the non-semimartingale nature of fractional Brownian motion and at obtaining a tractable stochastic calculus framework. Indeed, the fundamental martingale provides an alternative representation of the driving noise, allowing the model to be formulated in a semimartingale setting while preserving the dependence structure induced by the underlying fractional process.

Consequently, this transformation does not alter the empirical motivations that led to the adoption of fractional dynamics. The long-range dependence and heterogeneous scaling properties identified in Chapter 3 remain embedded in the model through the Hurst parameters governing the underlying fractional components. Therefore, the martingale representation should be viewed solely as a mathematical tool that facilitates model formulation and estimation, without affecting the empirical features motivating the fractional specification.

Chapter 5

Parameter estimation of normalized integrated fBm

In this part of the thesis, we investigate the statistical properties of the time-averaged fractional Brownian motion (fBm) and propose new estimators for its Hurst parameter. The time-averaged fBm is obtained by integrating the fBm over a fixed time window. This setting is motivated by the frequent use in the literature of fBm-based models for time series that have undergone averaging transformations, in many studies, researchers pre-process the data, often averaging it, before estimating H. This pre-processing step may introduce distortions that affect the accuracy of the exponent's estimation: in fact, nothing guarantees that a linear combination of increments of a fBm, like the typical result of this averaging process, is still a fBm. In particular in presence of large amounts of potentially memory-bearing data, a time averaging is often applied and it can change the structure of the underlying relationships and affect standard estimation procedures.

Our main motivating example comes from electricity markets. In fact, several empirical studies studied models based on fBm, finding that they adapt quite well to the dynamics of daily electricity prices. However, such approach is inconsistent with the way electricity prices are computed. Electricity markets operate on a much finer time scale, with trading intervals of one hour or 15 minutes in Europe, and even 5 minutes in some Australian markets. Daily prices are therefore obtained as averages of intraday prices (see, e.g., [78], [32]).

If the elementary price dynamics are assumed to follow an fBm, then the resulting daily prices, being time averages of this process, cannot themselves be fBm, but should instead be modeled as time-averaged versions of it. This averaging operation significantly alters the dependence structure of the original process. Another example is that two common ways to measure insolation in a given location are solar radiance, which is an instantaneous measurement of solar radiation, and solar insolation, which is the solar radiance averaged over a given time period. Thus, if one assumes that solar radiance follows a fBm, as a logical consequence, solar insolation should follow a nifBm.

A wide range of methods has been proposed to estimate the Hurst exponent and characterize short- or long-range dependence, relying on the behavior of the autocovariance function and on self-similarity properties, as discussed in previous chapters. A critical issue, which we aim to

emphasize, is that many empirical studies apply such estimation procedures to pre-processed data, often obtained through averaging. Since linear combinations of fBm increments are not guaranteed to preserve the fBm structure, this pre-processing step may distort the dependence properties of the data and, consequently, affect the reliability of standard Hurst exponent estimators.

For these reasons, we introduce the normalized integral-mean process of fBm (nifBm) over a period $h > 0$ and investigate how this averaging impacts the dynamical features of the process. Within this framework, after exploiting the properties and computing the covariance function of nifBm we construct, using ergodic theory, strongly consistent estimators for the Hurst parameter specifically adapted to the transformed process. We establish their asymptotic normality and validate their finite-sample performance through an extensive simulation study. We then extend the analysis to linear combinations of two different time-averaged fBm processes, again deriving estimators for the parameters of interest. Moreover, assuming non-degeneracy of the covariance matrix, we introduce a maximum likelihood estimator (MLE) for the drift parameter of this process. Finally the present the numerical simulations that support our theoretical results.

The literature contains numerous works devoted to the study of this subject, both from a theoretical perspective and from an applied one. For instance, in [46] small ball estimates for integrated fBm are considered, in [56] such functionals of integrated fBm as the maximum, the position of the maximum, the occupation time above zero and some others are studied. In [55] the problem of the log-asymptotic behavior of the probability that the integrated fBm does not exceed a fixed level over a long time is solved. The authors of [6] consider the persistence exponent of integrated fBm, a problem that originates in theoretical physics, where the persistence exponent serves as a simple measure of how fast a complicated physical system returns from a disordered initial condition to its stationary state. In [3] the persistence exponent is studied numerically, while in [2] the mean and covariance of ifBm and of some other integrated Gaussian processes are investigated. In [63] biomarker measurement modeling with a longitudinal submodel is treated, and to overcome longitudinal submodel challenges, the authors replace random slopes with scaled integrated fBm.

5.1 Normalized integrated fractional Brownian motion

In this section we start with the definition of Normalized integrated fractional Brownian motion, then we study its properties.

Definition 5.1. *(Normalized integrated fractional Brownian motion)*
Let $B^H = \{B_t^H, t \geq 0\}$ be a fractional Brownian motion with Hurst parameter $H \in (0;1)$ with continuous trajectories a.s. (Definition 4.1) then for a given $h > 0$, we can consider the normalized Riemann integral for any $t > 0$

$$X_t^{h,H} := \frac{1}{h} \int_t^{t+h} B_u^H \, du, \tag{5.1}$$

this stochastic process is called normalized integrated fractional Brownian motion (nifBm).

If the parameter H is clear from the context, we will write simply X_t^h. Even when considered as a function of both parameters, t and h, nifBm is Gaussian and zero-mean process. Therefore, its main characteristics are identified through its covariance function. Some related work in this direction is to be found in [2], but we need to produce much more detailed analysis in order to get the statistical estimators.

We first compute the covariance function and present the main results below, postponing the proofs of the corresponding lemmas to Appendix A.

Lemma 5.1.1. *For any $s \geq t$*

$$\begin{aligned}\mathbb{E}[X_t^h X_s^h] = \frac{1}{2h(2H+1)}\big((s+h)^{2H+1} - s^{2H+1} + (t+h)^{2H+1} - t^{2H+1}\big) \\ + \frac{1}{2h^2(2H+1)(2H+2)}\big(2(s-t)^{2H+2} - (s-t+h)^{2H+2} - |s-t-h|^{2H+2}\big).\end{aligned} \tag{5.2}$$

In particular, for any $t \geq 0$

$$\mathbb{E}[(X_t^h)^2] = \frac{1}{h(2H+1)}\big((t+h)^{2H+1} - t^{2H+1}\big) - \frac{h^{2H}}{(2H+1)(2H+2)}. \tag{5.3}$$

Remark 5.1.1. *It is clear from formula* (5.2)*, as well as from* (5.3)*, that the process X^h is not stationary in t. If we analyze the value $\mathbb{E}[(X_t^h)^2]$ from* (5.3) *as $t \to \infty$, then*

$$(t+h)^{2H+1} - t^{2H+1} = t^{2H+1}\left(\left(1+\frac{h}{t}\right)^{2H+1} - 1\right) \sim t^{2H+1}(2H+1)\frac{h}{t},$$

whence $\mathbb{E}[(X_t^h)^2] \sim t^{2H}$ as $t \to \infty$, the same asymptotics as a fBm.

Since we need to employ the ergodic theorem (2.0.2) to build the statistical estimates, our goal is to construct a stationary process, starting from nifBm. In the following calculations the length h of the interval of integration will be fixed while t will be shifted. The increments of the process are:

$$\Delta X_t^h = (X_{t+h}^h - X_t^h) = \frac{1}{h}\left(\int_{t+h}^{t+2h} B_u^H\, du - \int_t^{t+h} B_s^H\, ds\right) = \frac{1}{h}\int_t^{t+h}\left(B_{s+h}^H - B_s^H\right)\, ds \tag{5.4}$$

We are going to compute the covariance and variance of these increments where shifting time t by a quantity nh, with $n \in \mathbb{N}$. This calculation will be different for $n = 0$ (variance, intervals of integration are completely overlapping), $n = 1$ (covariance, intervals are partially overlapping) and $n \geq 2$ (covariance, intervals are not overlapping). The following result on the structure of the covariance show also that the increments of the nifBm are stationary.

Theorem 5.1.1. *For any $t \geq 0$ and $n \geq 0$*

$$\mathbb{E}[(X_{t+h}^h - X_t^h)(X_{t+(n+1)h}^h - X_{t+nh}^h)] = h^{2H}\gamma(H,n). \tag{5.5}$$

with

$$\gamma(H,n) := \begin{cases} \dfrac{2(2^{2H}-1)}{(2H+1)(H+1)},\ n=0, \\ (2(2H+1)(2H+2))^{-1}(7-4\cdot 2^{2H+2}+3^{2H+2}),\ n=1, \\ (2(2H+1)(2H+2))^{-1}((n-2)^{2H+2}-4(n-1)^{2H+2} \\ +6n^{2H+2}-4(n+1)^{2H+2}+(n+2)^{2H+2}),\ n\geq 2, \end{cases} \tag{5.6}$$

that can be expressed in a more concise form as

$$\gamma(H,n) = \frac{(|n-2|^{2H+2}-4|n-1|^{2H+2}+6|n|^{2H+2}-4|n+1|^{2H+2}+|n+2|^{2H+2})}{4(2H+1)(H+1)},$$

Proof. The proof follows directly from an application of Lemma 5.1.1 to the increments and their sum. Here, we consider only the case $n=0$ in detail to show how the terms containing t cancel each other. The proof in cases $n=1$ and $n\geq 2$ follows the same lines. For $n=0$ expanding the square according to (5.3), we obtain

$$\mathbb{E}[(X^h_{t+h})^2] = \frac{1}{h(2H+1)}\big((t+2h)^{2H+1}-(t+h)^{2H+1}\big) - \frac{h^{2H}}{(2H+1)(2H+2)},$$

The mixed product $\mathbb{E}[X^h_t X^h_{t+h}]$ is given by (5.1.1) with $s=t+h$,

$$\mathbb{E}[X^h_t X^h_{t+h}] = \frac{1}{2h(2H+1)}\big((t+2h)^{2H+1}-t^{2H+1}\big)+\frac{1}{2h^2(2H+1)(2H+2)}\big(2h^{2H+2}-(2h)^{2H+2}\big).$$

Therefore together with (5.3) we may conclude

$$\begin{aligned} \mathbb{E}(X^h_{t+h}-X^h_t)^2 =& \frac{1}{h(2H+1)}\big[(t+2h)^{2H+1}-(t+h)^{2H+1}+(t+h)^{2H+1}-t^{2H+1} \\ & -(t+2h)^{2H+1}+t^{2H+1}\big] - \frac{2h^{2H}}{(2H+1)(2H+2)} - \frac{2h^{2H+2}-(2h)^{2H+2}}{h^2(2H+1)(2H+2)} \\ =& \frac{h^{2H}}{(2H+1)(2H+2)}\Big(2^{2H+2}-4\Big) \\ =& \frac{2h^{2H}}{(2H+1)(H+1)}\Big(2^{2H}-1\Big). \end{aligned} \tag{5.7}$$

□

By studying the sign of $\gamma(H,n)$ for $H\in(0,1)$ we can compare it with the autocorrelation function of fBm which is positive for $H>1/2$ and negative for $H<1/2$. The results can be summarized as follow.

Lemma 5.1.2. (i) *Let $H\in(0,1)$. The function $\gamma(H,1)$, is zero for $H=0$ and admits a unique $H_0\in(0,1)$ such that $\gamma(H_0,1)=0$, $\gamma(H,1)<0$ for $H\in(0,H_0)$ and $\gamma(H,1)>0$ for $H\in(H_0,1]$. Numerical computations give $H_0\simeq 0.2626229$. The graph of the function $\gamma(H,1)$ over the interval $(0,1)$ is shown in Figure 5.1.*

(ii) *For any* $n \geq 2$ *function* $\gamma(H, n)$, $H \in (0, 1)$ *is strictly negative for* $H \in (0, 1/2)$*, zero for* $H = 1/2$ *and strictly positive for* $H \in (1/2, 1)$.

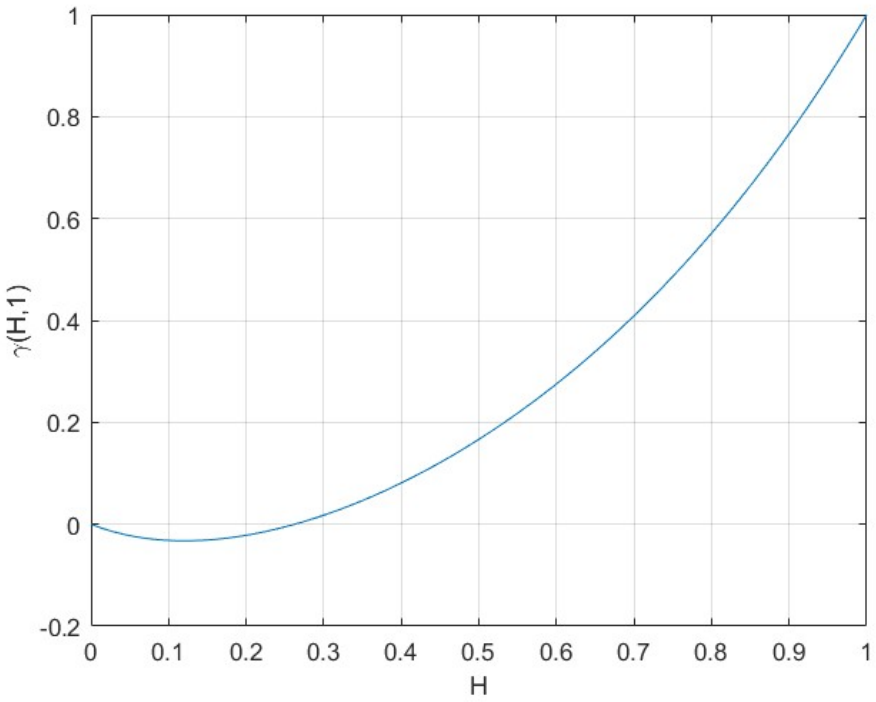

Figure 5.1: Graph of the function $\gamma(H, 1)$ for $H \in (0, 1)$. The function becomes zero at $H_0 \simeq 0.2626229$.

Remark 5.1.2. *Note that the covariance in* (5.5) *does not depend on* t*. Also,* X_t^h *is a Gaussian process in both arguments* t *and* h*. It means that choosing* t *proportional to* h *(as done in the main part),* $\Delta X_t^h = (X_{t+h}^h - X_t^h)$ *is a stationary Gaussian sequence . Furthermore, looking at the brackets in the right-hand side of* (5.5) *we find the coefficients of the binomial expansion for* $(a - b)^4$*. A similar structure can be observed even in the numerator of* $\gamma(H, 1)$ *that can be rewritten as* $3^{2H+2} - 4 \cdot 2^{2H+2} + 6 + 1$*. Indeed, when* $n = 1$*, the term* $|n - 2|^{2H+2}$ *equals* 1*, while the contribution corresponding to* $|n - 1|^{2H+2}$ *vanishes.*

Recall that the fBm is a self-similar process with self-similarity index H. This property, as we saw, is crucial in many estimation procedures. Here we want to establish the self-similarity of the process X_t^h, $t \geq 0$. Given that nifBm defined in (5.1) depends on t and h, we consider the following modified property of self-similarity.

Lemma 5.1.3. *For any* $h > 0$ *a nifBm* $X^h = \{X_t^h, t \geq 0\}$ *is self-similar with self-similarity parameter* H *in the sense that for all* $c > 0$

$$\{X_{ct}^{ch}, t \geq 0\} \stackrel{d}{=} \{c^H X_t^h, t \geq 0\}. \tag{5.8}$$

5.1.1 Asymptotic behavior of the covariance

To assess whether we can use the ergodic theorems [31, Chapter 2] for Gaussian sequences, we need to check if the covariance function (5.5) tends to zero as $n \to \infty$ for any $H \in (0,1)$.

Lemma 5.1.4. *For any $H \in (0,1)$ $\gamma(H,n), n \in \mathbb{N}_0$ defined by* (5.6)*, is a asymptotically negligible, i.e., tends to zero as $n \to \infty$. More precisely,*

$$\frac{n^{2-2H}\gamma(H,n)}{2H(2H-1)} \to 1,$$

as $n \to \infty$.

Proof. Let us rewrite $\gamma(H,n)$ for $n \geq 2$ by taking out the multiplier n^{2H+2}:

$$\gamma(H,n) = \frac{n^{2H+2}}{2(2H+1)(2H+2)} g(n^{-1}),$$

where

$$g(x) = \Big((1-2x)^{2H+2} - 4\,(1-x)^{2H+2} + 6 - 4\,(1+x)^{2H+2} + (1+2x)^{2H+2}\Big).$$

The asymptotic behavior of $\gamma(H,n)$ can be deduced from the Taylor expansion of $g(x)$ at the origin. Computing the derivatives of $g(x)$, we have

$$g'(x) = (2H+2)\left(-2(1-2x)^{2H+1} + 4(1-x)^{2H+1} - 4(1+x)^{2H+1} + 2(1+2x)^{2H+1}\right),$$

$$g''(x) = (2H+2)(2H+1)\left(4(1-2x)^{2H} - 4(1-x)^{2H} - 4(1+x)^{2H} + 4(1+2x)^{2H}\right),$$

$$g'''(x) = (2H+2)(2H+1)(2H)\left(-8(1-2x)^{2H-1} + 4(1-x)^{2H-1} - 4(1+x)^{2H-1} + 8(1+2x)^{2H-1}\right),$$

$$g^{(iv)}(x) = (2H+2)(2H+1)(2H)(2H-1)\left(16(1-2x)^{2H-2} - 4(1-x)^{2H-2} - 4(1+x)^{2H-2} + 16(1+2x)^{2H-2}\right).$$

Then $g(0) = g'(0) = g"(0) = g'''(0) = 0$, and the first nonzero term in the Taylor expansion of g at zero is the fourth derivative.

$$g^{(iv)}(0) = 24(2H+2)(2H+1)(2H)(2H-1),$$

Consequently

$$g(x) = (2H+2)(2H+1)(2H)(2H-1)x^4 + o(x^4).$$

Hence, as $n \to \infty$, $\gamma(H,n)$ behaves as $2H(2H-1)n^{2H-2}$, which implies that

$$\frac{n^{2-2H}\gamma(H,n)}{2H(2H-1)} \to 1,\ n \to \infty.$$

□

Remark 5.1.3. *It is interesting to note that the covariance of the increments of the process $\{X^h_{kh}\}_{k\geq 1}$ exhibits the same asymptotic behavior as that of a fractional Brownian motion. Specifically, when $H > \frac{1}{2}$, the function $\gamma^H(n)$ is strictly positive and decays slowly, whereas for $H < \frac{1}{2}$, $\gamma^H(n)$ is strictly negative and exhibits a faster decay. This can be easily explained if for $n \geq 2$ we transform the incremental covariance as follows:*

$$\begin{aligned}&\frac{1}{h^2}\mathbb{E}\int_0^h \big(B^H_{s+h} - B^H_s\big)ds \int_{nh}^{(n+1)h} \big(B^H_{t+h} - B^H_t\big)dt\\ &= \frac{1}{h^2}\int_0^h\int_0^h \mathbb{E}\big(B^H_{s+h} - B^H_s\big)\big(B^H_{t+(n+1)h} - B^H_{t+nh}\big)dsdt,\end{aligned}$$

Recall that the increments of fBm are positively (negatively) correlated if $H > 1/2$ ($H < 1/2$). Moreover, applying the expansion of $(1+x)^{2H}$, we obtain

$$\begin{aligned}&\mathbb{E}\big(B^H_{s+h} - B^H_s\big)\left(B^H_{t+(n+1)h} - B^H_{t+nh}\right)\\ &= \frac{1}{2}\Big[(t-s+(n+1)h)^{2H} + (t-s+(n-1)h)^{2H} - 2(t-s+nh)^{2H}\Big]\\ &= \frac{(nh)^{2H}}{2}\left[\left(1+\frac{t-s+h}{nh}\right)^{2H} + \left(1+\frac{t-s-h}{nh}\right)^{2H} - 2\left(1+\frac{t-s}{nh}\right)^{2H}\right]\\ &= \frac{H(2H-1)(nh)^{2H}}{2}\left[\left(\frac{t-s+h}{nh}\right)^{2} + \left(\frac{t-s-h}{nh}\right)^{2} - 2\left(\frac{t-s}{nh}\right)^{2} + o(n^{-2})\right]\\ &\sim H(2H-1)h^{2H}n^{2H-2}.\end{aligned}$$

and we can apply the Lebesgue dominated convergence theorem in order to get the same asymptotic behavior of standard and integrated fBm. Figures 5.2 and 5.3 illustrate the comparison of the incremental covariance of the integrated and standard fractional Brownian motions for $H = 0.3$ and $H = 0.7$, respectively.

Remark 5.1.4. *From Lemma 5.1.2, (ii), it follows that for $k \geq j+2$ and $H = \frac{1}{2}$, the respective increments are independent. Therefore, in this case $g_{1/2}(\frac{1}{n}) = 0, n \geq 2$, where*

$$g_{1/2}(x) = \left((1-2x)^3 - 4\,(1-x)^3 + 6 - 4\,(1+x)^3 + (1+2x)^3\right).$$

Moreover, equality $g_{1/2}(x) = 0$ can be easily checked for any x.

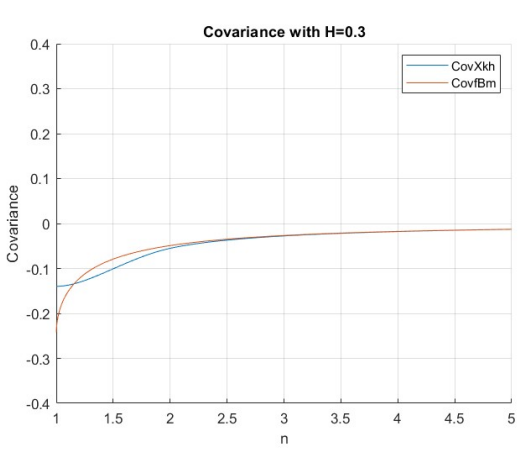

Figure 5.2: Comparison of the covariance of the increments in our process ΔX_k^h and the fractional Brownian motion with $H = 0.3$.

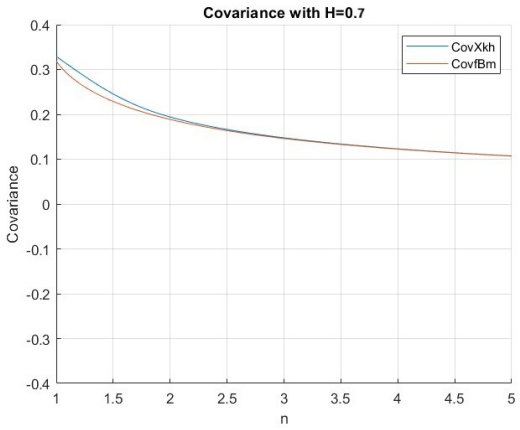

Figure 5.3: Comparison between the covariance of the increments in our process ΔX_k^h and the fractional Brownian motion with $H = 0.7$.

5.1.2 Nonsingularity of the incremental covariance matrix

Let fix some $h > 0$ and define the discrete-time increments $\Delta X_k^h := X_{(k+1)h}^h - X_{kh}^h$, $k \in \mathbb{N}_0$, which defines a Gaussian sequence $\Delta X^h = \{X_{(k+1)h}^h - X_{kh}^h, k \in \mathbb{N}_0\}$. From Theorem 5.1.1, it is immediate to notice that

$$\mathbb{E}[\Delta X_k^h \Delta X_{k+n}^h] = h^{2H}\gamma(H, n), \qquad \text{for all } k \in \mathbb{N}_0. \tag{5.9}$$

In the next proposition, we show that any covariance matrix of the increments ΔX_k^h is nonsingular.

Propotion 5.1.1. *If* $0 \leq k_1 < \ldots < k_m$ *with* $k_i \in \mathbb{N}$, *then* $\Sigma_{k_1,\ldots,k_m} := (\mathrm{Cov}(\Delta X_{k_i}^h, \Delta X_{k_j}^h))_{i,j=1}^m$ *has rank* m.

Proof. Let's prove this by contradiction. Assume that for some $0 \leq k_1 < \ldots < k_n$

$$\operatorname{rank} \Sigma_{k_1,\ldots,k_{m-1}} = \operatorname{rank} \Sigma_{k_1,\ldots,k_m} = m - 1$$

(if $\operatorname{rank} \Sigma_{k_1,\ldots,k_{m-1}} < m - 1$, a similar argument could be applied). Then it would be possible to express $\Delta X_{k_m}^h$ as a linear combination of the other components, i.e. there would exist $a_1, \ldots, a_{m-1} \in \mathbb{R}$ such that

$$\Delta X_{k_m}^h = \sum_{i=1}^{m-1} a_i \Delta X_{k_i}^h. \tag{5.10}$$

Note that

$$\Delta X_{k_m}^h = \frac{1}{h}\left(I_m + \zeta_m\right), \tag{5.11}$$

where $I_m = \int_{(k_m+1)h}^{(k_m+2)h} W_s^H ds$ and ζ_m is $\mathcal{F}_{(k_m+1)h}$-adapted. Also, $\sum_{i=1}^{m-1} a_i \Delta X_{k_i}^h$ is $\mathcal{F}_{(k_{m-1}+2)h} \subset \mathcal{F}_{(k_m+1)h}$-adapted. Taking into account this adaptedness and (5.10)-(5.11), we conclude that I_m

is $\mathcal{F}_{(k_m+1)h}$-adapted, and therefore $\mathbb{E}(I_m|\mathcal{F}_{(k_m+1)h}) = I_m$. However, according to representation (4.3),

$$\mathbb{E}(I_n|\mathcal{F}_{(k_m+1)h}) = \int_{(k_m+1)h}^{(k_m+2)h} \int_0^{(k_m+1)h} K_H(s,u)dB_u ds \neq I_m = \int_{(k_m+1)h}^{(k_m+2)h} \int_0^{s} K_H(s,u)dB_u ds,$$

whence the proof follows. □

Remark 5.1.5. *In fact, we did not use in the proof the stationarity of the increments ΔX_k^h. However, taking into account the stationarity and assuming that equality* (5.10) *holds, we get that for any $m \geq 0$*

$$\Delta X_{k_n+m}^h = \sum_{i=1}^{n-1} a_i \Delta X_{k_i+m}^h.$$

Now, by the same reason, we can present all $\Delta X_{k_i+m}^h$ with $k_i + m \geq k_n$ via linear combination of the increments with smaller indices. By induction, it means that assumption (5.10) *leads to the possibility to predict without error all the future increments ΔX_k^h for $k \geq k_n$ via increments until k_{n-1}. Such a property corresponds to a perfectly predictable stationary Gaussian sequence and is therefore incompatible with the stochastic structure of the increments considered here.*

5.1.3 Linear combination of two nifBms and its main properties

In this section we study the properties of linear combination of two independent incremental processes constructed from two nifBms.

Starting with the process (5.1), put in it $t = kh$ and define the following stochastic sequence:

$$\begin{aligned} \widetilde{X}_k^h &= \frac{a}{h} \int_{kh}^{(k+1)h} B_s^{H_1} ds + \frac{b}{h} \int_{kh}^{(k+1)h} B_s^{H_2} ds \\ &= aX_{kh}^{h,H_1} + bX_{kh}^{h,H_2}, \qquad k \in \mathbb{N}_0,\ h > 0, \end{aligned} \tag{5.12}$$

where $\mathbb{N}_0 = \mathbb{N} \cup \{0\}$. Here coefficients a and b are two real numbers, and W^{H_1}, W^{H_2} are two independent fractional Brownian motions with Hurst parameters $H_i \in (0,1)$, $i = 1, 2$. So, we are working with equidistant observations.

Remark 5.1.6. *As usual, taking into account the symmetry of the Gaussian processes W^{H_1} and W^{H_2}, we can assume that $a > 0$, $b > 0$. Otherwise, in what follows we can estimate $|a|$ and $|b|$.*

Of course, the sequence $\{\widetilde{X}_k^h,\ k \in \mathbb{N}_0\}$ is Gaussian but not stationary. Again, as in the case with one nifBm, to construct statistical estimators of all parameters basing on the ergodic theorem, we want to transform it into a stationary Gaussian stochastic sequence. The easiest way is to create an

incremental process of the form $\Delta\widetilde{X}_k^h := \widetilde{X}_{k+1}^h - \widetilde{X}_k^h$. Thus, we have

$$\begin{aligned}\Delta\widetilde{X}_k^h &= a(X_{(k+1)h}^{h,H_1} - X_{kh}^{h,H_1}) + b(X_{(k+1)h}^{h,H_2} - X_{kh}^{h,H_2}) \\ &= \frac{a}{h}\int_{kh}^{(k+1)h}\left(B_{s+h}^{H_1} - B_s^{H_1}\right)ds + \frac{b}{h}\int_{kh}^{(k+1)h}\left(B_{s+h}^{H_2} - B_s^{H_2}\right)ds \\ &=: a\Delta X_k^{h,H_1} + b\Delta X_k^{h,H_2}.\end{aligned}$$

Propotion 5.1.2. *The Gaussian sequence* $\{\Delta\widetilde{X}_k^h, k \in \mathbb{N}_0\}$ *is stationary, with* $\mathbb{E}[\Delta\widetilde{X}_k^h] = 0$ *for all* $k \in \mathbb{N}_0$ *and*

$$\mathbb{E}\left[\Delta\widetilde{X}_k^h\Delta\widetilde{X}_{k+n}^h\right] = a^2h^{2H_1}\gamma(H_1,n) + b^2h^{2H_2}\gamma(H_2,n), \tag{5.13}$$

for all $k, n \in \mathbb{N}_0$.

Proof. Since $\{\Delta\widetilde{X}_k^h, k \in \mathbb{N}_0\}$ is Gaussian, and $\mathbb{E}[\Delta\widetilde{X}_k^h] = 0$ for all $k \in \mathbb{N}_0$, it is sufficient to prove that its covariance $\mathbb{E}\left[\Delta\widetilde{X}_k^h\Delta\widetilde{X}_{k+n}^h\right]$ does not depend on k. To prove this, we take into account independence and zero mean of $\Delta X_k^{h,H_1}$ and $\Delta X_k^{h,H_2}$, and state that

$$\mathbb{E}\left[\Delta\widetilde{X}_k^h\Delta\widetilde{X}_{k+n}^h\right] = a^2\mathbb{E}\left[\Delta X_k^{h,H_1}\Delta X_{k+n}^{h,H_1}\right] + b^2\mathbb{E}\left[\Delta X_k^{h,H_2}\Delta X_{k+n}^{h,H_2}\right].$$

Now, in order to finish the proof, it is sufficient to note, that, in terms of (5.5),

$$\mathbb{E}\left[\Delta X_k^{h,H}\Delta X_{k+n}^{h,H}\right] = \mathbb{E}[(X_{t+h}^h - X_t^h)(X_{t+(n+1)h}^h - X_{t+nh}^h)],$$

with $t = kh$, and apply Theorem 5.1.1. □

5.2 Construction of statistical estimators

In this section, we construct estimators for the normalized integrated fractional Brownian motion. We begin with the simplest case, namely the process (5.1), where we set $t = kh$ and define the discrete time stochastic sequence:

$$X_k^{h,H} = \frac{a}{h}\int_{kh}^{(k+1)h} B_u^H\,du, \tag{5.14}$$

where $h > 0$ is fixed and $a \in \mathbb{R}$ denotes the diffusion coefficient. Observe that $X_k^{h,H}$ is not $\mathcal{F}_{kh}$-measurable, as it is defined through the integral of B^H over the interval $[kh, (k+1)h]$. Hence, the k-th observation becomes available only at time $(k+1)h$. Nevertheless, for notational convenience, we index the observations by k. Our first goal is the estimation of the Hurst exponent H and the coefficient a through the ergodic theorem (2.0.2) and the study of asymptotic properties such as strong consistency and asymptotic normality for this estimators. We then extend the analysis to

the mixed normalized integrated fBm (5.12) defined as

$$\widetilde{X}_k^h = \frac{a}{h}\int_{kh}^{(k+1)h} B_s^{H_1} ds + \frac{b}{h}\int_{kh}^{(k+1)h} B_s^{H_2} ds \qquad k \in \mathbb{N}_0,\ h > 0,$$

where $B_s^{H_1}$ and $B_s^{H_2}$ are two independent fBm with different Hurst parameters. In this case, the aim is to estimate the parameter vector $\{H_1, H_2, a, b\}$ and to investigate the corresponding properties.

In the final part of this section, we address the problem of drift estimation via maximum likelihood. In particular, we prove the non-degeneracy of the covariance matrix by considering a model of the form:

$$Y_k^h = \mu G_k^h + P_{kh}, \tag{5.15}$$

where P_{kh} can be either the process (5.14) or (5.12), and G is a known deterministic function. We assume that H and a in the case (5.14) or $H_1, H_2 \in (0,1)$ and that the coefficients $a, b \in \mathbb{R}\setminus\{0\}$ in the mixed case, are known, an essential prerequisite for applying MLE. The objective is to estimate the drift parameter $\mu \in \mathbb{R}$ from discrete observations. Simulation studies on the performance of the proposed estimators are discussed at the end of each subsection.

5.2.1 Estimation of the parameters H and a^2 in the model with one nifBm

Consider the case when we have only one nifBm (5.14). We call this model *"model with one nifBm"*. We need only two statistics to compute the estimators for H and a^2. The first estimator, ξ_N^1 is based directly on the stationary incremental process $\Delta X_k^h = X_{k+1}^h - X_k^h$ and other estimator is based on the increments

$$\Delta X_k^{jh} = X_{k+1}^{jh} - X_k^{jh} \tag{5.16}$$

for $j = 2$, whose stationarity can be established similarly to ΔX_k^h. So, we introduce the following statistics:

$$\xi_N^j := \frac{1}{N}\sum_{k=0}^{N-1}\left(X_{k+1}^{jh} - X_k^{jh}\right)^2 = \frac{1}{N}\sum_{k=0}^{N-1}\left(\Delta X_k^{jh}\right)^2, \quad j = 1, 2. \tag{5.17}$$

Observe that the stationarity of the increment sequences is a crucial assumption in this procedure, since it allows the application of the ergodic theorem (2.0.2).

Remark 5.2.1. *We can observe that the number of observations considered differs between the two statistics. In fact, in ξ_N^2 the mean is taken over an interval of length $2h$, so the sum contains only half as many elements as in ξ_N^1. This difference does not represent an issue, since we rely on the ergodic theorem as $N \to \infty$.*

Lemma 5.2.1. *The following a.s. convergences hold for $N \to \infty$:*

$$\xi_N^j \to \mathbb{E}(\xi_1^j) = Aa^2\big(2^{2H} - 1\big)j^{2H}, \tag{5.18}$$

where $j = 1, 2$ *and*

$$A = \frac{2h^{2H}}{(2H+1)(H+1)}, \quad i = 1, 2.$$

Proof. Since the random sequence $\{\Delta X_k^h,\, k \geq 0\}$ is stationary and ergodic for any $h > 0$, the proof of all a.s. convergence follows directly from the ergodic Theorem 2.0.2 with $Q(x) = x^2$, the values of $\mathbb{E}(\xi_1^i)$ that are calculated in accordance with formula (5.5). □

Using these statistics, we can state and prove the following theorem:

Theorem 5.2.1. *Consider the model with one nifBm, and let* $0 < H < 1$ *and* $a^2 > 0$*. Then the estimator* $\hat{\theta}_N = (\widehat{H}_N, \hat{a}_N^2)$*:*

$$\widehat{H}_N = \frac{1}{2\log 2} \log\left(\frac{\xi_N^2}{\xi_N^1}\right), \quad \widehat{A}_N = \frac{2h^{2\widehat{H}_N}}{\big(2\widehat{H}_N + 1\big)\big(\widehat{H}_N + 1\big)}. \tag{5.19}$$

and

$$\hat{a}_N^2 = \frac{\xi_N^1}{\widehat{A}_N\big(2^{2\widehat{H}_N} - 1\big)}, \tag{5.20}$$

is a strongly consistent estimator of $\theta = (H, a^2)$*.*

Proof. Considering the statistics (5.17) ξ_N^1 and ξ_N^2, by ergodic theorem $\xi_N^1 \to \mathbb{E}(\xi_0^1)$ and $\xi_N^2 \to \mathbb{E}(\xi_0^2)$ a.s, recalling $x = 2^{2H}$ in the equation (5.42), we obtain this two equations

$$Aa^2(x-1) = \xi_N^1 \tag{5.21}$$

$$Aa^2x(x-1) = \xi_N^2 \tag{5.22}$$

x is obtained dividing the second one by the first one:

$$x = \frac{\xi_N^2}{\xi_N^1}$$

Since $x = 2^{2H}$

$$H = \frac{1}{2}\log_{2+}\left(\frac{\xi_N^2}{\xi_N^1}\right)$$

where

$$\log_+ x = \begin{cases} \log x, & \text{if } x > 0, \\ 0, & \text{if } x \leq 0, \end{cases}$$

Changing the basis of the logarithm, we obtain the estimator (5.19). The estimator for a^2 can be computed from the equation (5.21). □

5.2.2 Asymptotic normality.

In this part we want prove the asymptotic normality of the estimator $\widehat{\theta}_N = (\widehat{H}_N, \widehat{a}_N^2)$ defined in (5.19)–(5.20). The asymptotic normality means that as the sample size goes to infinity, the

distribution of the estimator converges to a normal distribution. We begin by establishing the asymptotic normality of the underlying statistics, and then we extend the result to the estimator.

Remark 5.2.2. *Note that if we fix a final time T and follow the trajectory of our process up to T, the number of the terms in the summations of each statistic ξ^1, ξ^2, will be different, since for each statistic we consider increments of different amplitude, in particular ξ^1 has $2N$ elements while ξ^2, N elements. Thus, for notation convenience we replace ξ^1_N with ξ^1_{2N}.*

Following this Remark, we employ the modified notation for the statistics, ξ^1_{2N} and ξ^2_N. By (5.42), as $N \to \infty$,

$$\xi^1_{2N} \to \mathbb{E}(\xi^1_1) = A_1 a^2(2^{2H}-1) =: f_1(\theta), \quad \xi^2_N \to \mathbb{E}(\xi^2_1) = A_1 a^2(2^{2H}-1)2^{2H} =: f_2(\theta) \text{ a.s.} \tag{5.23}$$

The next theorem establishes their joint asymptotic normality.

Theorem 5.2.2. *Let $0 < H < \frac{3}{4}$[1]. Consider the vectors $\bar{\xi}_N = (\xi^1_{2N}, \xi^2_N)^\top$, $\bar{\eta} = (\mathbb{E}(\xi^1_1), \mathbb{E}(\xi^2_1))^\top$. Then $\bar{\xi}_N$ is asymptotically normal, that is,*

$$\sqrt{N}(\bar{\xi}_N - \bar{\eta}) = \sqrt{N}\begin{pmatrix} \xi^1_{2N} - \mathbb{E}(\xi^1_1) \\ \xi^2_N - \mathbb{E}(\xi^2_1) \end{pmatrix} \xrightarrow{d} \mathcal{N}\big(0, \widetilde{\Sigma}\big), \quad \textit{as } N \to \infty,$$

where the asymptotic covariance matrix $\widetilde{\Sigma}$ is given by

$$\widetilde{\Sigma} = \begin{pmatrix} \widetilde{\Sigma}_{11} & \widetilde{\Sigma}_{12} \\ \widetilde{\Sigma}_{12} & \widetilde{\Sigma}_{22} \end{pmatrix},$$

with entries

$$\widetilde{\Sigma}_{11} = h^{4H} \sum_{i=-\infty}^{\infty} \gamma(H,i)^2, \qquad \widetilde{\Sigma}_{22} = 2^{4H+1} h^{4H} \sum_{i=-\infty}^{\infty} \gamma(H,i)^2, \tag{5.24}$$

$$\widetilde{\Sigma}_{12} = h^{4H} \sum_{i=-\infty}^{\infty} \gamma(H,i)\big(3\gamma(H,i) + 4\gamma(H,i+1) + \gamma(H,i+2)\big). \tag{5.25}$$

Before going into the details of the proof, we need to introduce the following lemma concerning the convergence of the series and a remark on the increments.

Lemma 5.2.2. *For any $H < \frac{3}{4}$ and for all $\alpha, \beta \in \mathbb{Z}$,*

$$\sum_{i=-\infty}^{\infty} |\gamma(H, i+\alpha)\gamma(H, i+\beta)| < \infty \tag{5.26}$$

[1]The condition $H < 3/4$ is required for the application of the Breuer–Major theorem. Since the autocorrelation of the fractional Gaussian noise behaves as $\rho(k) \sim C_H k^{2H-2}$, the summability condition $\sum_{k\geq 1} \rho(k)^2 < \infty$ is satisfied only when $H < 3/4$. This guarantees a Gaussian limit and hence the asymptotic normality of the estimator; see [61] for details.

Proof. By Cauchy-Schwarz inequality, we get for all $\alpha, \beta \in \mathbb{Z}$

$$\sum_{i=-\infty}^{\infty} |\gamma(H, i+\alpha)\gamma(H, i+\beta)| \leq \sqrt{\sum_{i=-\infty}^{\infty} |\gamma(H, i+\alpha)^2| \cdot \sum_{i=-\infty}^{\infty} |\gamma(H, i+\beta)^2|} = \sum_{i=-\infty}^{\infty} \gamma(H, i)^2 < \infty,$$

by Lemma (5.1.4). □

Remark 5.2.3. *As our estimators will use also the process X^{2h}, we notice that we can represent it in terms of the process X^h*

$$\begin{aligned} X_k^{2h} &= \frac{1}{2h} \int_{2hk}^{2h(k+1)} aB_u^H du \\ &= \frac{1}{2} \left(\frac{1}{h} \int_{2hk}^{2hk+h} aB_u^H du + \frac{1}{h} \int_{(2k+1)h}^{(2k+2)h} aB_u^H du \right) \\ &= \tfrac{1}{2} \left(X_{2k}^h + X_{2k+1}^h \right). \end{aligned} \tag{5.27}$$

More generally, we obtain

$$\widetilde{X}_k^{jh} = \frac{1}{j} \sum_{l=0}^{j-1} \widetilde{X}_{jk+l}^h, \quad j \in \mathbb{N}. \tag{5.28}$$

However, to be consistent, we write

$$\Delta X_k^{2h} := X_{2h(k+1)}^{2h} - X_{2hk}^{2h}, \quad k = 0, \ldots, N-1.$$

Now we are ready to prove the asymptotic normality.

Proof. The proof consists of two parts. In the first part, we establish that $\sqrt{N}(\bar{\xi}_N - \bar{\eta})$ converges to a bivariate normal distribution. In the second part, we compute the entries of the asymptotic covariance matrix.

Step 1: Asymptotic normality. Recall that

$$\xi_{2N}^1 = \frac{1}{2N} \sum_{k=0}^{2N-1} \left(\Delta X_k^h\right)^2, \qquad \xi_N^2 = \frac{1}{N} \sum_{k=0}^{N-1} \left(\Delta X_k^{2h}\right)^2,$$

where $\Delta X_k^h = X_{(k+1)h}^h - X_{kh}^h$. By (5.27) express $\{\Delta X_k^{2h}\}$ in terms of $\{\Delta X_k^h\}$.

$$X_{kh}^{2h} = \tfrac{1}{2}\left(X_{2kh}^h + X_{(2k+1)h}^h\right),$$

which implies

$$\begin{aligned} \Delta X_k^{2h} &= \tfrac{1}{2}\left(X_{(2k+3)h}^h + X_{(2k+2)h}^h - X_{(2k+1)h}^h - X_{2kh}^h\right) && (5.29) \\ &= \tfrac{1}{2}\left(\Delta X_{2k+2}^h + 2\Delta X_{2k+1}^h + \Delta X_{2k}^h\right). && (5.30) \end{aligned}$$

Let us define $Y_k = (Y_k^{(1)}, Y_k^{(2)}, Y_k^{(3)})$, $k \in \mathbb{N}_0$, by

$$Y_k^{(1)} = \Delta X_{2k}^h, \qquad Y_k^{(2)} = \Delta X_{2k+1}^h, \qquad Y_k^{(3)} = \Delta X_{2k+2}^h. \tag{5.31}$$

Then

$$\xi_{2N}^1 = \frac{1}{2N}\sum_{k=0}^{N-1}\Big(\big(Y_k^{(1)}\big)^2 + \big(Y_k^{(2)}\big)^2\Big), \quad \xi_N^2 = \frac{1}{4N}\sum_{k=0}^{N-1}\big(Y_k^{(1)} + 2Y_k^{(2)} + Y_k^{(3)}\big)^2.$$

To prove the asymptotic normality of $(\xi_{2N}^1, \xi_N^2)^\top$, we use the so called Cramér–Wold device. Let $\alpha, \beta \in \mathbb{R}$ with $\alpha^2 + \beta^2 \neq 0$ and define

$$F(y) = \frac{\alpha}{2}(y_1^2 + y_2^2) + \frac{\beta}{4}(y_1 + 2y_2 + y_3)^2, \qquad y = (y_1, y_2, y_3)^\top \in \mathbb{R}^3.$$

then

$$\alpha\xi_{2N}^1 + \beta\xi_N^2 = \frac{1}{N}\sum_{k=0}^{N-1} F(Y_k).$$

Hence we need to show that

$$\sqrt{N}\Big(\alpha(\xi_{2N}^1 - \mathbb{E}[\xi_1^1]) + \beta(\xi_N^2 - \mathbb{E}[\xi_1^2])\Big) = \frac{1}{\sqrt{N}}\sum_{k=0}^{N-1}(F(Y_k) - \mathbb{E}[F(Y_k)]) \tag{5.32}$$

converges in distribution to a Gaussian law. This is proved by applying the Breuer–Major theorem for stationary Gaussian vectors [5, 61] ; see Theorem B.0.3 in the Appendix. To apply this result, we have to verify that

$$\sum_{n\in\mathbb{Z}} |r^{(p,l)}(n)|^q < \infty, \quad \text{for all} \quad p, l \in \{1, 2, 3\} \tag{5.33}$$

where

$$r^{(p,l)}(n) := \mathbb{C}\mathrm{ov}(Y_k^{(p)}, Y_{k+n}^{(l)}),$$

for $n \in \mathbb{Z}$, where k is any large enough number such that $k, k+n \geq 0$, and q is the Hermite rank[2] of f with respect to Y_1. In our case, we have $q \geq 2$. The identification of the Hermite rank relies on the same argument presented in [68]. Since $q \geq 2$, in order to verify the condition (5.33), it is suffices to prove that

$$\sum_{n\in\mathbb{Z}} |r^{(p,l)}(n)|^2 < \infty, \quad \text{for all} \quad p, l \in \{1, 2, 3\}. \tag{5.34}$$

This can be proven, using (5.31), the definition of $\gamma(H, n)$ and its asymptotic behavior (Lemma

[2]The function $f : \mathbb{R}^d \to \mathbb{R}$ is said to have Hermite rank equal to q with respect to a random vector X if (a) $\mathbb{E}[(f(x) - \mathbb{E}[f(x)])p_m(X)] = 0$ for every polynomial p_m (on $\mathbb{R}^d$) of degree $m \leq q-1$; and (b) there exists a polynomial p_q of degree q such that$\mathbb{E}[(f(x) - \mathbb{E}[f(x)])p_q(X)] \neq 0$. More details in [61].

5.1.4). Indeed, we can express $r^{(p,l)}$ as follows:

$$
\begin{aligned}
&r^{(1,1)}(n) = \mathbb{C}ov(Y_1^{(1)}, Y_{1+n}^{(1)}) = h^{2H}\gamma(H, 2n), && r^{(1,2)}(n) = \mathbb{C}ov(Y_1^{(1)}, Y_{1+n}^{(2)}) = h^{2H}\gamma(H, 2n+1),\\
&r^{(1,3)}(n) = \mathbb{C}ov(Y_1^{(1)}, Y_{1+n}^{(3)}) = h^{2H}\gamma(H, 2n+2), && r^{(2,1)}(n) = \mathbb{C}ov(Y_1^{(2)}, Y_{1+n}^{(1)}) = h^{2H}\gamma(H, 2n-1),\\
&r^{(2,2)}(n) = \mathbb{C}ov(Y_1^{(2)}, Y_{1+n}^{(2)}) = h^{2H}\gamma(H, 2n), && r^{(2,3)}(n) = \mathbb{C}ov(Y_1^{(2)}, Y_{1+n}^{(3)}) = h^{2H}\gamma(H, 2n+1),\\
&r^{(3,1)}(n) = \mathbb{C}ov(Y_1^{(3)}, Y_{1+n}^{(1)}) = h^{2H}\gamma(H, 2n-2), && r^{(3,2)}(n) = \mathbb{C}ov(Y_1^{(3)}, Y_{1+n}^{(2)}) = h^{2H}\gamma(H, 2n-1),\\
&r^{(3,3)}(n) = \mathbb{C}ov(Y_1^{(3)}, Y_{1+n}^{(3)}) = h^{2H}\gamma(H, 2n).
\end{aligned}
$$

Now, considering, for example, the series

$$\sum_{n=-\infty}^{\infty} (r^{(1,1)})^2(n) = h^{4H} \sum_{n=-\infty}^{\infty} \gamma(H, 2n)^2,$$

it is easy to see that by Lemma 5.2.2, this series converges for $H < \frac{3}{4}$. The other cases are analogous. Consequently, the conditions required by the Breuer–Major theorem for stationary vectors are fulfilled, which implies that (5.32) converges weakly to a centered normal distribution.

Step 2: Identification of the asymptotic covariance matrix.
To determine the form of the covariance matrix of the limiting distribution, we analyze the asymptotic behavior as $N \to \infty$ of the following variances and covariances:

$$N\,\mathrm{Var}(\xi_{2N}^1), \quad N\,\mathrm{Var}(\xi_N^2), \quad N\,\mathrm{Cov}(\xi_{2N}^1, \xi_N^2).$$

We start by computing the variances. By exploiting the stationarity of the sequence $\{\Delta X_k^h\}_k$ and using the formula (B.2), we obtain Hence

$$
\begin{aligned}
N\,\mathrm{Var}(\xi_{2N}^1) &= \frac{1}{4N}\mathrm{Var}\Big(\sum_{k=0}^{2N-1}(\Delta X_k^h)^2\Big) = \frac{1}{4N}\sum_{k=0}^{2N-1}\sum_{j=0}^{2N-1}\mathrm{cov}\Big((\Delta X_k^h)^2, (\Delta X_j^h)^2\Big)\\
&= \frac{h^{4H}}{2N}\sum_{k=0}^{2N-1}\sum_{j=0}^{2N-1}\gamma(H, k-j)^2.
\end{aligned}
$$

Upon rearrangement of the sum[3], we get

$$\begin{aligned} N\operatorname{Var}(\xi^1_{2N}) &= \frac{h^{4H}}{2N}\sum_{k=0}^{2N-1}\sum_{i=k-2N+1}^{k}\gamma(H,i)^2 \\ &= \frac{h^{4H}}{2N}\sum_{i=-2N+1}^{0}\sum_{k=0}^{2N-1+i}\gamma(H,i)^2 + \frac{h^{4H}}{2N}\sum_{i=1}^{2N-1}\sum_{k=i}^{2N-1}\gamma(H,i)^2 \\ &= h^{4H}\sum_{i=-2N+1}^{2N-1}\Big(1-\frac{|i|}{2N}\Big)\gamma(H,i)^2 \to h^{4H}\sum_{i=-\infty}^{\infty}\gamma(H,i)^2, \end{aligned} \tag{5.35}$$

as $N\to\infty$, where the interchange of limit and summation is justified by the dominated convergence theorem, as ensured by Lemma 5.1.4.

Analogous computations yield

$$N\operatorname{Var}(\xi^2_N) \to 2^{4H+1}h^{4H}\sum_{i=-\infty}^{\infty}\gamma(H,i)^2, \quad \text{as } N\to\infty.$$

We now compute the asymptotic behavior of the covariance between ξ^1_{2N} and ξ^2_N.

$$\begin{aligned} N\operatorname{cov}\left(\xi^1_{2N},\xi^2_N\right) &= N\operatorname{cov}\left(\frac{1}{2N}\sum_{k=0}^{2N-1}(\Delta X^h_k)^2, \frac{1}{N}\sum_{j=0}^{N-1}(\Delta X^{2h}_j)^2\right) \\ &= \frac{1}{8N}\operatorname{cov}\left(\sum_{k=0}^{N-1}\left((\Delta X^h_{2k})^2+(\Delta X^h_{2k+1})^2\right), \sum_{j=0}^{N-1}(\Delta X^h_{2j+2}+2\Delta X^h_{2j+1}+\Delta X^h_{2j})^2\right) \\ &= \frac{1}{8N}\sum_{k=0}^{N-1}\sum_{j=0}^{N-1}\operatorname{cov}\Big((\Delta X^h_{2k})^2+(\Delta X^h_{2k+1})^2, (\Delta X^h_{2j+2}+2\Delta X^h_{2j+1}+\Delta X^h_{2j})^2\Big) \\ &= \frac{1}{4N}\sum_{k=0}^{N-1}\sum_{j=0}^{N-1}\Big[\Big(\operatorname{cov}\left(\Delta X^h_{2k}, \Delta X^h_{2j+2}+2\Delta X^h_{2j+1}+\Delta X^h_{2j}\right)\Big)^2 \\ &\qquad + \Big(\operatorname{cov}\left(\Delta X^h_{2k+1}, \Delta X^h_{2j+2}+2\Delta X^h_{2j+1}+\Delta X^h_{2j}\right)\Big)^2\Big], \end{aligned}$$

where we used formula (B.2).

Expressing the covariances in terms of $\gamma(H,n)$, we obtain

$$\begin{aligned} N\operatorname{cov}(\xi^1_{2N},\xi^2_N) = \frac{h^{4H}}{4N}\sum_{k=0}^{N-1}\sum_{j=0}^{N-1}\Big[&\big(\gamma(H,2k-2j-2)+2\gamma(H,2k-2j-1)+\gamma(H,2k-2j)\big)^2 \\ &+\big(\gamma(H,2k-2j-1)+2\gamma(H,2k-2j)+\gamma(H,2k-2j+1)\big)^2\Big]. \end{aligned}$$

[3]The weight $\left(1-\frac{|i|}{N}\right)$ comes from rewriting the double sum $\frac{1}{N}\sum_{k=0}^{N-1}\sum_{j=0}^{N-1}f(j-k)$ as $\sum_{i=-N+1}^{N-1}(1-|i|/N)f(i)$, since for each fixed $i\in\{-N+1,\dots,N-1\}$ there are $N-|i|$ pairs (j,k) with $j-k=i$.

Proceeding as in (5.35), by rearranging the sums and passing to the limit as $N \to \infty$, we obtain

$$\begin{aligned} N\,\mathrm{cov}(\xi^1_{2N}, \xi^2_N) \to \frac{h^{4H}}{2} \sum_{i=-\infty}^{\infty} \Big[\big(\gamma(H,2i-2) + 2\gamma(H,2i-1) + \gamma(H,2i)\big)^2 \\ + \big(\gamma(H,2i-1) + 2\gamma(H,2i) + \gamma(H,2i+1)\big)^2 \Big] \\ = \frac{h^{4H}}{2} \sum_{j=-\infty}^{\infty} \big(\gamma(H,j) + 2\gamma(H,j+1) + \gamma(H,j+2)\big)^2. \end{aligned}$$

Finally, expanding the square and exploiting the shift-invariance of the sums yields the expression for $\widetilde{\Sigma}_{12}$ stated in the theorem. This completes the proof. □

We now want prove the asymptotic normality of $\hat{\theta}_N = (\widehat{H}_N, \hat{a}^2_N)$. Consider the vector-valued function $f(\theta) = (f_1(\theta), f_2(\theta))$, with $f_1(\theta) = \mathbb{E}(\xi^1_n)$ and $f_2(\theta) = \mathbb{E}(\xi^2_n)$, computed in Lemma 5.2.1.

Theorem 5.2.3. *Let $0 < H < \frac{3}{4}$. The estimator $\hat{\theta}_N = (\widehat{H}_N, \hat{a}^2_N)^\top$ is asymptotically normal, that is*

$$\sqrt{N}(\hat{\theta}_N - \theta) = \sqrt{N} \begin{pmatrix} \widehat{H}_N - H \\ \hat{a}^2_N - a^2 \end{pmatrix} \xrightarrow{d} \mathcal{N}\big(0, \Sigma_0\big),$$

with the asymptotic covariance matrix Σ_0 given by

$$\Sigma_0 = \big(f'(\theta)\big)^{-1} \widetilde{\Sigma} \,(\big(f'(\theta)\big)^{-1})^\top, \tag{5.36}$$

where f' is the Jacobian matrix of f and $\widetilde{\Sigma}$ is defined in Theorem 5.2.2.

Proof. We apply delta method (B.0.2) for function q constructed in Theorem 5.2.1 as a vector of two component, in particular $q_1 = \hat{H}(\xi^1_{2N}, \xi^2_N)$ and $q_2 = \hat{a}^2(\xi^1_{2N}, \xi^2_N)$ considering that for the sequence $\bar{\xi}_N$ we proved asymptotic normality in Theorem 5.2.2. To apply the delta method, it is necessary to compute the derivative matrix of q and verify its nonsingularity. However, due to the complexity of q, we instead calculate the derivative matrix of f at θ, since by the inverse function theorem, $q' = (f')^{-1}$. Showing that $f'(\theta)$ is nonsingular thus ensures that q' exists and is nonsingular as well, allowing the application of the delta method. Thus, we first evaluate the partial derivative of f. We have

$$f_1(\theta) = \frac{2h^{2H}}{(2H+1)(H+1)} a^2 \big(2^{2H} - 1\big),$$

hence

$$\frac{\partial f_1}{\partial H} = 2a^2 h^{2H} \frac{\big[2\ln(h)(2^{2H}-1) + 2\ln(2)\,2^{2H}\big]\,(2H+1)(H+1) - (2^{2H}-1)(4H+3)}{\big((2H+1)(H+1)\big)^2} \tag{5.37}$$

and

$$\frac{\partial f_1}{\partial a^2} = \frac{2h^{2H}}{(2H+1)(H+1)}\big(2^{2H}-1\big) \tag{5.38}$$

Consider now,

$$f_2(\theta) = \frac{2a^2h^{2H}2^{2H}(2^{2H}-1)}{(2H+1)(H+1)}.$$

Letting

$$N(\theta) = 2a^2h^{2H}2^{2H}(2^{2H}-1), \qquad D(\theta) = (2H+1)(H+1),$$

$$\begin{aligned}\frac{\partial D}{\partial H} &= \big((2H+1)(H+1)\big) = 2(H+1)+(2H+1) = 4H+3,\\ \frac{\partial N}{\partial H} &= 2a^2\left[h^{2H}2^{2H}(2\log h+2\log 2)(2^{2H}-1)+h^{2H}2^{2H}\big(2\log 2\cdot 2^{2H}\big)\right],\end{aligned}$$

whence,

$$\begin{aligned}\frac{\partial f_2}{\partial H} &= \frac{2a^2h^{2H}2^{2H}}{((2H+1)(H+1))^2}\\ &\times\left[\big((2\log h+2\log 2)(2^{2H}-1)+2\log 2\cdot 2^{2H}\big)(2H+1)(H+1)-(2^{2H}-1)(4H+3)\right].\end{aligned}$$

and

$$\frac{\partial f_2}{\partial a^2} = \frac{h^{2H}2^{2H+1}(2^{2H}-1)}{(2H+1)(H+1)}. \tag{5.39}$$

By computing the determinant of the Jacobian matrix $f' = \begin{pmatrix}\partial f_1/\partial H & \partial f_1/\partial a^2\\ \partial f_2/\partial H & \partial f_2/\partial a^2\end{pmatrix}$, we obtain

$$\det\big(f'(\theta)\big) = -\frac{a^2h^{4H}2^{2H+3}\log 2\big(2^{2H}-1\big)^2}{(2H+1)^2(H+1)^2}.$$

It is easy to see that the determinant is strictly negative for all positive a, h, and H. This guarantees the invertibility of the matrix $f'(\bar{\theta})$ in the considered parameter domain. The application of the delta method concludes the proof. □

Remark 5.2.4. *For $H > \frac{3}{4}$, the dependence structure becomes too strong and the classical central limit theorem generally fails. Therefore, asymptotic normality cannot be guaranteed. In this regime, suitably normalized statistics may converge to non-Gaussian limits.*

Simulation: Hurst parameter and diffusion coefficient in the model with one nifBm We assess the numerical performance of the estimator $\hat{\theta}_N = (\widehat{H}_N, \hat{a}^2_N)$ defined in equations (5.19) and (5.20).

For a fixed step size h, we generate the increments ΔX^h using the Cholesky method based on the covariance structure. The realization of ΔX^{2h} is then computed according to (5.30), so that it incorporates half of the increments present in ΔX^h. From these processes, we compute the

statistics ξ_N^j, $j = 1, 2$, to study the behavior of the estimator. For each combination of H and h, we simulate a trajectory and apply the estimators to obtain estimates of H and a^2. We report the empirical mean and the standard deviation over 100 replications and, using the covariance matrix (5.36), we also compute the theoretical standard deviation, the value of a is fixed to 1.

Table 5.1 presents the performance of the estimators $\widehat{H}_N$ and $\widehat{a}_N^2$ for $H \in \{0.1, 0.3, 0.5, 0.7\}$, $h \in \{2, 2^2, 2^4\}$, and sample sizes $N = 2^n$, $n \in \{6, 8, 10, 12\}$. In the table, the empirical mean of the estimators is denoted by $\mathbf{m}(\cdot)$, while $\boldsymbol{\sigma}_{\mathbf{e}}(\cdot)$ represents the empirical standard deviation. The symbol $\boldsymbol{\sigma}_{\mathbf{t}}(\cdot)$ denotes the corresponding theoretical standard deviation. The estimator $\widehat{H}_N$ shows almost unbiased behavior in all Hurst parameters, with only slight deviations for small N and extreme H values, particularly $H = 0.1$. Its empirical standard deviation $\boldsymbol{\sigma}_{\mathbf{e}}(\widehat{H}_N)$ decreases rapidly with N and closely matches the theoretical standard deviation $\boldsymbol{\sigma}_{\mathbf{t}}(\widehat{H}_N)$ for moderate and large samples, confirming the accuracy of the theoretical variance formula. The increment size h exerts minimal influence on $\widehat{H}_N$, slightly affecting variability only for small N.

In contrast, the diffusion coefficient estimator $\widehat{a}_N^2$ is considerably more sensitive to both sample size N and averaging window h. For small N and large h, it exhibits pronounced bias and elevated variability, especially for small Hurst indices ($H = 0.1$ or 0.3). As N increases, both bias and variability diminish and the empirical standard deviation converges toward the theoretical value.

These results indicate that $\widehat{H}_N$ provides stable and reliable estimates even for moderate N, whereas accurate estimation of $\widehat{a}_N^2$ requires sufficiently large samples and moderate values of h.

5.2.3 Estimation of the parameters H_1, H_2, a^2, and b^2 in the model with two nifBms

We aim to estimate the parameter vector $\theta = (H_1, H_2, a^2, b^2)$ of the process

$$\widetilde{X}_k^h = aX_{kh}^{h,H_1} + bX_{kh}^{h,H_2}. \qquad a, b \neq 0. \tag{5.40}$$

Since four parameters must be estimated, we apply Theorem 2.0.2 and construct four corresponding statistics. The first two coincide with those introduced in the previous section, while two additional statistics are defined for $j = 4, 8$. In this way, we obtain a family of statistics based on the increments

$$\Delta\widetilde{X}_k^{jh} = \widetilde{X}_{k+1}^{jh} - \widetilde{X}_k^{jh},$$

for $j = 1, 2, 4, 8$, whose stationarity can be established similarly to $\Delta\widetilde{X}_k^h$. Thus, let us denote:

$$\xi_N^j := \frac{1}{N}\sum_{k=0}^{N-1}\left(\widetilde{X}_{k+1}^{jh} - \widetilde{X}_k^{jh}\right)^2 = \frac{1}{N}\sum_{k=0}^{N-1}\left(\Delta\widetilde{X}_k^{jh}\right)^2, \quad j = 1, 2, 4, 8. \tag{5.41}$$

All are constructed in the same manner, differing only in the time step used to compute the increment of the process (5.12). This strategy ensures that, all the power functions appearing in the estimating equations are powers of 2, which considerably simplifies the explicit derivation of the

Table 5.1: Estimators $\widehat{H}_N$ and $\widehat{a}^2_N$ in the model with one nifBm.

	$h=2$				$h=2^2$				$h=2^4$			
	$N=2^6$	2^8	2^{10}	2^{12}	2^6	2^8	2^{10}	2^{12}	2^6	2^8	2^{10}	2^{12}
$H=0.1$												
$\mathbf{m}(\widehat{H}_N)$	0.0746	0.0834	0.1022	0.1000	0.0952	0.1002	0.0967	0.1026	0.1096	0.1055	0.1001	0.1015
$\boldsymbol{\sigma}_\mathbf{e}(\widehat{H}_N)$	0.1713	0.0833	0.0352	0.0198	0.1483	0.0669	0.0362	0.0195	0.1635	0.0752	0.0357	0.0196
$\boldsymbol{\sigma}_\mathbf{t}(\widehat{H}_N)$	0.1087	0.0544	0.0272	0.0136	0.1087	0.0544	0.0272	0.0136	0.1087	0.0544	0.0272	0.0136
$\mathbf{m}(\widehat{a}^2_N)$	2.0548	1.7555	1.2109	1.0352	2.4617	2.0531	1.7098	1.0147	3.9263	0.8146	1.8697	1.0452
$\boldsymbol{\sigma}_\mathbf{e}(\widehat{a}^2_N)$	16.830	7.0895	0.8605	0.0867	26.357	7.1395	3.1218	0.2407	31.873	5.3269	6.3387	0.3355
$\boldsymbol{\sigma}_\mathbf{t}(\widehat{a}^2_N)$	1.0176	0.5088	0.2544	0.0718	1.1663	0.5831	0.2916	0.1458	1.4649	0.7325	0.3662	0.1831
$H=0.3$												
$\mathbf{m}(\widehat{H}_N)$	0.2715	0.2961	0.3000	0.3004	0.3067	0.2948	0.3052	0.2993	0.2875	0.2934	0.2980	0.3004
$\boldsymbol{\sigma}_\mathbf{e}(\widehat{H}_N)$	0.1325	0.6090	0.0320	0.0159	0.1377	0.0594	0.0327	0.0153	0.1435	0.0622	0.0358	0.0141
$\boldsymbol{\sigma}_\mathbf{t}(\widehat{H}_N)$	0.1194	0.0597	0.0298	0.0149	0.1194	0.0597	0.0298	0.0149	0.1194	0.0597	0.0298	0.0149
$\mathbf{m}(\widehat{a}^2_N)$	1.1625	1.0719	1.0082	1.0023	4.2266	1.0948	0.9937	1.0066	0.8646	1.2299	1.0609	1.0041
$\boldsymbol{\sigma}_\mathbf{e}(\widehat{a}^2_N)$	4.3630	0.3158	0.1328	0.0597	9.9780	0.3462	0.1743	0.0768	7.3627	0.7895	0.3227	0.1095
$\boldsymbol{\sigma}_\mathbf{t}(\widehat{a}^2_N)$	0.4354	0.2177	0.1089	0.0544	0.5904	0.2952	0.1476	0.0738	0.9115	0.4557	0.2279	0.1139
$H=0.5$												
$\mathbf{m}(\widehat{H}_N)$	0.4826	0.5024	0.4990	0.4998	0.4936	0.4957	0.4952	0.5002	0.4981	0.4977	0.5031	0.4979
$\boldsymbol{\sigma}_\mathbf{e}(\widehat{H}_N)$	0.1175	0.0523	0.0311	0.0121	0.1161	0.0529	0.0277	0.0118	0.1187	0.0548	0.0252	0.0125
$\boldsymbol{\sigma}_\mathbf{t}(\widehat{H}_N)$	0.1104	0.0552	0.0276	0.0138	0.1104	0.0552	0.0276	0.0138	0.1104	0.0522	0.0276	0.0138
$\mathbf{m}(\widehat{a}^2_N)$	1.1302	1.0085	1.0113	1.0023	1.2494	1.0489	1.0231	0.9995	1.3550	1.0952	0.9873	1.0181
$\boldsymbol{\sigma}_\mathbf{e}(\widehat{a}^2_N)$	0.4158	0.1355	0.0729	0.0311	1.2327	0.2178	0.1098	0.0484	1.1090	0.4620	0.1572	0.0795
$\boldsymbol{\sigma}_\mathbf{t}(\widehat{a}^2_N)$	0.3023	0.1512	0.0759	0.0378	0.4351	0.2176	0.1088	0.0544	0.7252	0.3626	0.1813	0.0906
$H=0.7$												
$\mathbf{m}(\widehat{H}_N)$	0.6804	0.6940	0.7006	0.6976	0.6854	0.6959	0.6970	0.7007	0.6826	0.6943	0.6967	0.7006
$\boldsymbol{\sigma}_\mathbf{e}(\widehat{H}_N)$	0.0787	0.0429	0.0232	0.0117	0.0989	0.0514	0.0234	0.0129	0.0864	0.0459	0.0253	0.0139
$\boldsymbol{\sigma}_\mathbf{t}(\widehat{H}_N)$	0.0902	0.0535	0.0294	0.0157	0.0902	0.0535	0.0294	0.0157	0.0902	0.0535	0.0294	0.0157
$\mathbf{m}(\widehat{a}^2_N)$	1.0750	0.9855	1.0005	0.9987	1.0805	1.0192	1.0101	0.9968	1.2327	1.0766	1.0194	0.9950
$\boldsymbol{\sigma}_\mathbf{e}(\widehat{a}^2_N)$	0.2457	0.0831	0.0463	0.0215	0.3890	0.1537	0.0564	0.0357	0.7304	0.2976	0.1283	0.0627
$\boldsymbol{\sigma}_\mathbf{t}(\widehat{a}^2_N)$	0.3042	0.1729	0.0934	0.0492	0.4713	0.2664	0.1436	0.0754	0.7583	0.4313	0.2331	0.1227

estimator $\hat{\theta}$ of vector θ.

Lemma 5.2.3. *The following a.s. convergences hold as $N \to \infty$:*

$$\xi_N^j \to \mathbb{E}(\xi_1^j) = A_1 a^2 \big(2^{2H_1} - 1\big) j^{2H_1} + A_2 b^2 \big(2^{2H_2} - 1\big) j^{2H_2}, \tag{5.42}$$

where $j = 1, 2, 4, 8$ and

$$A_i = \frac{2h^{2H_i}}{(2H_i + 1)(H_i + 1)}, \quad i = 1, 2.$$

Proof. The result follows directly from Lemma 5.2.1, using the independence of the processes B^{H_i}, $i = 1, 2$, together with the expression of $\mathbb{E}(\xi_1^j)$ obtained from formula (5.5) by replacing h with jh, for $j = 1, 2, 4, 8$. □

Now we are going to construct strongly consistent estimators of the parameter $\theta = (H_1, H_2, a^2, b^2)^\top$.

The subsequent notation will be used:

$$\log_+ x = \begin{cases} \log x, & \text{if } x > 0, \\ 0, & \text{if } x \le 0, \end{cases} \qquad \sqrt[+]{x} = \begin{cases} \sqrt{x}, & \text{if } x > 0, \\ 0, & \text{if } x \le 0. \end{cases}$$

Also, for any $N \ge 1$, we denote

$$D_N = \left(\xi_N^4 \xi_N^2 - \xi_N^8 \xi_N^1\right)^2 - 4\left(\xi_N^4 \xi_N^1 - \left(\xi_N^2\right)^2\right)\left(\xi_N^8 \xi_N^2 - \left(\xi_N^4\right)^2\right),$$
$$x_N = \frac{\xi_N^8 \xi_N^1 - \xi_N^4 \xi_N^2 + \sqrt[+]{D_N}}{2(\xi_N^4 \xi_N^1 - (\xi_N^2)^2)}, \qquad y_N = \frac{\xi_N^8 \xi_N^1 - \xi_N^4 \xi_N^2 - \sqrt[+]{D_N}}{2(\xi_N^4 \xi_N^1 - (\xi_N^2)^2)}.$$

Theorem 5.2.4. *Let $0 < H_2 < H_1 < 1$. The random vector $\hat{\theta}_N = (\widehat{H}_{1,N}, \widehat{H}_{2,N}, \hat{a}_N^2, \hat{b}_N^2)$, where*

$$\widehat{H}_{1,N} = \frac{1}{2\log 2} \log_+ (x_N), \tag{5.43}$$

$$\widehat{H}_{2,N} = \frac{1}{2\log 2} \log_+ (y_N), \tag{5.44}$$

$$\hat{a}_N^2 = \frac{\big(2\widehat{H}_{1,N} + 1\big)\big(\widehat{H}_{1,N} + 1\big)\,(\xi_N^2 - y_N \xi_N^1)}{2h^{2\widehat{H}_{1,N}}(x_N - y_N)(x_N - 1)}, \tag{5.45}$$

and

$$\hat{b}_N^2 = \frac{\big(2\widehat{H}_{2,N} + 1\big)\big(\widehat{H}_{2,N} + 1\big)\,(\xi_N^2 - x_N \xi_N^1)}{2h^{2\widehat{H}_{2,N}}(y_N - x_N)(y_N - 1)} \tag{5.46}$$

is a strongly consistent estimator of $\theta = (H_1, H_2, a^2, b^2)$.

Remark 5.2.5. *Condition of Theorem 5.2.4 does not mean that we should "know what index is bigger". It just means that taking x_N we estimate bigger index, and taking y_N we estimate the smaller one.*

Proof. Denote

$$x = 2^{2H_1}, \quad y = 2^{2H_2}, \quad A = a^2 A_1, \quad B = b^2 A_2,$$

$$\eta_j = \mathbb{E}(\xi_1^j),\ j = 1, 2, 4, 8.$$

Then the equalities in the right-hand side of (5.42) from Lemma 5.2.1 can be rewritten in the form

$$\eta_1 = A(x-1) + B(y-1), \tag{5.47}$$

$$\eta_2 = Ax(x-1) + By(y-1), \tag{5.48}$$

$$\eta_4 = Ax^2(x-1) + By^2(y-1), \tag{5.49}$$

$$\eta_8 = Ax^3(x-1) + By^3(y-1). \tag{5.50}$$

Solving the system of linear (w.r.t. A and B) equations (5.47) and (5.48), we can present the variables A and B as functions of x and y:

$$A = \frac{\eta_2 - y\eta_1}{(x-y)(x-1)}, \quad B = \frac{\eta_2 - x\eta_1}{(y-x)(y-1)}. \tag{5.51}$$

Inserting into (5.49) expressions (5.51) obtained for A and B, we get that

$$\begin{aligned}
\eta_4 &= \frac{\eta_2 - y\eta_1}{x-y}x^2 + \frac{\eta_2 - x\eta_1}{y-x}y^2 \\
&= \frac{1}{x-y}\big(\eta_2 x^2 - \eta_1 x^2 y - \eta_2 y^2 + \eta_1 x y^2\big) \\
&= \frac{1}{x-y}\big(\eta_2(x^2-y^2) - \eta_1 xy(x-y)\big) = \eta_2(x+y) - \eta_1 xy,
\end{aligned} \tag{5.52}$$

whence

$$x = \frac{\eta_4 - \eta_2 y}{\eta_2 - \eta_1 y}. \tag{5.53}$$

Note that $\eta_2 - \eta_1 y = A(x-1)(x-y)$, $A > 0$ (A is positive and can be zero only if $a = 0$ but this is the degenerate case with only one component for the process X_k^h), $x = 2^{H_1} > 0$, $x = 1$ if $H_1 = 0$ and $x - y = 0$ if $H_1 = H_2$. If we assume $H_1 \neq H_2$, the denominator is nonzero.

Similarly, it follows from (5.50) and (5.51) that

$$\begin{aligned}
\eta_8 &= \frac{\eta_2 - y\eta_1}{x-y}x^3 + \frac{\eta_2 - x\eta_1}{y-x}y^3 \\
&= \frac{1}{x-y}\big(\eta_2 x^3 - \eta_1 x^3 y - \eta_2 y^3 + \eta_1 x y^3\big) \\
&= \frac{1}{x-y}\big(\eta_2\left(x^3 - y^3\right) - \eta_1 xy(x^2 - y^2)\big) \\
&= \frac{1}{x-y}\big(\eta_2(x-y)(x^2+xy+y^2) - \eta_1 xy(x-y)(x+y)\big) \\
&= \eta_2\left(x^2 + xy + y^2\right) - \eta_1 xy(x+y).
\end{aligned} \tag{5.54}$$

Multiplying the right-hand side of (5.52) by $(x+y)$ and subtracting the right-hand side of (5.54),

we get that

$$\eta_2(x+y)^2 - \eta_2\left(x^2+xy+y^2\right) = \eta_4(x+y) - \eta_8,$$

whence

$$x = \frac{\eta_8 - \eta_4 y}{\eta_4 - \eta_2 y}. \tag{5.55}$$

Again, the denominator is nonzero. It follows from equations (5.53) and (5.55) that

$$\frac{\eta_8 - \eta_4 y}{\eta_4 - \eta_2 y} = \frac{\eta_4 - \eta_2 y}{\eta_2 - \eta_1 y},$$

and we obtain the following quadratic equation w.r.t. y:

$$y^2\left(\eta_1\eta_4 - \eta_2^2\right) + y(\eta_2\eta_4 - \eta_1\eta_8) + \left(\eta_2\eta_8 - \eta_4^2\right) = 0. \tag{5.56}$$

It is evident that x satisfies the same quadratic equation due to symmetry. Hence, x and y with $(x > y)$ are the two roots of equation (5.56),

$$x, y = \frac{(\eta_1\eta_8 - \eta_2\eta_4) \pm \sqrt{D}}{2(\eta_1\eta_4 - \eta_2^2)}, \tag{5.57}$$

where the denominator is again nonzero if $H_1 \neq H_2$, and

$$D = (\eta_2\eta_4 - \eta_1\eta_8)^2 - 4(\eta_1\eta_4 - \eta_2^2)(\eta_2\eta_8 - \eta_4^2). \tag{5.58}$$

Let us check if the discriminant D is nonnegative. We use the equalities (5.47)–(5.54) and conclude that

$$\begin{aligned}
\eta_2\eta_4 - \eta_1\eta_8 &= AB(x-1)(y-1)(xy^2 + x^2y - y^3 - x^3) && (5.59)\\
&= -AB(x-1)(y-1)(x+y)(x-y)^2 < 0,\\
\eta_1\eta_4 - \eta_2^2 &= AB(x-1)(y-1)(x^2 - 2xy + y^2) && (5.60)\\
&= AB(x-1)(y-1)(x-y)^2 > 0,\\
\eta_2\eta_8 - \eta_4^2 &= AB(x-1)(y-1)(xy^3 - 2xy^2 + x^3y) && (5.61)\\
&= AB(x-1)(y-1)xy(x-y)^2 > 0.
\end{aligned}$$

Thus

$$\begin{aligned}
D &= A^2B^2(x-1)^2(y-1)^2(x+y)^2(x-y)^4 - 4A^2B^2(x-1)^2(y-1)^2xy(x-y)^4\\
&= A^2B^2(x-1)^2(y-1)^2(x-y)^6 > 0.
\end{aligned}$$

Since D is positive, we have two different roots

$$x = \frac{\eta_1\eta_8 - \eta_2\eta_4 + \sqrt{D}}{2(\eta_1\eta_4 - \eta_2^2)}, \qquad y = \frac{\eta_1\eta_8 - \eta_2\eta_4 - \sqrt{D}}{2(\eta_1\eta_4 - \eta_2^2)} \tag{5.62}$$

Since $x = 2^{2H_1}$ and $y = 2^{2H_2}$, we get from (5.62) that

$$H_1 = \frac{1}{2\log 2}\log\left(\frac{\eta_1\eta_8 - \eta_2\eta_4 + \sqrt{D}}{2(\eta_1\eta_4 - \eta_2^2)}\right), \quad H_2 = \frac{1}{2\log 2}\log\left(\frac{\eta_1\eta_8 - \eta_2\eta_4 - \sqrt{D}}{2(\eta_1\eta_4 - \eta_2^2)}\right) \tag{5.63}$$

Recall that a^2 and b^2 can be obtained from equations (5.51):

$$a^2 = \frac{(2H_1+1)(H_1+1)(\eta_2 - y\eta_1)}{2h^{2H_1}(x-y)(x-1)}, \qquad b^2 = \frac{(2H_2+1)(H_2+1)(\eta_2 - x\eta_1)}{2h^{2H_2}(y-x)(y-1)}. \tag{5.64}$$

Now, in order to obtain the estimators, we substitute η_j with ξ_N^j in (5.62) and (5.63) and obtain D_N, x_N, y_N, $\widehat{H}_{1,N}$ and $\widehat{H}_{2,N}$. Then we substitute in (5.64) $\widehat{H}_{i,N}$, instead of H_i, $i = 1, 2$ obtaining $\hat{a}_N^2$ and $\hat{b}_N^2$. Note that the random denominators are asymptotically nonzero with probability 1. Strong consistency of these estimators follows from strong consistency of ξ_N^j. □

Remark 5.2.6. *The estimators for H_1 and H_2 do not depend explicitly on h, but only indirectly through the estimators ξ_N^j for $j = 1, 2, 4, 8$.*

Asymptotic normality in the model with two nifBms We now generalize theorems 5.2.2 and 5.2.3 to the case of the linear combination of two processes. The proof is omitted, since it relies on the same arguments as in the two-dimensional case, with only a substantial increase in algebraic complexity.

Remark 5.2.7. *In the spirit of the Remark 5.2.2 we consider a modified estimator $\widehat{\theta}_N$, where the statistics ξ_N^1, ξ_N^2, and ξ_N^4 are replaced by ξ_{8N}^1, ξ_{4N}^2, and ξ_{2N}^4, respectively. Accordingly, we introduce*

$$\bar{\xi}_N = (\xi_{8N}^1, \xi_{4N}^2, \xi_{2N}^4, \xi_N^8)^\top, \qquad \bar{\eta} = (\mathbb{E}(\xi_1^1), \mathbb{E}(\xi_1^2), \mathbb{E}(\xi_1^4), \mathbb{E}(\xi_1^8))^\top =: f(\theta),$$

where the expectations $\mathbb{E}(\xi_1^j)$, $j = 1, 2, 4, 8$, are given by (5.42).

Theorem 5.2.5. *Let $0 < H_1 < H_2 < \frac{3}{4}$. Then $\bar{\xi}_N$ is asymptotically normal, that is*

$$\sqrt{N}(\bar{\xi}_N - \bar{\eta}) = \sqrt{N}\begin{pmatrix} \xi_{8N}^1 - \mathbb{E}(\xi_1^1) \\ \xi_{4N}^2 - \mathbb{E}(\xi_1^2) \\ \xi_{2N}^4 - \mathbb{E}(\xi_1^4) \\ \xi_N^8 - \mathbb{E}(\xi_1^8) \end{pmatrix} \xrightarrow{d} \mathcal{N}\big(0, \widetilde{\Sigma}\big), \quad \text{as } N \to \infty.$$

Moreover, the estimator $\widehat{\theta}_N = (\widehat{H}_{1,N}, \widehat{H}_{2,N}, \widehat{a}_N^2, \widehat{b}_N^2)^\top$ *is asymptotically normal, that is*

$$\sqrt{N}(\widehat{\theta}_N - \theta) = \sqrt{N} \begin{pmatrix} \widehat{H}_{1,N} - H \\ \widehat{H}_{2,N} - H \\ \widehat{a}_N^2 - a^2 \\ \widehat{b}_N^2 - b^2 \end{pmatrix} \xrightarrow{d} \mathcal{N}\big(0, \Sigma_0\big), \quad \text{as } N \to \infty.$$

with the asymptotic covariance matrix Σ_0 *given by*

$$\Sigma_0 = \big(J_f(\theta)\big)^{-1} \widetilde{\Sigma} \left(\big(J_f(\theta)\big)^{-1}\right)^\top,$$

where J_f *is the Jacobian matrix of* f*.*

Simulation: Hurst parameters and diffusion coefficients in a model with two nifBm. For the estimation of the parameter vector $\theta = (H_1, H_2, a^2, b^2)$, we employ the estimators from Theorem 5.2.4, which relies on the statistics ξ_N^j for $j = 1, 2, 4, 8$.

The one-dimensional simulation procedure is inefficient here, since computing $\Delta\widetilde{X}_k^{jh}$ via (5.30) reduces the number of realizations, slowing estimator convergence. While asymptotically valid, this approach requires a larger number of observations N for reasonable accuracy.

To overcome this, we directly simulate the increments $\Delta\widetilde{X}_k^{jh}$ using Cholesky decomposition and compute ξ_N^j from the covariance structure:

$$\mathbb{E}\left[\Delta\widetilde{X}_k^{jh}\, \Delta\widetilde{X}_{k+n}^{jh}\right] = a^2(jh)^{2H_1}\gamma(H_1, n) + b^2(jh)^{2H_2}\gamma(H_2, n), \quad n = 0, \ldots, N,\ j = 1, 2, 4, 8. \tag{5.65}$$

Since the covariance differs only by the factor jh, it suffices to compute it once for $j = 1$, and the other statistics can be obtained by rescaling. This reduces computational cost, eliminates repeated increment calculations, and ensures the same number of observations for all statistics. Stationarity of $\Delta\widetilde{X}_k^{jh}$ further simplifies computation, as the covariance matrix is Toeplitz.

Table 5.2 presents the results for the estimator parameter vector $\theta = (H_1, H_2, a^2, b^2)$ across five different pairs of H_1 and H_2 with $H_1 < H_2$, where the scale parameters a and b are both set to 2. The simulation results indicate that the Hurst estimators $\widehat{H}_{1,N}$ and $\widehat{H}_{2,N}$ are generally unbiased and become increasingly precise as the sample size N grows, with $\widehat{H}_{2,N}$ showing particularly robust performance across all scenarios. Estimating a very small H_1 in the presence of a larger H_2 proves more challenging, resulting in slight bias and increased variance, especially for small N and larger increment sizes h. The scale parameter estimator $\widehat{b}_N^2$ remains consistently accurate and stable, whereas $\widehat{a}_N^2$ can exhibit considerable variance and bias under these challenging conditions but stabilizes with larger N or smaller h. Overall, all estimators perform well for moderate Hurst parameters ($H \geq 0.3$), with precision improving as N increases and h decreases, highlighting the robustness of $\widehat{H}_{2,N}$ and $\widehat{b}_N^2$ and the sensitivity of $\widehat{H}_{1,N}$ and $\widehat{a}_N^2$ in difficult regimes. Notably, when $N \geq 2^{10}$, all parameters are estimated with high accuracy and stability across all configurations.

Table 5.2: Estimators $\widehat{H}_{1,N}$, $\widehat{H}_{2,N}$, $\widehat{a}^2_N$ and $\widehat{b}^2_N$ in the model with two nifBms.

	$h=2$				$h=2^2$				$h=2^4$			
	$N=2^6$	2^8	2^{10}	2^{12}	2^6	2^8	2^{10}	2^{12}	2^6	2^8	2^{10}	2^{12}
						$H_1=0.1$, $H_2=0.3$						
$\mathbf{m}(\widehat{H}_1)$	0.0904	0.0992	0.0997	0.1000	0.0999	0.0998	0.0997	0.0999	0.0970	0.0995	0.0995	0.0999
$\boldsymbol{\sigma}_{\mathbf{e}}(\widehat{H}_1)$	0.0204	0.0064	0.0032	0.0016	0.0200	0.0078	0.0037	0.0019	0.0301	0.0108	0.0050	0.0025
$\mathbf{m}(\widehat{H}_2)$	0.3018	0.3001	0.3001	0.3000	0.3000	0.3000	0.3001	0.3000	0.3000	0.3000	0.3000	0.3000
$\boldsymbol{\sigma}_{\mathbf{e}}(\widehat{H}_2)$	0.0047	0.0014	0.0007	0.0004	0.0032	0.0013	0.0007	0.0003	0.0025	0.0010	0.0005	0.0003
$\mathbf{m}(\widehat{a}^2)$	4.0911	4.1431	4.0196	4.0080	4.2818	4.1285	4.0211	4.0083	8.9166	4.1510	4.0266	4.0094
$\boldsymbol{\sigma}_{\mathbf{e}}(\widehat{a}^2)$	0.6753	0.4501	0.2311	0.0947	0.9985	0.4037	0.2288	0.0935	45.583	0.3691	0.2178	0.0888
$\mathbf{m}(\widehat{b}^2)$	3.7943	3.9307	4.0233	4.0146	4.0705	3.9818	4.0235	4.0148	4.0594	3.9781	4.0246	4.0143
$\boldsymbol{\sigma}_{\mathbf{e}}(\widehat{b}^2)$	1.0540	0.3951	0.1964	0.0979	0.8183	0.4022	0.1939	0.0967	0.8020	0.3958	0.1898	0.0949
						$H_1=0.1$, $H_2=0.5$						
$\mathbf{m}(\widehat{H}_1)$	0.0912	0.1007	0.0993	0.1000	0.0646	0.0999	0.0988	0.0999	0.0420	0.0931	0.0965	0.0996
$\boldsymbol{\sigma}_{\mathbf{e}}(\widehat{H}_1)$	0.0710	0.0218	0.0108	0.0047	0.3199	0.0297	0.0143	0.0062	0.5585	0.0626	0.0260	0.0109
$\mathbf{m}(\widehat{H}_2)$	0.5000	0.4999	0.5000	0.5000	0.5001	0.4999	0.5000	0.5000	0.5004	0.5000	0.5000	0.5000
$\boldsymbol{\sigma}_{\mathbf{e}}(\widehat{H}_2)$	0.0042	0.0017	0.0009	0.0004	0.0033	0.0013	0.0007	0.0003	0.0017	0.0008	0.0004	0.0002
$\mathbf{m}(\widehat{a}^2)$	3.8037	4.1390	4.0716	4.0197	4.6736	5.5225	4.1137	4.0256	0.0849	3.5420	4.5804	4.0641
$\boldsymbol{\sigma}_{\mathbf{e}}(\widehat{a}^2)$	3.5598	0.5714	0.2013	0.0976	8.7652	11.2864	0.2976	0.1231	48.779	6.0159	2.0301	0.2967
$\mathbf{m}(\widehat{b}^2)$	4.0703	4.0809	4.0120	4.0029	4.0614	4.0776	4.0119	4.0028	3.9782	4.0721	4.0118	4.0026
$\boldsymbol{\sigma}_{\mathbf{e}}(\widehat{b}^2)$	0.7711	0.3679	0.1921	0.0882	0.7615	0.3631	0.1896	0.0874	0.9350	0.3572	0.1866	0.0863
						$H_1=0.3$, $H_2=0.5$						
$\mathbf{m}(\widehat{H}_1)$	0.3012	0.3005	0.3002	0.3000	0.2998	0.3000	0.3001	0.3000	0.2999	0.2997	0.3000	0.3000
$\boldsymbol{\sigma}_{\mathbf{e}}(\widehat{H}_1)$	0.0203	0.0065	0.0034	0.0017	0.0211	0.0072	0.0036	0.0018	0.0300	0.0105	0.0050	0.0025
$\mathbf{m}(\widehat{H}_2)$	0.5001	0.5000	0.5000	0.5000	0.5001	0.5000	0.5000	0.5000	0.5000	0.5000	0.5000	0.5000
$\boldsymbol{\sigma}_{\mathbf{e}}(\widehat{H}_2)$	0.0041	0.0016	0.0008	0.0004	0.0033	0.0013	0.0007	0.0003	0.0017	0.0008	0.0004	0.0002
$\mathbf{m}(\widehat{a}^2)$	4.0112	4.0211	4.0135	4.0081	4.0145	4.0120	4.0105	4.0078	4.0123	4.0105	4.0089	4.0075
$\boldsymbol{\sigma}_{\mathbf{e}}(\widehat{a}^2)$	0.4421	0.2151	0.1108	0.0543	0.3981	0.1983	0.1021	0.0502	0.3652	0.1856	0.0952	0.0467
$\mathbf{m}(\widehat{b}^2)$	4.0110	4.0132	4.0100	4.0080	4.0108	4.0125	4.0103	4.0080	4.0105	4.0120	4.0101	4.0079
$\boldsymbol{\sigma}_{\mathbf{e}}(\widehat{b}^2)$	0.4012	0.1920	0.0961	0.0482	0.3920	0.1873	0.0928	0.0465	0.3845	0.1821	0.0912	0.0453
						$H_1=0.3$, $H_2=0.7$						
$\mathbf{m}(\widehat{H}_1)$	0.3001	0.3000	0.3000	0.3000	0.3001	0.3000	0.3000	0.3000	0.3002	0.3000	0.3000	0.3000
$\boldsymbol{\sigma}_{\mathbf{e}}(\widehat{H}_1)$	0.0202	0.0064	0.0033	0.0017	0.0210	0.0071	0.0035	0.0017	0.0299	0.0104	0.0049	0.0025
$\mathbf{m}(\widehat{H}_2)$	0.7000	0.7000	0.7000	0.7000	0.7000	0.7000	0.7000	0.7000	0.7000	0.7000	0.7000	0.7000
$\boldsymbol{\sigma}_{\mathbf{e}}(\widehat{H}_2)$	0.0035	0.0015	0.0007	0.0003	0.0027	0.0010	0.0005	0.0002	0.0016	0.0008	0.0004	0.0002
$\mathbf{m}(\widehat{a}^2)$	4.0102	4.0121	4.0105	4.0078	4.0108	4.0118	4.0104	4.0079	4.0105	4.0117	4.0102	4.0078
$\boldsymbol{\sigma}_{\mathbf{e}}(\widehat{a}^2)$	0.4441	0.2120	0.1090	0.0530	0.3960	0.1952	0.1018	0.0495	0.3615	0.1835	0.0938	0.0453
$\mathbf{m}(\widehat{b}^2)$	4.0112	4.0125	4.0103	4.0079	4.0109	4.0120	4.0102	4.0078	4.0106	4.0118	4.0101	4.0078
$\boldsymbol{\sigma}_{\mathbf{e}}(\widehat{b}^2)$	0.4010	0.1915	0.0958	0.0478	0.3921	0.1865	0.0924	0.0462	0.3825	0.1815	0.0909	0.0451
						$H_1=0.5$, $H_2=0.7$						
$\mathbf{m}(\widehat{H}_1)$	0.5000	0.5000	0.5000	0.5000	0.5000	0.5000	0.5000	0.5000	0.5000	0.5000	0.5000	0.5000
$\boldsymbol{\sigma}_{\mathbf{e}}(\widehat{H}_1)$	0.0042	0.0017	0.0008	0.0004	0.0033	0.0013	0.0007	0.0003	0.0017	0.0008	0.0004	0.0002
$\mathbf{m}(\widehat{H}_2)$	0.7000	0.7000	0.7000	0.7000	0.7000	0.7000	0.7000	0.7000	0.7000	0.7000	0.7000	0.7000
$\boldsymbol{\sigma}_{\mathbf{e}}(\widehat{H}_2)$	0.0035	0.0015	0.0007	0.0003	0.0027	0.0010	0.0005	0.0002	0.0016	0.0008	0.0004	0.0002
$\mathbf{m}(\widehat{a}^2)$	4.0105	4.0120	4.0103	4.0078	4.0108	4.0117	4.0102	4.0078	4.0105	4.0116	4.0101	4.0078
$\boldsymbol{\sigma}_{\mathbf{e}}(\widehat{a}^2)$	0.4425	0.2125	0.1095	0.0532	0.3952	0.1955	0.1020	0.0496	0.3618	0.1837	0.0939	0.0454
$\mathbf{m}(\widehat{b}^2)$	4.0111	4.0124	4.0102	4.0078	4.0109	4.0120	4.0101	4.0078	4.0106	4.0117	4.0100	4.0078
$\boldsymbol{\sigma}_{\mathbf{e}}(\widehat{b}^2)$	0.4012	0.1918	0.0959	0.0479	0.3920	0.1867	0.0925	0.0463	0.3827	0.1817	0.0910	0.0452

5.2.4 NifBm with drift: model description and drift parameter estimation

In this section, we focus on the estimation of the drift parameter. We extend the previously analyzed models by adding a deterministic drift component and consider the process $Y = \{Y_t,\, t \geq 0\}$

$$Y_t = \mu G(t) + P_t \tag{5.66}$$

where $\mu \in \mathbb{R}$ is an unknown constant, and G is a known deterministic function while the process P_t can be the normalized integrated fractional Brownian motion $X_t^{h,H}$ defined in (5.1) either the model with two nifBms $\widetilde{X}_k^h$ defined in (5.40). Suppose that the process Y is observed at discrete time points $t_k = kh$, for $k = 1, \ldots, N$. The corresponding observations $Y_1, \ldots, Y_N$ are given by

$$Y_k^h = \mu G_k^h + P_{kh}, \quad k = 1, \ldots, N, \tag{5.67}$$

Where we denote $G_k^h \coloneqq G(kh)$. In what follows, we assume that $G_k^h \neq 0$ at least for one k.
In this section, we assume that all the coefficients of the nifBm are known. The goal is to estimate the drift parameter $\mu \in \mathbb{R}$ based on the discrete observations.

Let $G_0^h \coloneqq 0$. Define the vector of increments $\Delta Y^{(N)} = (\Delta Y_0, \ldots, \Delta Y_{N-1})^\top$, where, for $k = 0, \ldots, N-1$,

$$\Delta Y_k = Y_{(k+1)h} - Y_{kh} = \mu \Delta G_k^h + \Delta P_k,$$

and $\Delta G_k^h = G_{k+1}^h - G_k^h$, $\Delta P_k = P_{k+1} - P_k$. Clearly, the vector $\Delta Y^{(N)}$ is Gaussian with distribution $\mathcal{N}(\mu \Delta G^{(N)}, \Sigma^{(N)})$, where $\Delta G^{(N)} = \left(\Delta G_0^h, \ldots, \Delta G_{N-1}^h\right)^\top$, and $\Sigma^{(N)}$ is the covariance matrix of the Gaussian vector

$$\Delta P^{(N)} \coloneqq \left(\Delta P_0, \ldots, \Delta \widetilde{P}_{N-1}\right)^\top.$$

Note that in the present setting the drift parameter cannot be estimated by simply taking the arithmetic average of the observations. Indeed, the increments of a nifBm are correlated and their covariance structure is described by a non-diagonal matrix $\Sigma^{(N)}$. The arithmetic mean would ignore this dependence structure, whereas the MLE explicitly incorporates the inverse covariance matrix and therefore fully accounts for the correlation of the noise.

1. The case $P_k \coloneqq \widetilde{X}_k^h = a X_{kh}^{h,H_1} + b X_{kh}^{h,H_2}$.

   Due to the independence of X^{h,H_1} and X^{h,H_2}, the covariance matrix decomposes as

   $$\Sigma^{(N)} = a^2 \Sigma_{H_1}^{(N)} + b^2 \Sigma_{H_2}^{(N)},$$

   where $\Sigma_{H_i}^{(N)}$ is the covariance matrix of $(\Delta X_0^{h,H_i}, \ldots, \Delta X_{N-1}^{h,H_i})^\top$, $i = 1, 2$. By Proposition 5.1.1, both $\Sigma_{H_1}^{(N)}$ and $\Sigma_{H_2}^{(N)}$ are positive definite, and hence $\Sigma^{(N)}$ is positive definite and non-singular whenever $a^2 + b^2 > 0$.

   Following the methodology of [52], the maximum likelihood estimator (MLE) of the drift

parameter μ is given by

$$\hat{\mu}_N = \frac{(\Delta G^{(N)})^\top \left(\widetilde{\Sigma}^{(N)}\right)^{-1} \Delta Y^{(N)}}{(\Delta G^{(N)})^\top \left(\widetilde{\Sigma}^{(N)}\right)^{-1} \Delta G^{(N)}}. \tag{5.68}$$

Propotion 5.2.1. *Let $a \neq 0$, $b \neq 0$, and $H_1, H_2 \in (0,1)$.*

(a) The MLE $\hat{\mu}_N$ is unbiased and normally distributed with variance

$$\mathrm{Var}(\hat{\mu}_N) = \frac{1}{(\Delta G^{(N)})^\top \left(\widetilde{\Sigma}^{(N)}\right)^{-1} \Delta G^{(N)}}. \tag{5.69}$$

(b) If

$$\frac{N^{H_1 \vee H_2}}{G_N^h} \to 0 \quad \text{as } N \to \infty, \tag{5.70}$$

then the estimator $\hat{\mu}_N$ is consistent both in L^2 and almost surely.

Proof. a) Since the process Y is Gaussian and the estimator $\hat{\mu}_n$ is a linear functional of the observations, it is normally distributed. From the model representation

$$\Delta Y^{(N)} = \mu \Delta G^{(N)} + \Delta \widetilde{X}^{(N)},$$

it follows that

$$\hat{\mu}_N = \mu + \frac{\left(\Delta G^{(N)}\right)^\top \left(\widetilde{\Sigma}^{(N)}\right)^{-1} \Delta \widetilde{X}^{(N)}}{\left(\Delta G^{(N)}\right)^\top \left(\widetilde{\Sigma}^{(N)}\right)^{-1} \Delta G^{(N)}},$$

which shows that $\hat{\mu}_N$ is unbiased and has variance given by (5.69).

b) According to [53, Theorem 1], a sufficient condition for both L^2-consistency and strong consistency of $\hat{\mu}_N$ is that

$$\frac{\mathbb{V}ar\left(\widetilde{X}_N^h\right)}{\left(G_N^h\right)^2} \to 0 \quad \text{as } N \to \infty.$$

This condition holds under assumption (5.70), since

$$\mathbb{V}ar\left(\widetilde{X}_N^h\right) = \mathbb{V}ar\left(aX_{Nh}^{h,H_1} + bX_{Nh}^{h,H_2}\right) \sim a^2(Nh)^{2H_1} + b^2(Nh)^{2H_2}, \quad \text{as } N \to \infty,$$

see Remark 5.1.1. □

Remark 5.2.8. *In this section, we assumed that the process Y is observed on an equidistant grid $\{h, 2h, \ldots, Nh\}$. However, the same results for the MLE of the drift parameter μ remain valid for any grid of the form $\{k_1 h, k_2 h, \ldots, k_N h\}$, where $k_1 < k_2 < \cdots < k_N$.*

The L^2- and strong consistency of the corresponding MLE holds under assumption (5.70)*, provided that $k_N \to \infty$ as $N \to \infty$.*

It is important to note that the ergodic-type estimators of H_1, H_2, a, and b crucially depend on the equidistant nature of the observation grid. Accordingly, we maintain the same equidistant observation scheme in the present section.

Let us consider a simpler alternative estimator based on two observations only:

$$\widetilde{\mu}_N = \frac{Y_N^h - Y_0^h}{G_N^h}. \tag{5.71}$$

Observe that this estimator can be interpreted as the MLE of μ based on the last and first observation. Therefore, taking into account Remark 5.2.8 and Proposition 5.2.1, we immediately obtain the following result.

Propotion 5.2.2. *Let $a \neq 0$, $b \neq 0$, and $H_1, H_2 \in (0,1)$.*

(a) The estimator $\widetilde{\mu}_N$ is unbiased and normal with

$$\mathbb{V}ar(\widetilde{\mu}_N) = \frac{\mathbb{V}ar\left(\widetilde{X}_N^h - \widetilde{X}_0^h\right)}{\left(G_N^h\right)^2}. \tag{5.72}$$

(b) Under assumption (5.70)*, the estimator $\widetilde{\mu}_N$ is consistent both in L^2 and almost surely.*

Remark 5.2.9. *(a) The MLE $\hat{\mu}_N$ is more efficient than the estimator $\widetilde{\mu}_N$, in the sense that $\mathrm{Var}(\hat{\mu}_N) \leq \mathrm{Var}(\widetilde{\mu}_N)$. This result follows from [52, Corollary 1], where the variances of MLEs based on samples of different sizes are compared.*

(b) A key advantage of the estimator $\widetilde{\mu}_N$ is its independence from the noise parameters H_1, H_2, a, and b, which may be unknown in practice.

(c) Under the stronger assumption that $N = O(G_N^h)$ as $N \to \infty$, the strong consistency of $\widetilde{\mu}_N$ can be derived from the ergodic Theorem 2.0.2. Indeed, this theorem implies

$$\frac{\widetilde{X}_N^h - \widetilde{X}_0^h}{N} = \frac{1}{N}\sum_{k=0}^{N-1} \Delta\widetilde{X}_k^h \to \mathbb{E}\left[\Delta\widetilde{X}_0^h\right] = 0 \quad \textit{a.s., as } N \to \infty,$$

which yields, under the stated assumption, that $\widetilde{\mu}_N = \mu + \frac{N}{G_N^h} \cdot \frac{\widetilde{X}_N^h - \widetilde{X}_0^h}{N} \to \mu$, a.s., as $N \to \infty$.

2. The case $P_k \coloneqq X_t^{h,H}$

Also in this case, the covariance matrix Σ_H^N is positive definite and non-singular, the MLE

of the drift parameter μ is given by

$$\hat{\mu}_N = \frac{\left(\Delta G^{(N)}\right)^\top \left(\Sigma_H^{(N)}\right)^{-1} \Delta Y^{(N)}}{\left(\Delta G^{(N)}\right)^\top \left(\Sigma_H^{(N)}\right)^{-1} \Delta G^{(N)}}, \tag{5.73}$$

where $\Sigma_H^{(N)}$ denotes the covariance matrix of the vector $(\Delta X_0^{h,H}, \dots, \Delta X_{N-1}^{h,H})^\top$.

The following result summarizes the properties of the estimator (5.73). It follows directly from the results of [52, 53], using the same approach as in Proposition 5.2.1. For this reason, the proof is omitted.

Propotion 5.2.3. *Let $a \neq 0$ and $H \in (0,1)$.*

(a) The MLE $\hat{\mu}_N$, defined in (5.73)*, is unbiased and normally distributed with variance*

$$\mathbb{V}ar(\hat{\mu}_N) = \frac{a^2}{\left(\Delta G^{(N)}\right)^\top \left(\Sigma_H^{(N)}\right)^{-1} \Delta G^{(N)}}. \tag{5.74}$$

(b) Suppose that

$$\frac{N^H}{G_N^h} \to 0 \quad \text{as } N \to \infty. \tag{5.75}$$

Then the MLE $\hat{\mu}_N$ is consistent both in the L^2-sense and almost surely.

The following result gives the properties of an alternative estimator in the model with drift and one nifBm.

Propotion 5.2.4. *Let $a \neq 0$ and $H \in (0,1)$.*

(a) The estimator

$$\widetilde{\mu}_N = (Y_N^h - Y_0^h)/G_N^h \tag{5.76}$$

is unbiased and normally distributed with variance

$$\mathbb{V}ar(\widetilde{\mu}_N) = a^2 \mathbb{E}[(X_{Nh}^{h,H} - X_0^{h,H})^2]/(G_N^h)^2.$$

(b) Under assumption (5.75)*, then the estimator $\widetilde{\mu}_N$ is consistent both in the L^2-sense and almost surely.*

Remark 5.2.10. *For $\mu \neq 0$, the random sequence $\{\Delta Y_k^h,\ k \geq 0\}$, where Y_k^h is defined by* (5.66)*, is not ergodic. However, in this case an analogue of Lemma 5.2.1 can be obtained. For the modified observations*

$$\widetilde{Y}_k^h := Y_k^h - \widetilde{\mu}_N G_k^h = P_k + (\mu - \widetilde{\mu}_N)\, G_k^h. \tag{5.77}$$

define

$$\widetilde{\xi}_N^j := \frac{1}{N}\sum_{k=0}^{N-1}\left(\widetilde{Y}_{k+1}^{jh} - \widetilde{Y}_k^{jh}\right)^2 = \frac{1}{N}\sum_{k=0}^{N-1}\left(\Delta\widetilde{Y}_k^{jh}\right)^2, \quad j \in \{1,2,4,8\}.$$

Then

$$\widetilde{\xi}_N^j = \frac{1}{N}\sum_{k=0}^{N-1}\left(\Delta P_k + (\mu - \widetilde{\mu}_N)\,\Delta G_k^{jh}\right)^2$$

$$\widetilde{\xi}_N^j = \xi_N^j + (\mu - \widetilde{\mu}_N)^2\,\frac{1}{N}\sum_{k=0}^{N-1}\left(\Delta G_k^{jh}\right)^2 + (\mu - \widetilde{\mu}_N)\,\frac{2}{N}\sum_{k=0}^{N-1}\Delta P_k \Delta G_k^{jh}. \tag{5.78}$$

If assumption (5.70) *holds, then* $\widetilde{\mu}_N \to \mu$ *a.s. as* $N \to \infty$*, by Proposition 5.2.2. Therefore, under the additional assumption*

$$\sum_{k=0}^{N-1}\left(\Delta G_k^{jh}\right)^2 = O(N), \quad N \to \infty, \tag{5.79}$$

we obtain the almost sure convergence

$$\widetilde{\xi}_N^j \to \mathbb{E}(\xi_0^j), \quad N \to \infty. \tag{5.80}$$

for $j = 1, 2$ *in the case* $P_k := X_t^{h,H}$ *or* $j = 1, 2, 4, 8$ *in the case with two nifBm processes. Indeed, the first term on the right-hand side of* (5.78) *converges to the stated limit by* (5.42)*; the second term tends to zero due to* (5.79)*, and the third term also vanishes, since it can be bounded via the first two terms using the Cauchy–Schwarz inequality.*

The convergence in (5.80) *guarantees the strong consistency, in the model with drift, of the estimators for the model parameters, where* $\widetilde{\xi}_N^j$ *are used instead of* ξ_N^j*.*

Assumption (5.79) *is satisfied, for instance, if the sequence* $\{\Delta G_k^{jh}, k \geq 0\}$ *is bounded; in particular, for a linear drift function* $G(t) = t$*, we have* $\Delta G_k^{jh} = jh$ *for all* k *(in this case, condition* (5.70) *also holds). More generally,* (5.79) *is valid whenever* G *satisfies a Lipschitz or Hölder condition.*

Simulation for the drift parameter estimators

In this part, we investigate the performance of the drift estimators for both models: the one driven by a single nifBm and the one driven by two nifBm processes. Specifically, we fix the true parameter value $\mu = 4$ and consider the function $G(t) = 5\cos t - e^{-4t} + 2t^2$, which satisfies condition (5.70) for arbitrary values of the Hurst exponents. The diffusion coefficients are set to $a = b = 1$. We begin with the estimation of the drift parameter in the model with a single nifBm with drift. The estimators $\widehat{\mu}_N$ and $\widetilde{\mu}_N$, defined in (5.73) and (5.76), respectively, are evaluated for several values of the Hurst parameter, $H \in \{0.1, 0.3, 0.5, 0.7, 0.9\}$, and for two values of the averaging window, $h \in \{2, 2^2\}$.

The discrete-time increments process,

$$\Delta X_k^h = X_{(k+1)h}^h - X_{kh}^h,$$

is simulated using the Cholesky method, based on the analytical expression of the covariance matrix given in equation (5.6). Once realizations of ΔX_k^h are generated, the increments of the function $G(t)$ are added to obtain the process $\Delta Y^{(N)}$.

For each configuration (H, h), we conduct 100 simulations. For every simulated trajectory, the estimator $\widehat{\mu}_N$ is computed according to (5.73) for various values of the number of observations N. The empirical mean $\mathbf{m}(\widehat{\mu})$ and standard deviation $\boldsymbol{\sigma}_\mathbf{e}(\widehat{\mu})$ are then calculated across the replications. In addition, the theoretical standard deviations $\boldsymbol{\sigma}_\mathbf{t}(\widehat{\mu})$ are derived from formula (5.74).

We also examine the performance of the alternative estimator $\widetilde{\mu}_N$ by comparing its empirical standard deviation $\boldsymbol{\sigma}_\mathbf{e}(\widetilde{\mu})$, obtained from simulations, with the corresponding theoretical value $\boldsymbol{\sigma}_\mathbf{t}(\widetilde{\mu})$ given by the square root of the variance of $\widetilde{\mu}_N$, computed as

$$\mathbb{V}ar(\widetilde{\mu}_N) = \frac{a^2 h^{2H}}{(G_N^h)^2(2H+1)(2H+2)}\Big[(N+1)^{2H+2} + (N-1)^{2H+2} - 2N^{2H+2} - 2\Big], \quad (5.81)$$

which follows from Proposition 5.2.4, using (5.2) and (5.3).

Table 5.3 reports the means, empirical and theoretical standard deviations of both estimators. The simulation results align closely with our theoretical findings. Both $\widehat{\mu}_N$ and $\widetilde{\mu}_N$ are essentially unbiased, with empirical means near the true value of drift. Empirical standard deviations match the theoretical values and decrease rapidly with increasing sample size N, confirming the consistency and asymptotic normality of both estimators.

Overall, $\widehat{\mu}_N$ is slightly more efficient than $\widetilde{\mu}_N$, particularly for small samples and large Hurst exponents H. For large N, both estimators achieve high precision, with empirical variability closely following theoretical predictions. The alternative estimator $\widetilde{\mu}_N$ shows greater variability, especially for H near one and small N, reflecting the loss of efficiency from using only two observations. Nevertheless, both theoretical and empirical standard deviations decrease consistently as N increases.

In summary, the simulations confirm the consistency of both estimators while highlighting the superior efficiency of the maximum likelihood approach.

Within the same framework, we consider the model with two independent nifBms and a drift term. We investigate the performance of the MLE $\widehat{\mu}_N$ of the drift parameter μ defined in equation (5.68). In addition, we examine the alternative estimator $\widetilde{\mu}_N$, introduced in equation (5.71), which relies on two observations.

To evaluate the accuracy of both methods, we compare the empirical standard deviations with their theoretical counterparts. For $\widehat{\mu}_N$, a closed-form variance expression is provided in equation (5.69), whereas for $\widetilde{\mu}_N$ the variance can be computed explicitly as $\mathbb{V}ar(\widetilde{\mu}_N) = a^2 T_1 + b^2 T_2$,

Table 5.3: Drift estimators $\widehat{\mu}_N$ and $\widetilde{\mu}_N$ in the model with one nifBm.

		$h = 2$			$h = 2^2$		
H		$N = 2^3$	$N = 2^5$	$N = 2^7$	$N = 2^3$	$N = 2^5$	$N = 2^7$
0.1	$\mathbf{m}(\widehat{\mu})$	3.99976	4.00004	4.00000	3.99945	4.00001	4.00000
	$\boldsymbol{\sigma}_{\mathbf{e}}(\widehat{\mu})$	0.00510	0.00053	0.00003	0.00561	0.00051	0.00000
	$\boldsymbol{\sigma}_{\mathbf{t}}(\widehat{\mu})$	0.00559	0.00048	0.00004	0.00599	0.00052	0.00000
	$\mathbf{m}(\widetilde{\mu})$	4.00045	3.99995	4.00001	4.00095	4.00004	3.99999
	$\boldsymbol{\sigma}_{\mathbf{e}}(\widetilde{\mu})$	0.00651	0.00045	0.00004	0.00568	0.00057	0.00005
	$\boldsymbol{\sigma}_{\mathbf{t}}(\widetilde{\mu})$	0.00733	0.00058	0.00004	0.00786	0.00062	0.00005
0.3	$\mathbf{m}(\widehat{\mu})$	4.00152	3.99994	3.99998	3.99881	3.99994	4.00002
	$\boldsymbol{\sigma}_{\mathbf{e}}(\widehat{\mu})$	0.01344	0.00140	0.00013	0.01625	0.00166	0.00018
	$\boldsymbol{\sigma}_{\mathbf{t}}(\widehat{\mu})$	0.01279	0.00141	0.00014	0.01575	0.00173	0.00017
	$\mathbf{m}(\widetilde{\mu})$	3.99817	3.99969	3.99991	3.99663	3.99942	3.99997
	$\boldsymbol{\sigma}_{\mathbf{e}}(\widetilde{\mu})$	0.01445	0.00165	0.00015	0.01417	0.00214	0.00019
	$\boldsymbol{\sigma}_{\mathbf{t}}(\widetilde{\mu})$	0.01676	0.00164	0.00016	0.02063	0.00203	0.00020
0.5	$\mathbf{m}(\widehat{\mu})$	3.99952	3.99936	4.00011	3.99924	3.99952	4.00002
	$\boldsymbol{\sigma}_{\mathbf{e}}(\widehat{\mu})$	0.02284	0.00311	0.00044	0.03116	0.00431	0.00061
	$\boldsymbol{\sigma}_{\mathbf{t}}(\widehat{\mu})$	0.02269	0.00320	0.00042	0.03209	0.00452	0.00059
	$\mathbf{m}(\widetilde{\mu})$	3.99907	3.99925	4.00005	3.99831	3.99984	4.00005
	$\boldsymbol{\sigma}_{\mathbf{e}}(\widetilde{\mu})$	0.02269	0.00338	0.00049	0.03375	0.00579	0.00071
	$\boldsymbol{\sigma}_{\mathbf{t}}(\widetilde{\mu})$	0.03077	0.00388	0.00049	0.04351	0.00548	0.00069
0.7	$\mathbf{m}(\widehat{\mu})$	3.99175	4.00051	3.99977	4.00518	4.00263	4.00031
	$\boldsymbol{\sigma}_{\mathbf{e}}(\widehat{\mu})$	0.03442	0.00606	0.00106	0.05696	0.01022	0.00185
	$\boldsymbol{\sigma}_{\mathbf{t}}(\widehat{\mu})$	0.03659	0.00665	0.00114	0.05944	0.01080	0.00184
	$\mathbf{m}(\widetilde{\mu})$	4.00987	3.99994	3.99991	4.00366	3.99717	3.99962
	$\boldsymbol{\sigma}_{\mathbf{e}}(\widetilde{\mu})$	0.04859	0.00904	0.00154	0.07372	0.01335	0.00221
	$\boldsymbol{\sigma}_{\mathbf{t}}(\widetilde{\mu})$	0.05437	0.00895	0.00148	0.08833	0.01453	0.00241
0.9	$\mathbf{m}(\widehat{\mu})$	3.99896	4.00091	3.99983	3.99089	4.00054	4.00060
	$\boldsymbol{\sigma}_{\mathbf{e}}(\widehat{\mu})$	0.04943	0.01187	0.00243	0.08474	0.02017	0.00450
	$\boldsymbol{\sigma}_{\mathbf{t}}(\widehat{\mu})$	0.04602	0.01090	0.00244	0.08588	0.02034	0.00455
	$\mathbf{m}(\widetilde{\mu})$	3.99131	3.99958	4.00013	3.99674	3.99842	3.99953
	$\boldsymbol{\sigma}_{\mathbf{e}}(\widetilde{\mu})$	0.07886	0.01719	0.00436	0.16066	0.03891	0.00819
	$\boldsymbol{\sigma}_{\mathbf{t}}(\widetilde{\mu})$	0.09515	0.02057	0.00449	0.17756	0.03839	0.00837

where

$$T_i = \frac{h^{2H_i}}{(G_N^h)^2(2H_i+1)(2H_i+2)}\left[(N+1)^{2H_i+2} + (N-1)^{2H_i+2} - 2N^{2H_i+2} - 2\right], \quad i = 1, 2.$$

As in the single-nifBm case, we consider $N \in \{2^3, 2^5, 2^7\}$ observation points and two averaging windows, $h \in \{2, 2^2\}$. For each configuration, 100 independent simulations are performed.

Table 5.4 reports the simulation results for the drift coefficient μ across different pairs of Hurst parameters (H_1, H_2). It presents the sample means of both estimators along with their empirical and theoretical standard deviations.

The results for the two-process model (Table 5.4) are consistent with those of the single-process case (Table 5.3). In both settings, the estimators are essentially unbiased, with empirical means very close to the true drift. Regarding variability, the MLE $\widehat{\mu}_N$ is systematically more efficient than the alternative estimator $\widetilde{\mu}_N$, particularly for larger sample sizes. Only in small-N scenarios two estimators exhibit similar performance; as N increases, the superiority of $\widehat{\mu}_N$ becomes evident across all parameter configurations.

This pattern is common to both the single- and two-process models, although the presence of two fractional components leads to higher overall variability, especially when at least one Hurst parameter is large. Thus, while both estimators are consistent, the MLE provides a more reliable and efficient estimation method, with the advantage most pronounced in smoother regimes and for larger samples.

Table 5.4: Drift estimators $\widehat{\mu}_N$ and $\widetilde{\mu}_N$ in the model with two nifBms.

			$h=2$			$h=2^2$		
H_1	H_2		$N=2^3$	$N=2^5$	$N=2^7$	$N=2^3$	$N=2^5$	$N=2^7$
0.1	0.3	$\mathbf{m}(\widehat{\mu})$	3.99938	4.00001	4.00001	3.99951	3.99968	4.00000
		$\boldsymbol{\sigma}_{\mathbf{e}}(\widehat{\mu})$	0.01306	0.00167	0.00015	0.01807	0.00165	0.00017
		$\boldsymbol{\sigma}_{\mathbf{t}}(\widehat{\mu})$	0.01399	0.00149	0.00015	0.01687	0.00181	0.00017
		$\mathbf{m}(\widetilde{\mu})$	3.99953	4.00016	3.99998	4.00385	4.00009	4.00001
		$\boldsymbol{\sigma}_{\mathbf{e}}(\widetilde{\mu})$	0.00819	0.00143	0.00016	0.02082	0.00226	0.00022
		$\boldsymbol{\sigma}_{\mathbf{t}}(\widetilde{\mu})$	0.00837	0.00175	0.00017	0.02211	0.00212	0.00020
0.1	0.5	$\mathbf{m}(\widehat{\mu})$	3.99824	4.00003	4.00004	3.99953	3.99963	4.00001
		$\boldsymbol{\sigma}_{\mathbf{e}}(\widehat{\mu})$	0.02263	0.00320	0.00037	0.03172	0.00472	0.00061
		$\boldsymbol{\sigma}_{\mathbf{t}}(\widehat{\mu})$	0.02349	0.00325	0.00042	0.03275	0.00456	0.00059
		$\mathbf{m}(\widetilde{\mu})$	3.99865	3.99956	4.00010	4.00025	3.99902	4.00005
		$\boldsymbol{\sigma}_{\mathbf{e}}(\widetilde{\mu})$	0.02565	0.00356	0.00051	0.03316	0.00515	0.00069
		$\boldsymbol{\sigma}_{\mathbf{t}}(\widetilde{\mu})$	0.03163	0.00392	0.00049	0.04421	0.00552	0.00069
0.3	0.5	$\mathbf{m}(\widehat{\mu})$	3.99990	4.00060	3.99993	3.99817	3.99997	3.99993
		$\boldsymbol{\sigma}_{\mathbf{e}}(\widehat{\mu})$	0.02745	0.00850	0.00045	0.03636	0.01463	0.00060
		$\boldsymbol{\sigma}_{\mathbf{t}}(\widehat{\mu})$	0.02615	0.00960	0.00044	0.03587	0.01326	0.00067
		$\mathbf{m}(\widetilde{\mu})$	3.99882	3.99976	4.00004	3.99829	3.99982	3.99997
		$\boldsymbol{\sigma}_{\mathbf{e}}(\widetilde{\mu})$	0.02907	0.00385	0.00046	0.03903	0.00551	0.00070
		$\boldsymbol{\sigma}_{\mathbf{t}}(\widetilde{\mu})$	0.03503	0.00421	0.00051	0.04815	0.00585	0.00072
0.3	0.7	$\mathbf{m}(\widehat{\mu})$	3.99509	4.00073	4.00010	4.00340	4.00009	4.00010
		$\boldsymbol{\sigma}_{\mathbf{e}}(\widehat{\mu})$	0.03863	0.00717	0.00116	0.06232	0.01110	0.00207
		$\boldsymbol{\sigma}_{\mathbf{t}}(\widehat{\mu})$	0.03947	0.00687	0.00115	0.06226	0.01101	0.00186
		$\mathbf{m}(\widetilde{\mu})$	3.99228	4.00021	3.99995	4.00442	4.00138	4.00025
		$\boldsymbol{\sigma}_{\mathbf{e}}(\widetilde{\mu})$	0.05530	0.00829	0.00159	0.07430	0.01515	0.00222
		$\boldsymbol{\sigma}_{\mathbf{t}}(\widetilde{\mu})$	0.05690	0.00910	0.00149	0.09071	0.01468	0.00241
0.5	0.7	$\mathbf{m}(\widehat{\mu})$	4.00221	4.00056	4.00014	3.99529	3.99930	4.00007
		$\boldsymbol{\sigma}_{\mathbf{e}}(\widehat{\mu})$	0.04494	0.00830	0.00121	0.06574	0.01188	0.00183
		$\boldsymbol{\sigma}_{\mathbf{t}}(\widehat{\mu})$	0.04352	0.00745	0.00122	0.06821	0.01181	0.00194
		$\mathbf{m}(\widetilde{\mu})$	3.99382	3.96247	4.00011	4.00016	4.00095	3.99986
		$\boldsymbol{\sigma}_{\mathbf{e}}(\widetilde{\mu})$	0.04386	0.01974	0.00164	0.00926	0.01521	0.00228
		$\boldsymbol{\sigma}_{\mathbf{t}}(\widetilde{\mu})$	0.06248	0.00127	0.00156	0.00975	0.01554	0.00250

Chapter 6

Model with fundamental martingale

In this chapter we introduce the Lucia–Schwartz model then we propose a modification of this model, taking into account the empirical findings discussed in Chapter 3 where we showed that the estimation results clearly indicate that a modeling framework based on fractional dynamics is appropriate for representing energy price fluctuations. At the same time, that analysis showed that the use of a single Hurst parameter is not sufficient to capture the full variability of the diffusive component, as the estimated Hurst exponent exhibits a pronounced dependence on the observation scale and on the dataset considered.

Moreover, modeling the price dynamics directly in terms of fractional Brownian motion would violate the martingale assumption for prices, under the risk-neutral measure, which is a fundamental requirement in arbitrage-free pricing frameworks. To overcome these limitations, we propose a modified model based on fundamental martingales. Starting from the classical Lucia–Schwartz model, we modify its second stochastic component by replacing it with a linear combination of processes defined in (4.8).

This construction allows us to preserve the martingale property of the spot price while simultaneously introducing multiple Hurst exponents into the dynamics, thereby providing greater flexibility in modeling the roughness of the stochastic component. Each Hurst parameter can be interpreted as capturing the roughness of the price dynamics over a specific regime, coherently with the scale-dependent behavior observed in the data. Within the theoretical framework developed in Chapter 1, the resulting spot price model is then used to derive the instantaneous forward price via conditional expectation. Finally, the forward price is obtained by integration over the delivery period, consistently with the structure of electricity forward contracts.

As a modeling choice, we adopt mean-reverting dynamics, which are widely regarded as the most appropriate specification for forward pricing in electricity markets.

Subsequently, the model is calibrated using market forward data. The calibration procedure is carried out in two steps. First, we exploit the quadratic variation techniques to estimate the diffusion coefficient of the stochastic component. Then, the drift parameters are estimated by means of different estimation techniques. Finally, model-implied forward prices are compared with observed market data.

6.0.1 The Lucia Schwartz model

Lucia-Schwartz models [48] were introduced as an extension of some widely used models in the late nineties, known as one-factor models, where the spot price $S(t)$ is given by the sum of two components

$$S(t) = \phi(t) + X_1(t), \tag{6.1}$$

where the first is a deterministic function of time $\phi(t)$ that tries to capture any relevant contribution arising from regular patterns in time, and the second is a stochastic process $X_1(t)$ following

$$dX_1(t) = -kX_1(t)dt + \sigma_1 dW_1(t),$$

with $k > 0$ and $W_1(t)$ a standard Brownian motion. Therefore, $X_1(t)$ is a stationary mean-reverting process, or Ornstein-Uhlenbeck process, with zero long-run mean and speed of adjustment k. Single-factor models became popular in commodity markets at the beginning of this century, as they provide a framework capable of capturing short-term deviations from an equilibrium level.
In [48] a second stochastic factor was added to the spot price described by (6.1), to account for the fact that changes in futures contracts prices with different maturities are not perfectly correlated one with another, as instead happens in the one-factor models (indeed, in any one-factor model, all futures prices are driven by the same underlying source of randomness, which implies perfect correlation across maturities, up to deterministic scaling effects). The introduction of an additional stochastic factor allows to overcome this structural limitation of the model by incorporating multiple sources of risk. As a result, the Lucia-Schwartz model assumes that:

$$S(t) = \phi(t) + X_1(t) + X_2(t), \tag{6.2}$$

$$dX_1(t) = -kX_1(t)dt + \sigma_1 dW_1(t), \tag{6.3}$$

$$dX_2(t) = \mu + \sigma_2 dW_2(t), \tag{6.4}$$

where the two Wiener processes $W_1(t)$ and $W_2(t)$ are correlated, with correlation coefficient ρ. The first factor $X_1(t)$ is a mean–reverting process that captures short–term fluctuations in electricity prices, typically associated with temporary supply–demand imbalances, weather conditions, and unexpected generation outages. In contrast, the second factor $X_2(t)$, modeled as an arithmetic Brownian motion, represents long–term uncertainty affecting the overall price level, such as technological developments, regulatory and political changes, and price dynamics in related commodity markets. This two–factor specification introduces additional flexibility into the model, allowing it to reproduce more realistic correlation structures across futures contracts with different maturities and to better capture both short–term dynamics and long–run price movements observed in electricity markets. The additive structure of the Lucia–Schwartz model allows the spot price to take negative values. Since both stochastic factors are Gaussian processes, the spot price is not constrained to be positive in contrast to geometric models. This feature is consistent with empirical

evidence from electricity markets, where negative prices may occur in fact in the recent years it happened in several national electricity markets.

6.1 A fractional Lucia-Schwartz model

In this section, we propose a modification of the Lucia–Schwartz model designed to preserve several stylized facts of electricity prices. In particular, the model is constructed to reproduce the roughness observed in high-frequency spot dynamics, the pronounced seasonal patterns in price levels, seasonality in volatility, as well as the Samuelson effect in derivative contracts[1]. At the same time, we want to preserve an arbitrage-free pricing framework for forward contracts. To this end, we work with a risk-neutral measure and employ an HJM-type approach. Moreover, we retain mean reversion as the key mechanism governing the term structure in electricity markets.

Simply modeling the stochastic component through a fractional Brownian motion is problematic from a pricing perspective, since fBm is not a martingale. We therefore rely on the class of Volterra-type processes introduced in Norros et al. [60], which are the so-called fundamental martingales. Specifically, we consider

$$M(t) = c_1 \int_0^t s^{\frac{1}{2}-H}(t-s)^{\frac{1}{2}-H} dB^H(s), \tag{6.5}$$

where $B^H(t)$ is a fractional Brownian motion with Hurst parameter $H \in (0,1) \setminus \{\frac{1}{2}\}$ and c_1 is a normalizing constant. The key properties of M are recalled in Section 4.2. The role of M in our construction is to introduce fractional roughness while preserving the martingale structure required by the pricing measure. Motivated by the empirical evidence, we allow for multiple fractional components. Let $\mathbf{B}^H(t) = (B_1^{H_1}(t), \dots, B_d^{H_d}(t))$ be a d-dimensional fractional Brownian motion (possibly with correlated components), and let $M_1, \dots, M_d$ denote the associated fundamental martingales defined as in (6.5), with Hurst parameters $H_1, \dots, H_d$.

We substitute the second factor X_2 of the Lucia–Schwartz model with a linear combination of these martingales. As we shall see later, the use of fundamental martingales, rather than fractional Brownian motions, preserves the affine structure of forward prices, as in [45]. The underlying idea is that the dynamics of the spot price should incorporate several coexisting factors with different degrees of roughness, possibly arising from different characteristics of the spot prices or from different time periods.

Under the chosen martingale measure $\mathbb{Q}$, we model the spot price as

$$S(t) = \phi(t) + X_0(t) + \sum_{i=1}^{d} g_i(t) X_i(t), \tag{6.6}$$

[1]The Samuelson effect refers to the empirical increase in forward (or futures) price volatility as time to maturity decreases, reflecting the higher sensitivity of short-term contracts to fundamental supply and demand shocks.

with $\phi(t)$ a deterministic seasonal component, $g_i(t)$ time-dependent functions to be determined and the $d+1$ hidden factors given by

$$\begin{aligned} X_0(t) &= \mathrm{e}^{-kt}X_0(0) + \int_0^t \mathrm{e}^{-k(t-s)}\sigma_0 dW_0^{\mathbb{Q}}(s) \\ X_i(t) &= X_i(0) + \mu_i t + \sigma_i M_i(t), \end{aligned} \tag{6.7}$$

The first factor X_0 is a stationary mean-reverting component, as in the original Lucia–Schwartz specification, and it is responsible for short-term fluctuations and for the Samuelson effect. The remaining factors incorporate fractional roughness through the martingales M_i. Under the risk neutral probability measure $\mathbb{Q}$, each fundamental martingale may be represented in the form (4.9)

$$M_i(t) = \int_0^t \frac{c_{H_i}}{2H_i} s^{\frac{1}{2}-H_i} dW_i^{\mathbb{Q}}(s),$$

with $W_0^{\mathbb{Q}}(t), W_1^{\mathbb{Q}}(t), \ldots, W_d^{\mathbb{Q}}(t)$ a $d+1-$dimensional Brownian motion with correlated components. Further analytical details on the spot price process are provided in Appendix C. Hence, using these dynamics, we obtain an explicit representation of $S(T)$

$$\begin{aligned} S(T) =& \phi(T) + X_0(t)\mathrm{e}^{-k(T-t)} + \sigma_0 \int_t^T \mathrm{e}^{-k(T-u)} dW_0^{\mathbb{Q}}(u) \\ &+ \sum_{i=1}^{d} g_i(T)\left[X_i(0) + \mu_i T + \sigma_i M_i(T)\right], \end{aligned} \tag{6.8}$$

and from this expression we may price the instantaneous forward by conditioning $S(T)$ with respect to $\mathcal{F}_t$

$$f(t,T) = \mathbb{E}_{\mathbb{Q}}(S(T)|\mathcal{F}_t),$$

where $\mathcal{F}_t$ is the natural filtration generated by $W_0^{\mathbb{Q}}(t), W_1^{\mathbb{Q}}(t), \ldots, W_d^{\mathbb{Q}}(t)$,

$$\begin{aligned} f(t,T) &= \mathbb{E}_{\mathbb{Q}}[S(T) \mid \mathcal{F}_t] \\ &= \phi(T) + X_0(t)\mathrm{e}^{-k(T-t)} + \sigma_0 \mathbb{E}_{\mathbb{Q}}\left(\int_t^T \mathrm{e}^{-k(T-u)}\, dW_0^{\mathbb{Q}}(u) \mid \mathcal{F}_t \right) \\ &\quad + \sum_{i=1}^{d} g_i(T)\left(X_i(0) + \mu_i T + \sigma_i \mathbb{E}_{\mathbb{Q}}[M_i(T) \mid \mathcal{F}_t]\right). \end{aligned} \tag{6.9}$$

By exploiting the martingale property of the stochastic integrals, we have

$$\mathbb{E}_{\mathbb{Q}}(\int_t^T \mathrm{e}^{-k(T-u)} dW_0^{\mathbb{Q}}(u)|\mathcal{F}_t) = 0, \quad \mathbb{E}_{\mathbb{Q}}(M_i(T)|\mathcal{F}_t) = M_i(t).$$

Hence,

$$f(t,T) = \phi(T) + X_0(t)\mathrm{e}^{-k(T-t)} + \sum_{i=1}^{d} g_i(T)\left(X_i(0) + \mu_i T + \sigma_i M_i(t)\right). \tag{6.10}$$

Using the identity $X_i(t) = X_i(0) + \mu_i t + \sigma_i M_i(t)$, we can rewrite the previous expression in affine form as

$$f(t,T) = \boldsymbol{\alpha}(t,T) \cdot \mathbf{X}(t) + \beta(t,T), \tag{6.11}$$

where $\mathbf{X}(t) = (X_0(t), \ldots, X_d(t))^\top \in \mathbb{R}^{d+1}$,

$$\beta(t,T) = \phi(T) + \sum_{i=1}^{d} g_i(T)\mu_i(T-t),$$

and the vector-valued function $\boldsymbol{\alpha}(t,T)$ has components

$$\alpha_0(t,T) = \mathrm{e}^{-k(T-t)}, \qquad \alpha_i(t,T) = g_i(T), \quad i = 1, \ldots, d.$$

Hence, the instantaneous forward price depends linearly on the hidden factors. This affine structure will be crucial both for calibration and for deriving closed-form expressions for forward prices over delivery periods.

On the other hand, by the martingale representation theorem (Theorem 2.0.1), the process $f(t,T)$ admits a stochastic integral representation with respect to the driving Brownian motions. In particular, it can be written as

$$f(t,T) = f(0,T) + \int_0^t \theta_0(s,T) dW_0^{\mathbb{Q}}(s) + \sum_{i=1}^{d} \int_0^t \theta_i(s,T) dW_i^{\mathbb{Q}}(s). \tag{6.12}$$

Comparing equations (6.10) and (6.12), we identify the deterministic and stochastic components of the representation:

$$\begin{aligned}
f(0,T) &= \phi(T) + \mathrm{e}^{-kT} X_0(0) + \sum_{i=1}^{d} g_i(T)(\mu_i T + X_i(0)), \\
\theta_0(s,T) &= \sigma_0 \mathrm{e}^{-k(T-s)}, \\
\theta_i(s,T) &= \sigma_i g_i(T) \frac{c_{H_i}}{2H_i} s^{\frac{1}{2}-H_i}.
\end{aligned}$$

It follows that the diffusion coefficients θ_i depend on the maturity T exclusively through the functions g_i.

Since our aim is to formulate, under the real-world probability measure $\mathbb{P}$, mean-reversion models both for the instantaneous forward $f(t,T)$ and the forward $F(t,T_1,T_2)$ for every maturity period $[T_1,T_2]$ (recalling that the forward and the instantaneous forward are linked by the relation (1.4)), we are interested in characterizing the *market price of risk*.

The market price of risk represents the adjustment that allows to move from the risk-neutral measure $\mathbb{Q}$, typically used for pricing, to the real world probability measure $\mathbb{P}$, which is relevant for estimation and forecasting. In energy markets, and especially in electricity markets where the non-storability of the commodity introduces additional sources of risk, this quantity plays a crucial role: it encapsulates the risk premia associated with seasonality, demand fluctuations, fuel costs, and unexpected shocks. In order to preserve a single arbitrage-free pricing measure for the entire forward curve, we assume that the change of measure from $\mathbb{P}$ to $\mathbb{Q}$ is driven by a unique market price of risk process. Consequently, the Girsanov kernel is independent of the maturity T. Any dependence on T is allowed to enter only through the volatility loadings of the forward dynamics and not through the measure change itself. We assume that under the real-world measure $\mathbb{P}$ the instantaneous forward price satisfies a mean-reverting stochastic differential equation of the form

$$df(t,T) = \big[-\lambda(t)f(t,T) + c(t,T)\big]dt + \eta_0(t,T)\,dW_0(t) + \sum_{i=1}^{d} \eta_i(t,T)\,dW_i(t), \tag{6.13}$$

where $\lambda(t)$ denotes the speed of mean reversion, $c(t,T)$ is a deterministic drift component, and $\eta_i(t,T)$ are the diffusion coefficients.

The specification of the coefficients λ, c, and η_i must be chosen so as to preserve the structural consistency of the model. In particular, we assume that the mean-reversion speed λ does not depend on the maturity T. This assumption is essential in order to maintain a closed mean-reverting structure when passing from instantaneous forwards to delivery-period forwards.

Indeed, if λ were allowed to depend on T, integrating the dynamics over the delivery interval $[T_1, T_2]$ would generate additional maturity-dependent drift terms that cannot be expressed solely in terms of $F(t,T_1,T_2)$. As a consequence, the affine structure of the model would be lost. A rigorous discussion of this structural requirement is provided in [45], while in [12] the same restriction is justified on the basis of no-arbitrage arguments.
Rewriting (6.13) in integral form and switching back to the risk neutral probability $\mathbb{Q}$ by Girsanov Theorem 2.0.3, we have

$$\begin{aligned} f(t,T) = f(0,T) &+ \int_0^t (-\lambda(s)f(s,T) + c(s,T))ds \\ &+ \int_0^t \eta_0(s,T)(dW_0^{\mathbb{Q}}(s) - \Lambda_0(s,T)ds) + \sum_{i=1}^{d} \int_0^t \eta_i(s,T)(dW_i^{\mathbb{Q}}(s) - \Lambda_i(s,T)ds), \end{aligned} \tag{6.14}$$

where the vector of Brownian motions under $\mathbb{Q}$ satisfies

$$d\boldsymbol{W}^{\mathbb{Q}}(s) = d\boldsymbol{W}(s) + \boldsymbol{\Lambda}(s)\,ds,,$$

where $\boldsymbol{\Lambda}$ represents the market price of risk process.
We assume that the market price of risk depends linearly on the hidden state variables. More

precisely, we postulate the affine structure

$$\boldsymbol{\Lambda}(s) = \boldsymbol{A}(s) \cdot \boldsymbol{X}(s) + \boldsymbol{b}(s), \tag{6.15}$$

where $\boldsymbol{A}(s)$ and $\boldsymbol{b}(s)$ are suitably defined $(d+1)$–dimensional deterministic vector-valued functions.

This specification guarantees that all forward contracts, regardless of maturity, are defined under the same risk-neutral probability measure $\mathbb{Q}$. The maturity dependence of the model is entirely captured by the volatility coefficients $\eta_i(s,T)$ and by the deterministic functions entering the forward representation, consistently with the HJM no-arbitrage framework.

Recall that under the risk-neutral probability measure, the forward price is a martingale. Therefore, the drift term of $f(t,T)$ in (6.14) must vanish, yielding the condition. This requirement yields the condition

$$-\lambda(s)f(s,T) + c(s,T) - \eta_0(s,T)\Lambda_0(s) - \sum_{i=1}^{d} \eta_i(s,T)\Lambda_i(s) = 0.$$

Exploiting the affine representations of $f(t,T)$ and $\boldsymbol{\Lambda}(t,T)$ (equations (6.11) and (6.15)), we obtain.

$$\begin{aligned}
&-\lambda(s)[\alpha_0(s,T)X_0 + \sum_{i=1}^{d} g_i(T)\alpha_i(s,T)X_i(s) + \beta(s,T)] + c(s,T) \\
&-\eta_0(s,T)[A_0(s)X_0 + b_0(s)] - \sum_{i=1}^{d} \eta_i(s,T)[A_i(s)X_i + b_i(s)] = 0.
\end{aligned}$$

Since the identity must hold for all realizations of the factors $X_i(s)$, the coefficients of the state variables and the constant term must vanish separately.

$$\begin{aligned}
&-\lambda(s)\alpha_0(s,T) - \eta_0(s,T)A_0(s) = 0 \\
&-\lambda(s)\alpha_i(s,T) - \eta_i(s,T)A_i(s) = 0 \\
&-\lambda(s)\beta(s,T) + c(s,T) - \eta_0(s)b_0(s) - \sum_{i=1}^{d} \eta_i(s,T)b_i(s) = 0.
\end{aligned}$$

From the previous equations, we can determine $A_0(s,T)$, $A_i(s,T)$ for $i = 1, \cdots, d$ and the coef-

ficient $c(s,T)$ once the diffusion coefficients $\eta_0(s,T)$ and $\eta_i(s,T)$ are specified. Indeed,

$$\begin{aligned}
A_0(s) &= -\frac{\lambda(s)\alpha_0(s,T)}{\eta_0(s,T)},\\
A_i(s) &= -\frac{\lambda(s)\alpha_i(s,T)}{\eta_i(s,T)},\\
c(s,T) &= \lambda(s)\beta(s,T) + \eta_0(s,T)b_0(s) + \sum_{i=1}^{d}\eta_i(s,T)b_i(s).
\end{aligned}$$

Comparing with (6.12) we get

$$\begin{aligned}
\eta_0(s,T) =& \theta_0(s,T) = \sigma_0 \mathrm{e}^{-k(T-s)},\\
\eta_i(s,T) =& \theta_i(s,T) = \sigma_i g_i(T)\frac{c_{H_i}}{2H_i}s^{\frac{1}{2}-H_i}.
\end{aligned}$$

Therefore,

$$\begin{aligned}
A_0(s) &= -\frac{\lambda(s)}{\sigma_0},\\
A_i(s) &= -\lambda(s)\frac{1}{\sigma_i\frac{c_{H_i}}{2H_i}s^{\frac{1}{2}-H_i}},\\
c(s,T) &= \lambda(s)(\phi(T) + \sum_{i=1}^{d} g_i(T)\mu_i(T-s)) + \sigma_0\mathrm{e}^{-k(T-s)}b_0(s,T) + \sum_{i=1}^{d}\sigma_i g_i(T)\frac{c_{H_i}}{2H_i}s^{\frac{1}{2}-H_i}b_i(s,T).
\end{aligned}$$

Hence, under the real-world measure $\mathbb{P}$, the instantaneous forward price satisfies

$$\begin{aligned}
f(t,T) =& f(0,T) + \int_0^t \sigma_0\mathrm{e}^{-k(T-s)}dW_0(s) + \sum_{i=1}^{d} g_i(T)\sigma_i\frac{c_{H_i}}{2H_i}\int_0^t s^{\frac{1}{2}-H_i}dW_i(s)\\
&+\int_0^t \lambda(s)\big[\phi(T) + \sum_{i=1}^{d} g_i(T)\mu_i(T-s) - f(s,T)\big]ds\\
&+\sigma_0\mathrm{e}^{-k(T-s)}\int_0^t \lambda(s)\Big[b_0(s,T) + \sum_{i=1}^{d}\sigma_i g_i(T)\frac{c_{H_i}}{2H_i}s^{\frac{1}{2}-H_i}b_i(s,T)\Big]ds.
\end{aligned}$$

Finally, in order to obtain a simpler formulation, we impose $\mu_i = 0$ for $i = 1,\dots,d$ and assume $\boldsymbol{b} \equiv 0$. Although a more general setting is theoretically admissible, introducing these additional drift components would increase the number of parameters without providing further structural insight.

Under this restriction, the drift under $\mathbb{P}$ reduces to a pure mean-reverting term toward the deter-

ministic seasonal level $\phi(T)$, resulting in a more tractable model specification.

$$\begin{aligned} f(t,T) =& f(0,T) + \int_0^t \lambda(s)(\phi(T) - f(s,T))ds + \int_0^t \sigma_0 \mathrm{e}^{-k(T-s)} dW_0(s) \\ &+ \sum_{i=1}^{d} g_i(T)\sigma_i \frac{c_{H_i}}{2H_i} \int_0^t s^{\frac{1}{2}-H_i} dW_i(s). \end{aligned}$$

Since the forward price $F(t,T_1,T_2)$ can be viewed as an average of instantaneous forward prices maturing over the delivery period $[T_1,T_2]$ equation (1.4). Substituting the dynamics of $f(t,u)$ and rearranging terms, we derive

$$\begin{aligned} F(t,T_1,T_2) =& \frac{1}{T_2-T_1}\int_{T_1}^{T_2} f(t,u)du \\ =& F(0,T_1,T_2) + \frac{1}{T_2-T_1}\int_{T_1}^{T_2}\int_0^t (\lambda(s)(\phi(u) - f(s,u))dsdu \\ &+ \frac{1}{T_2-T_1}\left[\int_{T_1}^{T_2}\int_0^t \sigma_0 \mathrm{e}^{-k(u-s)} dW_0(s)du + \sum_{i=1}^{d}\int_{T_1}^{T_2} g_i(u)\int_0^t \sigma_i \frac{c_{H_i}}{2H_i} s^{\frac{1}{2}-H_i} dW_i(s)du\right]. \end{aligned}$$

Applying Fubini's theorem and the Ito integration by parts formula, we may rewrite the above as

$$\begin{aligned} F(t,T_1,T_2) = F(0,T_1,T_2) &+ \int_0^t \lambda(s)\left(\frac{\int_{T_1}^{T_2}\phi(u)du}{T_2-T_1} - F(s,T_1,T_2)\right)ds \\ &+ \frac{\mathrm{e}^{-kT_1} - \mathrm{e}^{-kT_2}}{k(T_2-T_1)}\int_0^t \sigma_0 \mathrm{e}^{ks} dW_0(s) \\ &+ \frac{1}{T_2-T_1}\sum_{i=1}^{d}\int_{T_2}^{T_1} g_i(u)du \int_0^t \sigma_i \frac{c_{H_i}}{2H_i} s^{\frac{1}{2}-H_i} dW_i(s). \end{aligned}$$

Introducing the notation

$$\Lambda(t) = \int_0^t \lambda(s)ds, \qquad \Phi(T_1,T_2) = \frac{\int_{T_1}^{T_2}\phi(u)du}{T_2-T_1},$$

$$\Sigma(T_1,T_2) = \sigma_0 \frac{\mathrm{e}^{-kT_1} - \mathrm{e}^{-kT_2}}{k(T_2-T_1)}, \qquad G_i(T_1,T_2) = \frac{1}{T_2-T_1}\int_{T_2}^{T_1} g_i(u)du,$$

we can write the forward price in a more compact way

$$F(t,T_1,T_2) = F(0,T_1,T_2) + \Lambda(t)\Phi(T_1,T_2) - \int_0^t F(s,T_1,T_2)\lambda(s)ds \tag{6.16}$$
$$+\Sigma(T_1,T_2)\int_0^t \mathrm{e}^{ks}dW_0(s) + \sum_{i=1}^{d} G_i(T_1,T_2)\int_0^t \sigma_i \frac{c_{H_i}}{2H_i} s^{\frac{1}{2}-H_i} dW_i(s).$$

In conclusion, we derive a closed-form mean-reverting representation of the forward price in which the stochastic component is expressed as a linear combination of fundamental martingales driven by fractional-type factors with distinct Hurst parameters.

Through their respective Hurst exponents, these martingales determine the dependence structure of the spot price dynamics. In particular, the degree of roughness is generated by the fractional factors rather than being artificially imposed at the level of the model specification.

Allowing for multiple Hurst parameters significantly enhances the flexibility of the framework. Instead of constraining all sources of uncertainty to share the same degree of roughness, the model accommodates heterogeneous dependence structures across different components of the forward dynamics. This feature is particularly relevant from an empirical perspective: as shown in Section 3.3, the spot price dynamics often exhibit varying degrees of persistence depending on the time window under consideration. The proposed specification is therefore capable of reflecting this observed variability in a structurally consistent way.

In line with several models in the literature, forward prices are driven by different factors, X_i that appear in the dynamics of the spot but stay hidden in the forward dynamics. As in the Lucia-Schwartz model, we maintain the original specification of the factor X_0 as a stationary mean-reverting process, capturing short-term dynamics of the price curve and generating the Samuelson effect.

Finally, the availability of a closed-form solution for equation (6.16) enables explicit computation of both the expectation and the variance of the forward price, providing a solid analytical foundation for subsequent calibration procedures and pricing applications.

6.1.1 Closed form solution of the forward equation

Returning to the equation (6.16), under the real-world probability measure, the forward price is assumed to follow Ornstein–Uhlenbeck dynamics, for which a closed-form solution is available. For notational convenience, we denote

$$F(t,T_{i,1},T_{i,2}) = F_i(t),$$

The closed-form expression of $F_i(t)$ at maturity T is given by

$$\begin{aligned} F_i(T) =& e^{-\lambda(T-t)}F_i(t) + \int_t^T \lambda\Phi_i e^{-\lambda(T-s)}ds + \int_t^T \Sigma_i e^{ks}e^{-\lambda(T-s)}dW_0(s) \\ &+ \frac{1}{T_{i,2}-T_{i,1}}\sum_{j=1}^{n}\int_{T_{i,2}}^{T_{i,1}} g_j(u)\sigma_j\frac{c_{H_j}}{2H_j}\int_t^T s^{\frac{1}{2}-H_j}e^{-\lambda(T-s)}dW_j(s)du. \end{aligned} \tag{6.17}$$

Notice that the components in the forward vector process $\mathbf{F}(T) := (F_1(T), \cdots, F_N(T))$ are not mutually independent, as they are driven by the same Brownian motions. In particular, $\mathbf{F}(T)$ conditioned on $\mathcal{F}_t$ is a Gaussian vector:

$$\mathbf{F}(T) \mid \mathcal{F}_t \sim \mathcal{N}\left(e^{-\lambda(T-t)}\mathbf{F}(t) + \mathbf{\Phi}\left(1-e^{-\lambda(T-t)}\right), \boldsymbol{\sigma}(t,T)\right)$$

where $\mathbf{\Phi} := (\Phi_1, \cdots, \Phi_N)^\top$ and $\boldsymbol{\sigma}(t,T) := (\sigma_{ij}(t,T))_{i,j=1,\ldots,N}$. To compute the covariance matrix, we assume that the Brownian motions driving the forward contracts are uncorrelated. Introducing a correlated structure would increase the dimensionality of the model and reduce analytical tractability by generating additional cross-covariance terms, while also significantly increasing the numerical complexity of the calibration procedure.

Uncorrelation allows each factor to represent a distinct source of uncertainty whose contribution to the forward price volatility can be clearly identified. In particular, since the factors are characterized by different Hurst parameters, this assumption ensures that the observed roughness stems from their individual persistence properties rather than from cross-correlation effects. Define

$$G_{i,l} := \frac{1}{T_{i,2}-T_{i,1}}\int_{T_{i,1}}^{T_{i,2}} g_l(u)du$$

Since the deterministic part does not contribute to the covariance, we obtain:

$$\sigma_{ij}(t,T) = \int_t^T \left(\Sigma_i\Sigma_j \mathrm{e}^{2ks} + \sum_{l=1}^{d} G_{i,l}G_{j,l}\sigma_l^2\frac{c_{H_l}^2}{4H_l^2}s^{1-2H_l}\right)\mathrm{e}^{-2\lambda(T-s)}ds \tag{6.18}$$

Writing $e^{-2\lambda(T-s)} = e^{-2\lambda T}e^{2\lambda s}$, the integral in the covariance matrix can be solved using the power series expansion on the exponential function

$$\mathrm{e}^{2\lambda s} = \sum_{n=0}^{\infty}\frac{(2\lambda)^n}{n!}s^n. \tag{6.19}$$

The covariance entries can be expressed as

$$\begin{aligned}\sigma_{ij}(t,T) = &\frac{\Sigma_i \Sigma_j (\mathrm{e}^{2kT} - \mathrm{e}^{2kt-2\lambda(T-t)})}{k+\lambda} \\ &+ \sum_{l=1}^{d} G_{i,l} G_{j,l} \sigma_l^2 \frac{c_{H_l}^2}{4H_l^2} \mathrm{e}^{-2\lambda T} \sum_{n=2}^{\infty} \frac{(2\lambda)^{n-2}}{(n-2)!} \frac{1}{n-2H_l} (T^{n-2H_l} - t^{n-2H_l}).\end{aligned} \tag{6.20}$$

6.2 Calibration of the model

We now turn to the calibration of the model parameters using observed market forward prices. The estimation procedure is carried out in two steps. First, we exploit the quadratic variation of the price increments to estimate the diffusion parameters, including the volatility coefficients and the Hurst exponents associated with each fractional component. Then, conditional to the estimated diffusion structure, we recover the drift parameters by matching the theoretical dynamics of forward prices with observed market data.

6.2.1 Market setting

We consider an electricity market where the instantaneous spot price is assumed to follow the dynamics introduced in Section (6.1). Within this market, forward contracts are traded prior to delivery, and their dynamics are theoretically linked to the spot price through equation (1.4), leading to the closed-form representation given in (6.17).

A forward contract is a financial agreement specifying the delivery of electricity over a future time interval at a predetermined price. Each contract is characterized by two distinct phases: a trading period, during which the contract is actively traded on the market, and a delivery period, during which electricity is supplied, either physically or through financial settlement, at the agreed-upon price. Throughout the delivery period, the payoff of the contract is independent of the spot price fluctuations, reflecting the hedging nature of forward instruments.

At any given time, several forward contracts coexist, each characterized by a delivery interval $[T_{i,1}, T_{i,2}]$ and an associated trading period $[S_{i,1}, S_{i,2}]$, for $i = 1, \ldots, N$. Both delivery and trading periods vary across contracts, reflecting the coexistence of monthly, quarterly, and annual forwards within the same market. Monthly contracts are typically traded during the months preceding delivery, while quarterly and annual contracts may be traded several years in advance, up to the final trading day before the delivery period. Moreover, quarterly and annual contracts are subject to a cascade mechanism, where new contracts are introduced sequentially, ensuring continuous trading over future delivery horizons.

This heterogeneity in delivery maturities plays a crucial role in the calibration procedure. Forward prices are observed exclusively during their respective trading periods, while physical delivery takes place only after the end of trading. As a consequence, the calibration of the model relies solely on information available prior to the delivery period.

6.2.2 Model specification and parameters

We now recall the forward price dynamics derived in Section 6.1. We start from the forward contract price $F_i(t) := F(t, T_{i,1}, T_{i,2})$ given by (6.16). For each contract with delivery period $[T_{i,1}, T_{i,2}]$, under the historical probability measure $\mathbb{P}$, F_i satisfies:

$$\begin{aligned} F_i(t) =& F_i(0) + \Lambda(t)\Phi_i - \int_0^t F_i(s)\lambda(s)ds \\ &+ \Sigma_i \int_0^t \mathrm{e}^{ks} dW_0(s) + \sum_{j=1}^{d} G_{ij} \int_0^t \sigma_j \frac{c_{H_j}}{2H_j} s^{\frac{1}{2}-H_j} dW_j(s). \end{aligned}$$

We assume that the Brownian motions $\{W_i\}_{i=0}^d$ are mutually independent and $\Phi_i = \Phi(T_{i,1}, T_{i,2})$ and $\Sigma_i = \Sigma_i(T_{i,1}, T_{i,2})$ do not depend on t but only on the delivery period.
The functions $g_j(\cdot)$, which can be viewed as primitives of the coefficients G_{ij}, enter the fractional components are deterministic and capture the seasonal structure of the volatility. These functions weight the contribution of each fractional factor over the trading period and allow the model to accommodate heterogeneous seasonal effects across contracts. We discuss their specification later in this subsection.

The model depends on a set of parameters that can be classified according to their economic interpretation and probabilistic roles. In particular, the diffusion component is characterized by the volatility coefficients $\sigma_0, \sigma_1, \ldots, \sigma_d$, by the Hurst parameters $H_1, \ldots, H_d$ associated with the fractional components, and by the mean-reversion speed k of the component X_0 of the spot. To retain sufficient flexibility in the seasonal structure, we consider four distinct Hurst parameters and allow each fractional component to possess its own volatility coefficient σ_i, for $i = 1, \ldots, 4$. This choice improves identifiability when forward contracts span heterogeneous trading horizons and seasonal compositions. The parameters σ_0, σ_i for $i = 1, \ldots, 4$, and k are common to all forward contracts, as they directly stem from the dynamics of the underlying stochastic factors and therefore do not depend on the contract index.

The drift structure is governed by the mean-reversion parameter λ and by the contract-specific coefficients Φ_i, $i = 1, \ldots, N$, which encode the deterministic seasonal contribution to each forward price.

In line with standard practice in electricity markets, we assume a constant mean-reversion parameter λ.

The calibration of the model is carried out in two steps. In the first step, we estimate the diffusion parameters by exploiting the quadratic variation and covariation of the forward price increments, which is insensitive to the drift component.

The fractional Brownian motion has degenerate quadratic variation: it is identically zero when $H > \frac{1}{2}$ and infinite when $H < \frac{1}{2}$. This feature makes it unsuitable for our calibration procedure, which relies on quadratic variation–based arguments. In our setting, we introduced the associated

fundamental martingale, whose quadratic variation is finite and non–degenerate. Indeed, if we consider the expression of $M(t)$ in (4.9): $M(t) = \frac{c_H}{2H} \int_0^t s^{\frac{1}{2}-H} dW(s)$, then its quadratic variation can be easily computed:

$$\begin{aligned} < M_t, M_t > &= \left(\frac{c_H}{2H}\right)^2 \int_0^t (s^{\frac{1}{2}-H})^2 ds \\ &= \frac{c_H^2}{4H^2(2-2H)} t^{2-2H}. \end{aligned}$$

Then the goal of the first part of the calibration is to estimate the vector coefficients

$$p = (\sigma_0, \sigma_1, \sigma_2, \sigma_3, \sigma_4, k, H_1, H_2, H_3, H_4)$$

directly under $\mathbb{P}$. In the second step, we recover the drift parameters by matching the theoretical dynamics of forward prices with observed data. In particular, the estimation of λ is based on ordinary least squares (OLS) while the estimators for the coefficients Φ_i can be computed within a Gaussian likelihood framework. Details are provided in the next sections.

How to choose the functions g_i?
Let us consider a partition π of the time horizon $[0, \mathbb{T}]$ into subintervals

$$\pi_i = [t_i, t_{i+1}), \qquad i = 1, \dots, n,$$

which are meant to represent distinct periods, that can be seasons, months or different aggregation periods. Depending on the trading window of a given forward contract, different subsets of these intervals may be involved. For instance, one–month delivery forward contracts are typically traded six to seven months before the beginning of the delivery period.

It may happen that one of the partition intervals intersects both the trading period and the delivery period, as illustrated in Figure 6.1.

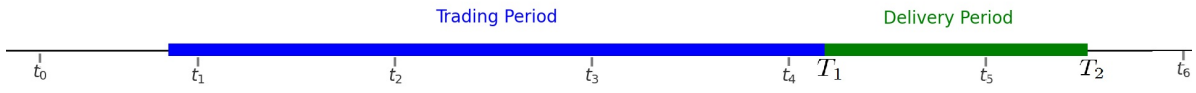

Figure 6.1: Timeline showing the partition of the time horizon, the trading period, and the delivery period.

Let F_k be a forward contract with delivery period $[T_{k,1}, T_{k,2}]$ and trading period $[\tau_k, T_{k,1}]$. The delivery starting time $T_{k,1}$ determines the end of the trading window and therefore identifies which intervals of the partition are relevant for the contract.

We define the functions g_i so as to weight the contribution of each partition interval depends

on the length of its overlap with the trading period. Specifically, for each $\pi_i = [t_i, t_{i+1})$ we set

$$g_i^{(k)}(u) := \left|[\tau_k, T_{k,1}] \cap [t_i, t_{i+1})\right| \, \mathbb{1}_{[T_{k,1}, T_{k,2}]}(u), \qquad u \in [0, \mathbb{T}].^2$$

With this choice, each function g_i activates a distinct stochastic component whose intensity is proportional to the length of the trading period falling within the corresponding interval of the partition. The delivery period enters only through the integration domain and acts as a common scaling factor.

6.2.3 Calibration of the diffusion coefficients

In this section we estimate the vector of diffusion parameters

$$\boldsymbol{p} = (\sigma_0, \sigma_1, \sigma_2, \sigma_3, \sigma_4, k, H_1, H_2, H_3, H_4)$$

To this end, we exploit the theoretical expressions of both quadratic variation and quadratic covariation of the forward price (6.16). These quantities allow for a direct comparison between model–implied second–order moments and their empirical counterparts computed from market data.

In addition to marginal quadratic variation, quadratic covariation between forward contracts is also incorporated in the estimation procedure. Cross–variation terms provide additional information on the common Brownian component and improve parameter identification.

Using the computations reported in Appendix D, and assuming that all Brownian motions driving the model are mutually independent, we consider N forward contracts with delivery periods $[T_{i,1}, T_{i,2}]$, $i = 1, \ldots, N$. The theoretical quadratic variation of the forward price F_i over its trading period $[\tau_{i,1}, \tau_{i,2}]$ is given by

$$\langle F_i, F_i \rangle_{\tau_{i,1}}^{\tau_{i,2}} = A_i + B_i,$$

where

$$A_i = \frac{\Sigma_i^2}{2k} \left(e^{2k\tau_{i,2}} - e^{2k\tau_{i,1}} \right),$$

and

$$B_i = \sum_{r=1}^{m_i} G_{i,r}^2 \, \frac{\sigma_r^2 c_{H_r}^2}{4H_r^2} \, \frac{\tau_{i,2}^{2-2H_r} - \tau_{i,1}^{2-2H_r}}{2 - 2H_r}.$$

However, for two distinct forward contracts F_i and F_j, the corresponding quadratic covariation involves products of the form $G_{i,r}G_{j,r}$, reflecting the exposure of both contracts to the same fractional component. Under the independence assumption, all mixed terms vanish, so that only diagonal contributions appear in the quadratic variation. In particular, the absence of correlation among the driving Brownian motions implies $\rho_{rv} = 0$ for $r \neq v$, and consequently all cross–variation terms disappear. This simplification leads to a more tractable expression and makes the

[2] We use the superscript (k) to indicate the dependence of the function g_i on the forward contract indexed by k.

calibration procedure computationally efficient.

We now introduce the realized quadratic variation of the forward prices F_i. Within each calibration window, forward prices are observed at discrete times

$$\pi = \{t_0 < t_1 < \cdots < t_n\},$$

with constant time step Δ. The realized quadratic variation is therefore computed using discrete observations over the trading period $[t_{l_1}, t_{l_2}]$, where $t_{l_1} = \tau_{i,1}$ and $t_{l_2} = \tau_{i,2}$, as

$$[F_i, F_i]_{\tau_{i,1}}^{\tau_{i,2}} := \sum_{k=l_1+1}^{l_2} \big(R_i(t_k) - R_i(t_{k-1})\big)^2,$$

where $R_i(t_k)$ denotes the observed market price of the forward contract F_i at time t_k. Similarly, for two forward contracts F_i and F_j traded over overlapping time intervals, we denote by

$$\tau_{ij,1} := \max\{\tau_{i,1}, \tau_{j,1}\}, \qquad \tau_{ij,2} := \min\{\tau_{i,2}, \tau_{j,2}\},$$

the common trading window, whenever $\tau_{ij,1} < \tau_{ij,2}$.

The realized quadratic covariation over the overlapping period $[\tau_{ij,1}, \tau_{ij,2}]$ is defined as

$$[F_i, F_j]_{\tau_{ij,1}}^{\tau_{ij,2}} := \sum_{k:\, t_k \in [\tau_{ij,1}, \tau_{ij,2}]} \big(R_i(t_k) - R_i(t_{k-1})\big)\big(R_j(t_k) - R_j(t_{k-1})\big).$$

Ideally, we impose that both realized quadratic variation and covariation match their theoretical counterparts, namely

$$[F_i, F_i]_{\tau_{i,1}}^{\tau_{i,2}} \simeq \langle F_i, F_i \rangle_{\tau_{i,1}}^{\tau_{i,2}}, \qquad i = 1, \ldots, N,$$

and

$$[F_i, F_j]_{\tau_{ij,1}}^{\tau_{ij,2}} \simeq \langle F_i, F_j \rangle_{\tau_{ij,1}}^{\tau_{ij,2}}, \qquad i \neq j.$$

The theoretical quadratic variation and covariation depend on the parameter vector $\mathbf{p}$. While each forward contract contributes one marginal quadratic variation equation, the inclusion of cross quadratic covariations substantially enlarges the set of conditions.

As a consequence, the estimation system is overdetermined, with the number of empirical conditions exceeding the number of parameters. This redundancy improves parameter identification and stabilizes the calibration procedure.

We estimate the parameter vector $\mathbf{p}$ by means of a least–squares approach. Specifically, we define the estimator $\hat{\mathbf{p}}$ as the solution of the following minimization problem, combining marginal and cross quadratic terms:

$$\widehat{\mathbf{p}} = \arg\min_{\mathbf{p} \in \mathcal{S}} \left\{ \sum_{i=1}^{N} w_i \big([F_i, F_i] - \langle F_i, F_i \rangle\big)^2 + \alpha \sum_{i<j} w_{ij} \big([F_i, F_j] - \langle F_i, F_j \rangle\big)^2 \right\}.$$

The weights w_i and w_{ij} account for heterogeneous trading lengths and for the different statistical reliability of the contracts. The scaling factor α balances the relative contribution of marginal and cross terms. In practice, it is calibrated so as to equalize their empirical order of magnitude, thereby preventing one component of the objective function from dominating the optimization.

The minimization problem is solved through an iterative block–coordinate procedure. More precisely, the parameter vector is partitioned into two subsets: (i) the fractional parameters (σ_r, H_r) associated with the seasonal components, and (ii) the parameters (k, σ_0) governing the common Brownian factor.

At each iteration, we alternate between the estimation of the fractional block, keeping (k, σ_0) fixed, and the estimation of (k, σ_0) conditional on the updated fractional parameters. This alternating strategy enhances numerical stability and improves the identifiability of the parameters. The procedure is repeated until convergence of the objective function.

6.2.4 Calibration of the drift

In what follows, the diffusion parameters are fixed at the robust estimates obtained in the previous step. We then concentrate on the calibration of the drift parameters of the model. As a first step, we recall the closed–form solution of the forward price dynamics (6.17) under the real–world probability measure $\mathbb{P}$, derived under the assumptions introduced in the previous sections.

$$F_i(T) = e^{-\lambda(T-t)} F_i(t) + \int_t^T \lambda \Phi_i e^{-\lambda(T-s)}\, ds + \int_t^T \Sigma_i e^{ks} e^{-\lambda(T-s)}\, dW_0(s) + \sum_{l=1}^{n} G_{il}\sigma_l \frac{c_{H_l}}{2H_l} \int_t^T s^{\frac{1}{2}-H_l} e^{-\lambda(T-s)}\, dW_l(s).$$

Conditioning on the information set $\mathcal{F}_t$, the forward vector

$$\mathbf{F}(T) := \big(F_1(T), \dots, F_N(T)\big)^\top$$

is Gaussian, with conditional distribution given by

$$\mathbf{F}(T) \mid \mathcal{F}_t \sim \mathcal{N}\big(e^{-\lambda(T-t)}\mathbf{F}(t) + \mathbf{\Phi}\big(1 - e^{-\lambda(T-t)}\big),\ \mathbf{\Sigma}(t,T)\big)\,,$$

where $\mathbf{\Phi} := (\Phi_1, \dots, \Phi_N)^\top$ and $\mathbf{\Sigma}(t,T) := (\sigma_{ij}(t,T))_{i,j=1,\dots,N}$ denotes the covariance matrix defined in (6.20).
It is worth pointing out that the covariance structure does not depend only on the diffusion parameters $(k, \sigma_0, \sigma_l, H_l)$, but also on the mean–reversion coefficient λ. This feature allows us to estimate λ by matching theoretical and empirical covariances.

Estimation of the mean–reversion parameter λ. Fix a final observation time $T = t_M$, corresponding to the end of the calibration window. We estimate λ by solving a nonlinear least–squares

problem of the form

$$\widehat{\lambda} = \arg\min_{\lambda} \sum_{i \leq j}^{N} \left(\sigma_{ij}(\lambda) - \mathrm{Cov}_{ij}^{\mathrm{emp}}\right)^2,$$

where the empirical covariance is computed as

$$\mathrm{Cov}_{ij}^{\mathrm{emp}} = \frac{1}{M-1} \sum_{l=1}^{M} \big(F_i(t_l) - \overline{F}_i\big)\big(F_j(t_l) - \overline{F}_j\big), \qquad \overline{F}_i = \frac{1}{M} \sum_{l=1}^{M} F_i(t_l).$$

The summation index runs over the set of observation times for which both forward contracts F_i and F_j are simultaneously traded. Hence, empirical covariances are computed over the overlapping trading interval of the two contracts. For consistency, sample means $\overline{F}_i$ and $\overline{F}_j$ are evaluated over the same overlapping period.

The objective function involves $\frac{N(N+1)}{2}$ distinct covariance terms, where N denotes the number of forward contracts included in the calibration. Once the diffusion parameters have been fixed in the previous step, this procedure yields an estimate of the mean–reversion coefficient λ.

Estimation of the vector $\mathbf{\Phi}$. Once obtained $\widehat{\lambda}$, we proceed to the estimation of the drift vector $\mathbf{\Phi} = (\Phi_1, \ldots, \Phi_N)^\top$. Consider daily observations of the forward prices on a uniform time grid $\pi = \{t_0 < t_1 < \cdots < t_n\}$, with $t_l - t_{l-1} = \Delta t$. From the conditional distribution of the increments we have

$$\mathbf{F}(t_l) - \mathbf{F}(t_{l-1}) \mid \mathcal{F}_{t_{l-1}} \sim \mathcal{N}\Big(\big(1 - e^{-\lambda \Delta t}\big)\big(\mathbf{\Phi} - \mathbf{F}(t_{l-1})\big),\ \mathbf{\Sigma}(t_{l-1}, t_l)\Big). \tag{6.21}$$

Exploiting the conditional mean, a natural estimator for each component Φ_j is given by

$$\widehat{\Phi}_j(\lambda) = \frac{1}{n} \sum_{l=1}^{n} \frac{F_j(t_l) - e^{-\lambda \Delta t} F_j(t_{l-1})}{1 - e^{-\lambda \Delta t}}, \qquad j = 1, \ldots, N.$$

In the empirical implementation we set $\Delta t = 1$, corresponding to daily observations. More generally, the estimator remains valid for any fixed time step Δt, provided that the increments are equally spaced. Under this condition, the estimator is consistent and coincides with the maximum likelihood estimator associated to the Gaussian density of the model (6.21) with a constant covariance.

Chapter 7

Empirical results

In this chapter we assess the empirical performance of the forward price model introduced in the previous chapters by calibrating it on real market data. The empirical analysis is carried out in two stages. First, we estimate the diffusion parameters by matching theoretical and realized quadratic variation and covariation of forward prices. Then, conditional on the estimated diffusion structure, we calibrate the drift parameters.

The diffusion calibration relies on a weighted least–squares procedure combining quadratic variations and cross quadratic covariations, implemented through an iterative block–coordinate strategy to enhance numerical stability and parameter identifiability. Robustness is assessed by repeating the estimation over different subsets of forward contracts and aggregating the resulting parameters.

Once the calibration procedure is completed, forward prices are simulated under the proposed model using the estimated parameters. The simulated outputs are compared with observed market data in order to evaluate the ability of the proposed framework to reproduce the main stylized features of forward price dynamics.

The chapter is organized as follows. The first section describes the dataset used in the empirical analysis. The subsequent sections present the diffusion and drift calibration procedures. Finally, we compare model–implied quantities with market observations, highlighting both strengths and limitations of the proposed approach.

7.1 Description of the dataset

In this section, we describe the dataset employed for the empirical analysis. We consider forward price data from the Italian electricity market over the time window from July 26, 2017, to December 27, 2019. The dataset consists of daily settlement prices of Phelix Base futures traded on the European Energy Exchange (EEX).

The initial dataset includes a total of 28 forward contracts, namely 18 monthly forwards, 7 quarterly forwards, and 3 yearly forwards.

However, in order to ensure numerical stability and reliable parameter identification in the diffusion calibration step, only a subset of contracts is retained for estimation. While all quarterly and yearly contracts are included, monthly contracts are selected more cautiously. Due to their relatively short trading windows, monthly forwards typically span only a limited number of seasonal regimes. As a consequence, they provide less information on the full seasonal structure of the volatility components and may generate instability in the estimation of the fractional parameters. For this reason, monthly contracts are incorporated in the calibration only when their inclusion improves robustness, according to the criteria discussed in the previous section.

Table 7.1 reports the forward contracts effectively used in the diffusion calibration procedure, together with the beginning and end of their trading period and the corresponding number of observed trading days.

The delivery period is not explicitly reported in the table, as it is indicated by the contract name. For instance, the contract *Mar-18* delivers over March 2018, while *Q2-18* has a delivery period ranging from April 2018 to June 2018.

Table 7.1: Forward contracts used in the calibration.

Contract	Trading start	Trading end	Trading days
Mar-18	31/08/2017	28-02-2018	127
Jul-18	02-01-2018	29-06-2018	126
Oct-18	04-04-2018	28-09-2018	128
Nov-18	02-05-2018	31-10-2018	131
Dec-18	31-05-2018	30-11-2018	132
Jan-19	02-07-2018	28-12-2018	127
Feb-19	31-07-2018	31-01-2019	128
Mar-19	31-08-2018	28-02-2019	125
Apr-19	01-10-2018	29-03-2019	125
May-19	31-10-2018	30-04-2019	123
Jun-19	30-11-2018	31-05-2019	123
Q2-18	26-07-2017	27-03-2018	172
Q3-18	26-07-2017	27-06-2018	235
Q4-18	26-07-2017	25-09-2018	299
Q1-19	26-07-2017	27-12-2018	363
Q2-19	15-01-2018	27-03-2019	305
Q3-19	15-01-2018	26-06-2019	367
Q4-19	15-01-2018	26-09-2019	433
Y-19	26-07-2017	27-12-2018	363
Y-20	26-07-2017	27-12-2019	617
Y-21	10-01-2018	27-12-2019	553

For each contract, we observe a discrete time series of forward prices over its trading period

$$[\tau_{i,1}, \tau_{i,2}],$$

with $\tau_{i,2} < T_{i,1}$, consistently with market practice, whereby trading ceases before the beginning of the delivery period. The observation times are denoted by

$$\tau_{i,1} = t_0 < t_1 < \cdots < t_{M_i} = \tau_{i,2},$$

and the corresponding observed prices are $\{F_i(t_l)\}_{l=0}^{M_i}$.

The dataset consists of partially overlapping time series across different forward contracts, allowing us to exploit both the time–series dimension of individual forwards and the cross–sectional

dimension induced by the coexistence of heterogeneous delivery horizons.

All prices are expressed in €/MWh and refer to settlement prices. Prior to calibration, the data are pre–processed to remove missing observations and to ensure consistency across contracts.

7.2 Numerical Results

In this section, we present the numerical results obtained from the calibration of the forward price model. Before entering into the details of the estimation procedure, we specify the modeling choices underlying the empirical implementation.

As discussed in the previous sections, the calibration is performed by first estimating the diffusive component of the model, characterized by the parameter vector $\boldsymbol{p}$. The vector $\boldsymbol{p}$ collects the coefficients associated with the stochastic drivers of the diffusion term, including the volatility parameters, the mean–reversion coefficient of the common factor, and the Hurst exponents of the fractional components.

Its dimension depends on the choice of d, the number of fundamental martingales used to model the diffusive dynamics of forward prices. In the empirical application, we set $d = 4$, corresponding to the four seasons of the year. Each season is associated with a distinct stochastic driver, allowing the diffusive component of the model to capture seasonally heterogeneous volatility patterns observed in electricity markets.

Within this framework, the functions g_i play a crucial role. They measure the exposure of each forward contract to the seasonal components over its trading horizon, thereby determining how seasonal effects are transmitted into the observed forward price dynamics.

7.2.1 Diffusion calibration results

The diffusion parameters are estimated within the robustness framework described in Section 6.2.3. The calibration is repeated over 20 different subsets of forward contracts, combining all quarterly and yearly contracts with alternative configurations of monthly forwards.

For each configuration, the model-implied quadratic covariations are compared with their empirical counterparts after calibration. In particular, we compute the correlation between the empirical and theoretical quadratic covariations as diagnostic indicator of the ability of the model to reproduce the cross-sectional dependence structure. This correlation is used to identify unstable calibrations, together with the inspection of boundary solutions. Configurations in which one or more parameters lie at the boundary of the admissible region are excluded, since such outcomes typically indicate weak identification or overfitting.

Final parameter estimates are obtained by taking the median across the retained runs. The interquartile interval is reported as a measure of dispersion. This choice is motivated by robustness considerations: since the ensemble procedure involves alternative subsets of contracts, the distribution of the resulting estimates may exhibit asymmetries or outliers. The median and interquartile

range provide summary statistics that are less sensitive to extreme configurations than the mean and standard deviation. The resulting diffusion parameters are reported in Table 7.2

Table 7.2: Estimates of the diffusion parameters. For each parameter we report the median, the first and third quartiles (Q25, Q75), and the interquartile range (IQR).

Parameter	**Median**	**Q25**	**Q75**	**IQR**
k	0.0017	0.0015	0.0025	0.0010
σ_0	0.8747	0.8493	0.9636	0.1143
H_1	0.2961	0.2799	0.3175	0.0376
H_2	0.2784	0.2570	0.2963	0.0392
H_3	0.2929	0.2903	0.2967	0.0064
H_4	0.2979	0.2887	0.3021	0.0135
σ_1	0.4452	0.4309	0.4616	0.0307
σ_2	0.2300	0.2039	0.2643	0.0604
σ_3	0.1141	0.0787	0.1355	0.0567
σ_4	0.1891	0.1424	0.2207	0.0783

The results reported in Table 7.2 highlight a satisfactory degree of robustness of the diffusion parameters across alternative contract selections. In particular, the mean–reversion coefficient of the common Brownian factor remains small but strictly positive, confirming the presence of a slow mean–reverting component shared across contracts. The volatility coefficient σ_0 associated with this common factor exhibits moderate dispersion, with a contained interquartile range, indicating that the aggregate level of market-wide uncertainty is stably identified across different calibration subsets.

The Hurst exponents exhibit limited dispersion, with interquartile ranges that remain moderate for the first two seasonal components and remarkably small for H_3 and H_4. This stability suggests that the fractional memory structure of the forward price dynamics is consistently identified by the data and is not driven by specific subsets of contracts.

All estimated Hurst parameters are strictly below 0.5, indicating a rough regime characterized by short–range dependence and anti–persistence in the increments of the associated fundamental martingales. This feature is consistent with the well–documented irregular behavior of electricity prices and supports the use of fractional components to capture high–frequency variability.

Regarding the volatility coefficients, the interquartile ranges are larger than those observed for the Hurst parameters, indicating that scale parameters are more sensitive to the specific composition of the contract subset. Nevertheless, the interquartile intervals remain reasonably contained, confirming that the ensemble procedure successfully filters out unstable configurations and delivers coherent diffusion estimates.

Overall, the limited variability across the retained runs validates the robustness framework

adopted in the calibration and provides a stable foundation for the subsequent estimation of the drift parameters.

7.2.2 Estimation of the Drift Component

After having calibrated the diffusion parameters of the model we turn to the estimation of the drift structure.

Under the adopted specification, the forward dynamics can be decomposed into a deterministic mean-reverting component and a stochastic martingale part. Once the diffusion parameters are fixed, the only remaining structural parameter governing the deterministic evolution is the mean-reversion speed λ, together with the long term mean of the forward Φ_j that is the maturity average of the seasonal component of the spot.

The estimation of λ is performed by matching the empirical covariance matrix of the forward prices with its theoretical counterpart implied by the model, via a nonlinear least-squares procedure. Given the estimate $\hat{\lambda}$, the contract-specific parameters Φ_j are subsequently recovered from the discrete-time representation of the forward dynamics, exploiting the mean-reverting structure of the deterministic component.

In order to assess the robustness of the drift estimation with respect to the cross-sectional composition of the calibration set, a balanced subsampling procedure is implemented.

Let n denote the total number of available forward contracts. At each replication stage, the full set of contracts is randomly permuted and partitioned into disjoint groups of fixed size m. Since m is chosen as a divisor of n, each permutation produces n/m non-overlapping groups covering the entire cross-section. We refer to this operation as one *round*.

In each round, every forward contract appears exactly once, and therefore contributes equally to the estimation procedure. Repeating this mechanism over R independent random permutations (rounds) yields a total of $R \cdot (n/m)$ subsamples, while guaranteeing that each contract is included exactly R times across the entire experiment.

For each subsample, the mean-reversion parameter λ is re-estimated by nonlinear least squares, and the associated deterministic levels Φ_j are subsequently recovered. This design ensures that the variability of the drift estimates is driven solely by cross-sectional composition effects, rather than by unequal sampling frequencies of specific contracts.

In the empirical application considered here, the contracts of the Table 7.1 are partitioned into groups of size $m = 7$, generating 3 disjoint groups per round. The procedure is repeated over $R = 13$ rounds, resulting in a total of 39 subsamples and exactly 13 inclusions for each forward contract. Summary statistics of the resulting λ estimates are reported in Table 7.3. while in Table 7.4 are reported the means and standard deviations of the estimated parameters Φ_j for $j = 1 \cdots 21$

	Mean	Std. Dev.	Median	IQR
λ	0.04353	0.00963	0.04016	0.01697

Table 7.3: Stability analysis of the drift parameter λ over 39 balanced subsamples (group size $m = 7$, 13 rounds).

Forward ID	$\overline{\Phi}_j$	Std. Dev.
Mar-18	51.755	0.00004
Jul-18	61.970	0.37029
Oct-18	70.842	0.83496
Nov-18	73.537	0.24087
Dic-18	71.472	0.06264
Jan-19	75.663	0.01469
Feb-19	72.722	0.11653
Mar-19	62.221	0.50660
Apr-19	54.981	0.58479
May-19	54.308	0.21263
Jun-19	53.785	0.73479
Q2-18	45.807	0.03690
Q3-18	55.160	0.26780
Q4-18	61.891	0.73876
Q1-19	62.012	0.34376
Q2-19	54.224	0.12052
Q3-19	59.214	0.04595
Q4-19	62.487	0.09909
Y-19	57.071	0.38195
Y-20	55.775	0.09394
Y-21	56.487	0.06325

Table 7.4: Mean and standard deviation of the estimated Φ_j parameters.

7.3 Forward Simulation

In the previous sections, the parameters governing both the diffusion and the drift components of the forward price dynamics have been estimated using empirical quadratic covariation and moment-based techniques. While these estimates provide a consistent parametric representation of the model, it remains essential to assess whether the resulting stochastic dynamics are capable of reproducing realistic forward price trajectories.

The simulation framework serves a dual purpose. First, it allows us to numerically verify the internal coherence of the estimated parameters, ensuring that the deterministic and stochastic components interact consistently. Second, it provides a graphical and statistical comparison between empirical forward trajectories and model-implied distributions.

In the literature on energy forward price modelling, stochastic dynamics such as multi-factor mean-reverting processes and Heath–Jarrow–Morton forward curve frameworks are commonly simulated using Monte Carlo and compared with observed forward series [10]. To this end, we implement a Monte Carlo simulation procedure based on the closed-form representation of the forward process. In particular, the simulation of the forward price trajectories is based on a time discretization of the integral representation of the model. Let $\{t_k\}$ be a uniform time grid with step Δt. The increments of the driving Brownian motion are generated as

$$\Delta W_k = \sqrt{\Delta t}\, Z_k, \quad Z_k \sim \mathcal{N}(0,1),$$

which corresponds to the standard Euler–Maruyama discretization. In practice, this is implemented by scaling independent standard Gaussian random variables by $\sqrt{\Delta t}$.
Analogously, for the fractional components, Gaussian increments are generated on the same grid and used to approximate the corresponding stochastic integrals through discrete summation. The resulting procedure can still be interpreted as an Euler-type discretization scheme applied to the integral representation of the model. This approach allows for an efficient simulation of the trajectories while preserving the correct covariance structure induced by the driving Gaussian processes.

For each forward contract, simulated paths are generated using the estimated drift parameter λ, the contract-specific long-term level Φ_i, and the calibrated diffusion structure, which includes both the Ornstein–Uhlenbeck component and the fractional stochastic factors. The deterministic conditional mean trajectory,

$$\mathbb{E}[F_i(t) \mid F_i(t_0)] = e^{-\lambda(t-t_0)}\mathbf{F}(t_0) + \Phi_i\big(1 - e^{-\lambda(t-t_0)}\big), \tag{7.1}$$

is compared against the Monte Carlo mean and against the empirical forward series. In addition, pointwise confidence bands are constructed from the empirical distribution of the simulated paths. More precisely, for each trading time t_k in the observed grid, a large number of Monte Carlo trajectories $\{F_i^{(s)}(t_k)\}_{s=1}^{N}$ is generated, and the empirical quantiles (typically the 5% and 95% levels) are computed. This yields a time-dependent interval

$$\big[q_{0.05}(t_k),\ q_{0.95}(t_k)\big],$$

which represents the model-implied range of plausible realizations at time t_k under the estimated parameters.

The empirical forward trajectory is then compared to these pointwise intervals. If the observed series remains predominantly within the simulated quantile bands, this provides evidence that the

magnitude of stochastic fluctuations implied by the calibrated diffusion component is consistent with the variability observed in the market data. Conversely, systematic deviations outside the bands would indicate either an underestimation or overestimation of volatility, or potential model misspecification.

It is important to stress that these are pointwise confidence bands rather than joint confidence regions; therefore, occasional excursions outside the interval are statistically expected. The purpose of this comparison is a qualitative validation of the structural properties of the proposed stochastic model.

A well-calibrated model should generate forward trajectories whose empirical realizations lie within plausible stochastic bounds assessing structural adequacy. The comparison between empirical data, theoretical mean dynamics, and simulated distributions therefore provides an additional robustness check for the full multi-factor specification.

The following figures display representative trajectories for three monthly contracts (Apr-19, May-19, Jun-19), two quarterly contract (Q2-19, Q3-19), and one yearly contract (Y-19).

In each figure, the black solid line represents the empirical forward price observed over the trading period. The blue dashed curve corresponds to the deterministic conditional mean (7.1) which is driven solely by the drift component and reflects the mean-reversion mechanism governed by λ and the contract-specific long-term level Φ_i. The red solid curve denotes the Monte Carlo average obtained from simulated trajectories of the stochastic model, incorporating both the Ornstein–Uhlenbeck factor and the fractional martingale components. The light grey region represents the pointwise confidence band, constructed from the empirical 5% and 95% quantiles of the simulated distribution at each trading date.

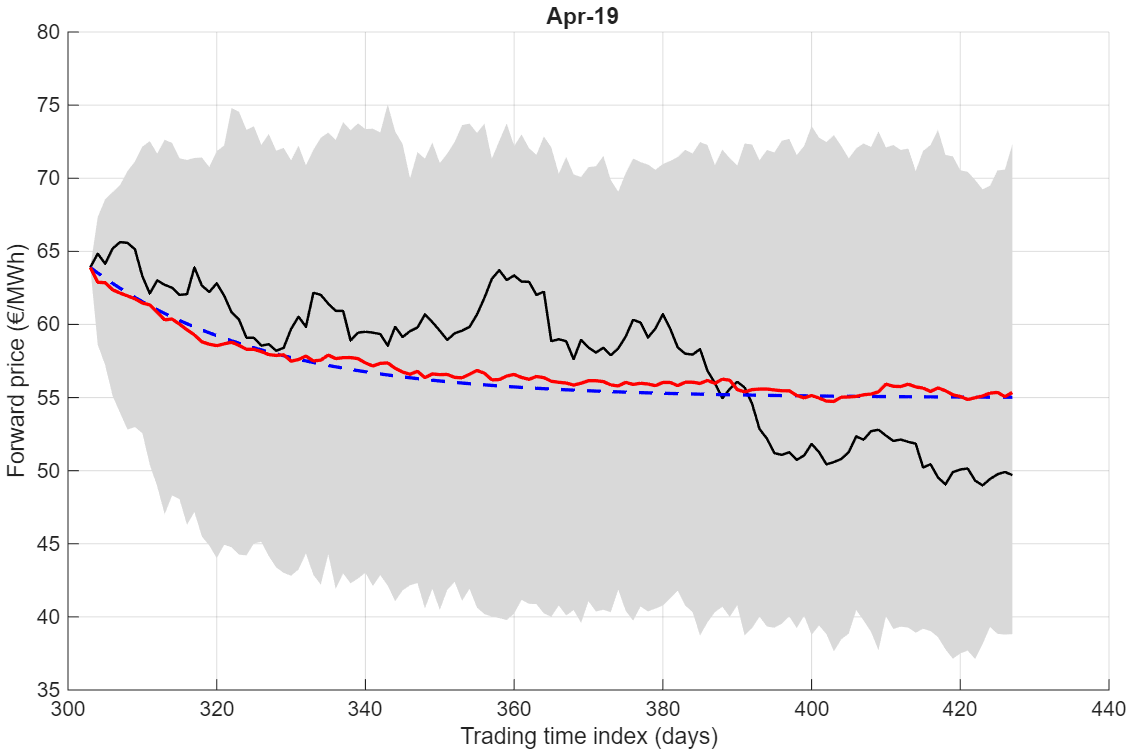

Figure 7.1: Empirical vs model comparison for the Apr-19 contract.

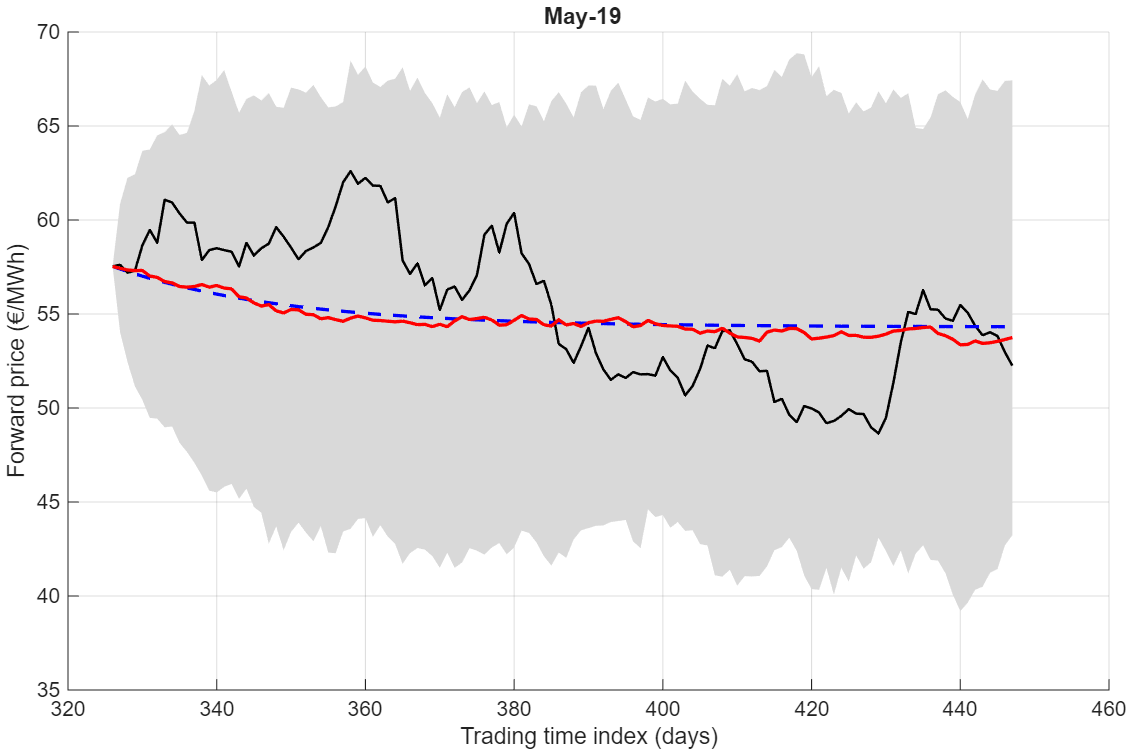

Figure 7.2: Empirical vs model comparison for the May-19 contract.

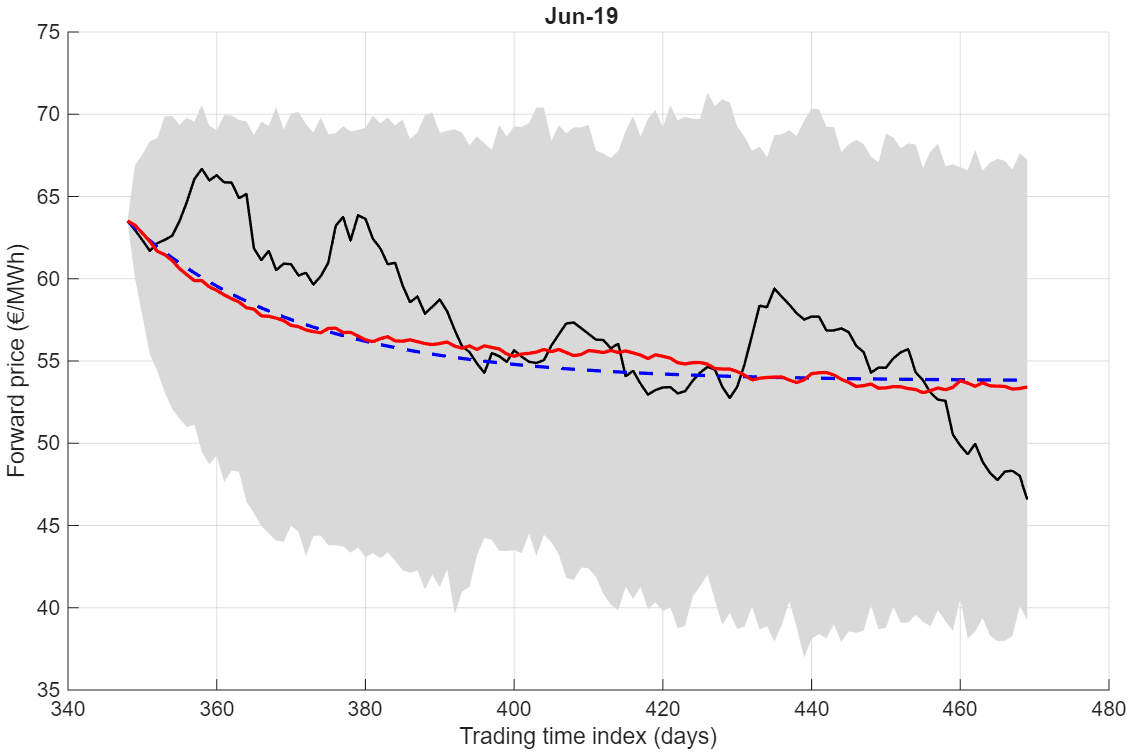

Figure 7.3: Empirical vs model comparison for the Jun-19 contract.

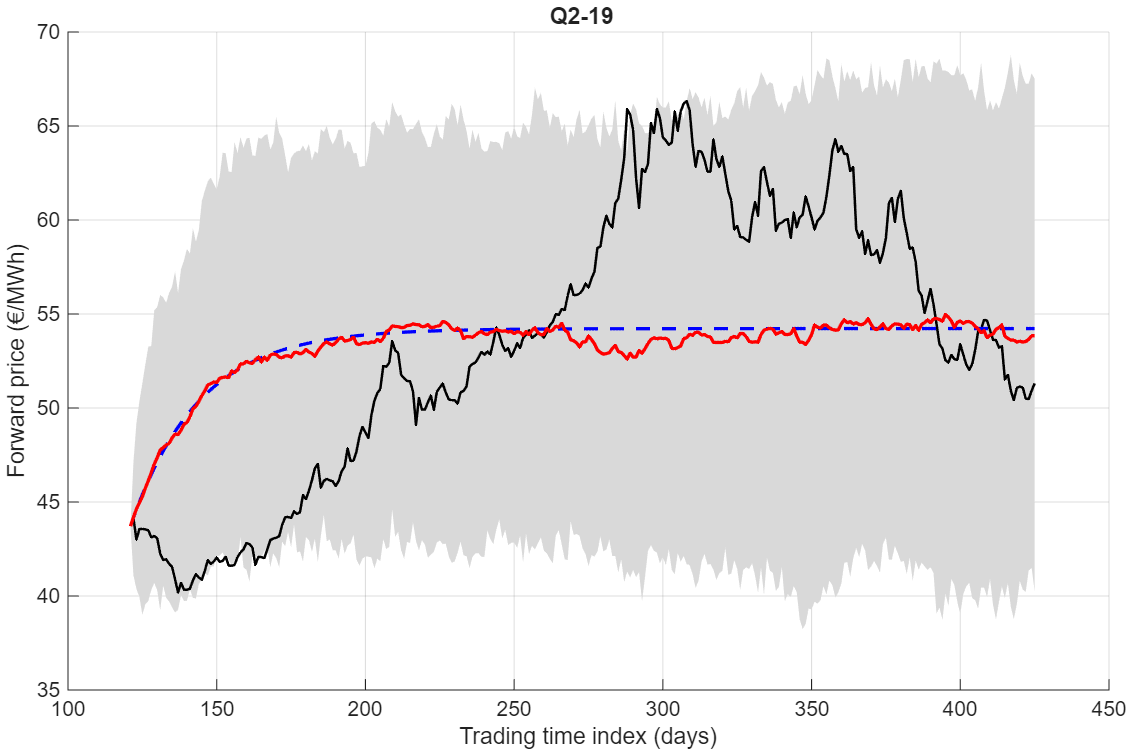

Figure 7.4: Empirical vs model comparison for the Q2-19 contract.

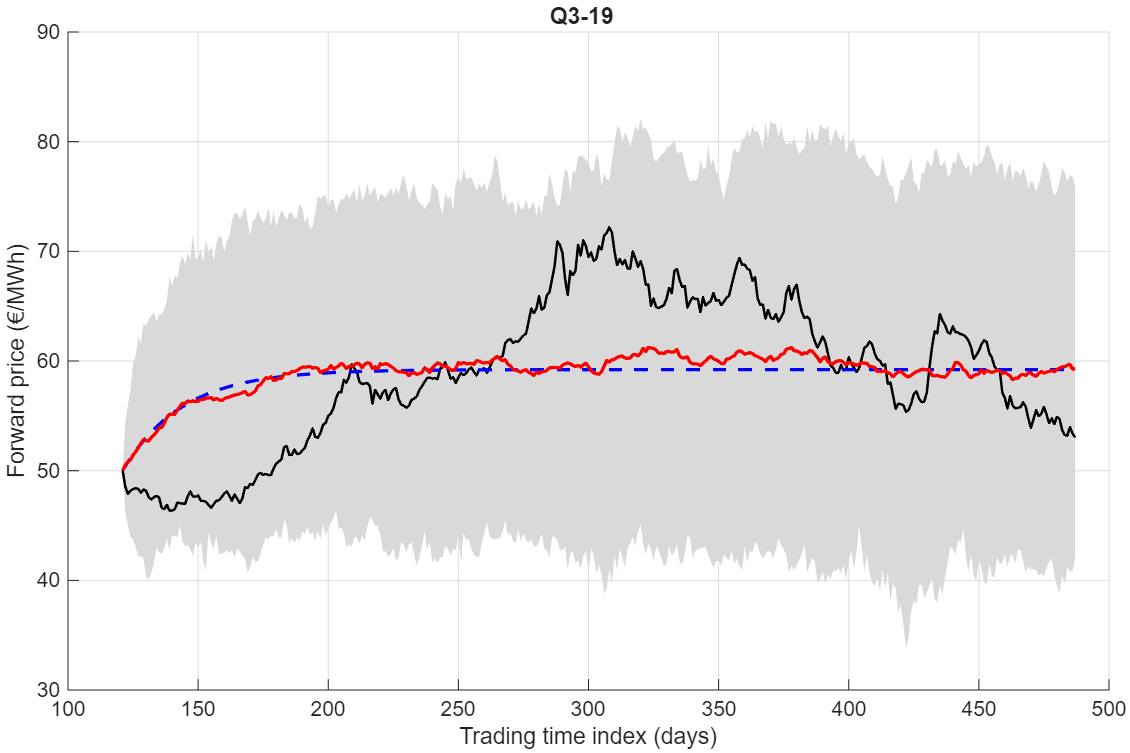

Figure 7.5: Empirical vs model comparison for the Q3-19 contract.

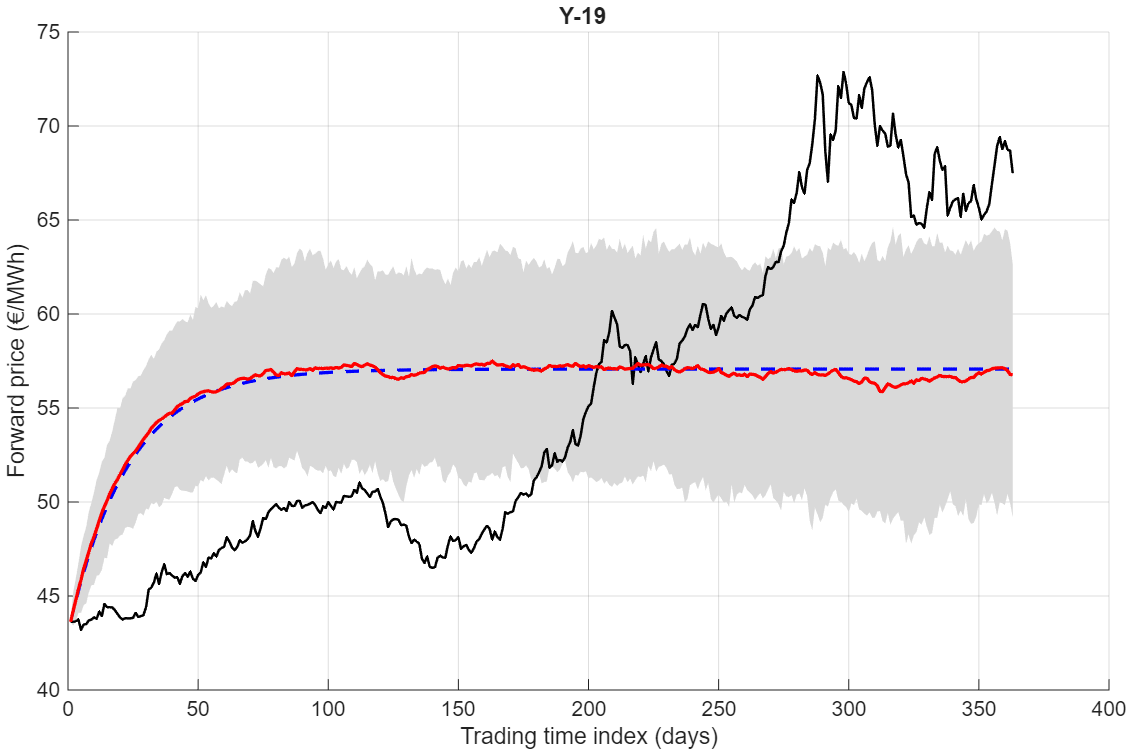

Figure 7.6: Empirical vs model comparison for the Y-19 contract.

Figures 7.1–7.6 illustrate the comparison between empirical forward trajectories and the model-implied dynamics for representative monthly, quarterly and yearly contracts.

In each figure, the black solid line represents the empirical forward price observed over the

trading period. The blue dashed curve corresponds to the deterministic conditional mean (7.1) which is driven solely by the drift component and reflects the mean-reversion mechanism governed by λ and the contract-specific long-term level Φ_i. The red solid curve denotes the Monte Carlo average obtained from simulated trajectories of the stochastic model, incorporating both the Ornstein–Uhlenbeck factor and the fractional martingale components. The light grey region represents the pointwise confidence band, constructed from the empirical 5% and 95% quantiles of the simulated distribution at each trading date.

For the monthly and quarterly contracts (e.g., Apr-19, May-19 and Q2-19), the empirical trajectory remains predominantly within the confidence band. Although temporary deviations occur, the observed forward prices are largely compatible with the variability generated by the calibrated diffusion structure. In these cases, the deterministic component captures the medium-term level towards which prices revert, while short-term oscillations are reasonably explained by the stochastic volatility induced by the Brownian and fractional factors. This suggests that the joint drift–diffusion specification provides an adequate representation of both central tendency and dispersion for shorter maturities.

For the yearly contracts (e.g., Y-19), a different pattern emerges. The empirical trajectory displays persistent and systematic departures from the model-implied mean, with extended portions of the observed path falling outside the simulated confidence band. This suggests that, at longer maturities, the calibrated diffusion component may underestimate the magnitude of price fluctuations, pointing to maturity-dependent effects that are not fully captured by the current specification.

One possible explanation is that the number of stochastic factors adopted in the model is sufficient to describe short- and medium-dated contracts, but may be too restrictive for long-dated forwards. In the present framework, four martingale components are introduced in order to assign one stochastic degree of freedom to each season. While this choice provides flexibility in the seasonal structure, it does not guarantee that four factors are optimal across all maturities. A natural extension would therefore be to investigate data-driven criteria to select the appropriate number of stochastic components (and, if needed, the corresponding seasonal partition), with the aim of improving the fit for yearly contracts.

The Monte Carlo analysis presented here should be interpreted primarily as an in-sample validation of the calibrated specification. While the comparison between empirical trajectories and model-implied confidence bands provides evidence that the proposed framework is capable of reproducing the main statistical features of the observed forward dynamics, a more stringent assessment would require an out-of-sample analysis. In particular, future research could investigate the forecasting performance of the model on contracts not used during calibration and compare its predictive accuracy against standard benchmark specifications. Such analysis would provide additional insight into the practical benefits of incorporating multiple fractional martingale components in electricity forward price modeling.

Chapter 8

Option pricing

In this chapter we construct the arbitrage-free price of options written on electricity forward contracts within the modeling framework introduced in the previous sections.
Since electricity cannot be stored, the spot price is not directly tradable and exhibits pronounced spikes and discontinuities. Consequently, options in electricity markets are typically written on forward contracts rather than on the spot price itself.

In classical financial markets, European options written on forwards are typically priced using the Black (1976) model, which assumes that the forward price follows a lognormal dynamics under the risk-neutral measure. In this framework, the forward price remains strictly positive and the option value admits a closed-form expression analogous to the Black–Scholes formula.

However, the lognormal assumption is not always appropriate in commodity markets. In particular, forward and spot prices of certain commodities, including electricity, gas, and oil, may have extreme fluctuations and may even become negative.

This issue became particularly evident during the COVID-19 crisis in 2020. Due to the collapse in demand and storage constraints, several commodity prices turned negative. A well-known example is the WTI crude oil futures contract, which traded below zero in April 2020 [73]. In such a setting, lognormal models are no longer adequate, as they exclude negative prices by construction.

For this reason, market practice increasingly relies on the Bachelier model, in which the forward price follows a Gaussian dynamics under the risk-neutral measure. Applications of the Bachelier framework to commodity markets during the COVID-19 period can be found, for instance, in [7], where a robust and parsimonious description of the oil option market is provided.

In electricity markets, where negative prices are structurally possible due to non-storability and supply-demand imbalances, the normal modeling framework appears particularly natural. Moreover, in models where forward prices are Gaussian, such as the affine structures driven by Brownian and fractional Brownian components considered in this work, the Bachelier formula arises directly from the distributional properties of the underlying process. For example closed formulas for the price of options written on forward electricity contracts using Bachelier model are derived in [54].

For these reasons, the Bachelier model provides a coherent and mathematically consistent framework for option valuation in the present setting.

In the following, we briefly recall the definition of European call and put options together with the arbitrage-free pricing principle. We do not enter into technical details or derivations, for a detailed and comprehensive treatment, we refer to [17]. We then discuss also the main differences between the Black and Bachelier approaches; a detailed and insightful comparison between the two models can be found in [22]. Finally, we apply the Bachelier model to our framework on the electricity forward dynamics developed in this thesis.

8.1 European Call and Put Options general overview

An option is a financial derivative granting its holder the right, but not the obligation, to buy or sell an underlying asset at a predetermined price K (the *strike price*) at a specified future date T (the *maturity*).
A *European call option* written on an underlying asset S with maturity T has payoff

$$(S(T) - K)^+, \tag{8.1}$$

where $(x)^+ := \max\{x, 0\}$. Similarly, a *European put option* with the same maturity and strike has payoff

$$(K - S(T))^+. \tag{8.2}$$

The payoff is inherently asymmetric: it is non-negative for the holder, while the potential gain depends on the type of option. For a call, it is theoretically unbounded as the underlying price may increase without bound; for a put, it is bounded above by the strike, since the underlying price cannot fall below zero.

Under standard no-arbitrage assumptions and suitable integrability conditions, the Fundamental Theorem of Asset Pricing guarantees the existence of an equivalent martingale measure $\mathbb{Q}$. Under such a measure, discounted asset prices evolve as martingales. In an arbitrage-free continuous-time framework, an option is fully characterized by its terminal payoff. Its value at time $t \leq T$ is defined as the conditional expectation of the discounted payoff under an equivalent martingale measure $\mathbb{Q}$, namely

$$V(t) = e^{-r(T-t)}\mathbb{E}^{\mathbb{Q}}\big[\Pi(T) \mid \mathcal{F}_t\big], \tag{8.3}$$

where r denotes the constant risk-free rate and $\{\mathcal{F}_t\}_{t\geq 0}$ the underlying filtration.
Therefore, option pricing reduces to specifying the risk-neutral dynamics of the underlying asset and computing the corresponding conditional distribution at maturity.

An important structural relation between European call and put options with the same strike K and maturity T is given by the *put–call parity*. Let $c(t)$ and $p(t)$ denote respectively the arbitrage-free prices at time $t \leq T$ of a European call and put written on the same underlying asset S. The absence of arbitrage implies

$$c(t) - p(t) = S(t) - Ke^{-r(T-t)}. \tag{8.4}$$

The relation follows from the replication argument obtained by comparing a portfolio consisting of a long call and a short put with a forward contract on the underlying asset. When options are written on forward contracts $F(t,T)$ rather than directly on the spot price, the parity relation becomes

$$c(t) - p(t) = e^{-r(T-t)}\big(F(t,T) - K\big), \tag{8.5}$$

which reflects the martingale property of forward prices under the risk-neutral measure.

The fundamental difference between the Bachelier (1900) and the Black–Scholes (1973) frameworks lies in the assumed dynamics of the underlying asset under the risk-neutral measure. In the Black–Scholes model, the underlying price S follows a geometric Brownian motion

$$dS(t) = rS(t)\,dt + \sigma S(t)\,dW(t), \tag{8.6}$$

so that $S(T)$ is log-normally distributed, thereby guaranteeing strict positivity of prices. The corresponding European call price is given by

$$C^{BS}(t) = S(t)N(d_1) - Ke^{-r(T-t)}N(d_2), \tag{8.7}$$

where

$$d_{1,2} = \frac{\ln\left(\frac{S(t)}{K}\right) + \left(r \pm \frac{1}{2}\sigma^2\right)(T-t)}{\sigma\sqrt{T-t}}.$$

and N denotes the cumulative distribution function of the standard normal distribution.

Unlike the Black–Scholes framework, the Bachelier model allows the underlying (in particular forward prices) to attain negative values. Hence it follows an additive Gaussian dynamics

$$dF(t) = \sigma\,dW(t), \tag{8.8}$$

so that $F(T)$ is normally distributed, in particular $F(T) \mid \mathcal{F}_t \sim \mathcal{N}(F(t),\, \sigma^2(T-t))$. Then the European call price at time t takes the form

$$C^{Bach}(t) = e^{-r(T-t)}\left[(F(t)-K)N(d) + \sigma\sqrt{T-t}\,n(d)\right], \tag{8.9}$$

where N and n denote respectively the cumulative distribution function and the probability density function of the standard normal distribution, and

$$d = \frac{F(t)-K}{\sigma\sqrt{T-t}}.$$

The two models are closely related. When the volatility–time product $\sigma\sqrt{T-t}$ is small relative to the underlying level, and the option is close to at-the-money $(S(t) = K)$, the lognormal distribution can be approximated by a normal distribution through a first-order expansion of the logarithm. In this regime, the Black–Scholes price admits a linear approximation that coincides with the

Bachelier formula. Hence, the Bachelier model can be interpreted as the first-order approximation of the multiplicative Black–Scholes dynamics [22].

8.2 Call and put option in energy markets

In electricity markets, vanilla European options are typically written on forward contracts rather than directly on the spot price. In our framework, the mean-reverting structure is imposed under the physical measure $\mathbb{P}$, while under the risk-neutral measure $\mathbb{Q}$ the instantaneous forward price admits a martingale representation. More precisely, the instantaneous forward $f(t,T)$ satisfies

$$f(t,T) = f(0,T) + \int_0^t \psi_0(s,T)\, dW_0^{\mathbb{Q}}(s) + \sum_{i=1}^{n} \int_0^t \psi_i(s,T)\, dW_i^{\mathbb{Q}}(s), \tag{8.10}$$

where

$$\psi_0(s,T) = \sigma_0 e^{-k(T-s)}, \qquad \psi_i(s,T) = \frac{c_{H_i}\sigma_i}{2H_i}\, g_i(T)\, s^{\frac{1}{2}-H_i},$$

and $\{W_i^{\mathbb{Q}}\}_{i=0}^n$ are correlated Brownian motions with correlation matrix (ρ_{ij}).

Since $f(t,T)$ is expressed as a stochastic integral of deterministic functions with respect to Brownian motions, it is Gaussian. For $t \le \tau \le T$, the conditional distribution of $f(\tau,T)$ given $\mathcal{F}_t$ is normal with mean

$$\mathbb{E}^{\mathbb{Q}}[f(\tau,T) \mid \mathcal{F}_t] = f(t,T),$$

and conditional variance

$$\sigma_f^2(t,\tau;T) = \int_t^\tau \left(\psi_0^2(s,T) + 2\psi_0(s,T) \sum_{i=1}^{n} \psi_i(s,T)\rho_{0i} + \sum_{i=1}^{n}\sum_{j=1}^{n} \psi_i(s,T)\psi_j(s,T)\rho_{ij} \right) ds. \tag{8.11}$$

In this setting, we can price vanilla put and call options on the instantaneous forward with strike price K. Considering a discount rate $r = 0$ the risk neutral price at time t of a vanilla call option with exercise time τ written on the instantaneous forward contract with maturity time $T > \tau$ is given by:

$$c(f,t,\tau,K) = \mathbb{E}^{\mathbb{Q}}((f(\tau,T) - K)_+ | \mathcal{F}_t), \tag{8.12}$$

while the put option with the same strike and exercise time is:

$$p(f,t,\tau,K) = \mathbb{E}^{\mathbb{Q}}((K - f(\tau,T))_+ | \mathcal{F}_t), \tag{8.13}$$

Since $f(\tau,T)$ in the risk-neutral probability framework is represented as in (8.10), and is conditionally Gaussian under $\mathbb{Q}$ with mean $f(t,T)$ and variance $\sigma_f^2(t,\tau;T)$, the price of these European options can be computed using the Bachelier formula, as in [76]. Moreover, this model is widely used in commodity pricing because it accommodates negative underlying prices and allows for option contracts with negative strikes.

Under this model the call option in (8.12) becomes:

$$c(f,t,\tau,K) = (f(t,T) - K)N(d) + \sqrt{\sigma_f^2(t,\tau;T)}n(d), \tag{8.14}$$

where N and n are the cumulative distribution function and the probability density function of a standard normal random variable and

$$d = \frac{f(t,T) - K}{\sqrt{\sigma_f^2(t,\tau;T)}}$$

.

Since we assume a zero interest rate, the call–put parity (8.5) reduces to

$$c(f,t,\tau,K) - p(f,t,\tau,K) = f(t,T) - K,$$

we can also price the put as:

$$p(f,t,\tau,K) = (f(t,T) - K)(N(d) - 1) + \sqrt{\sigma_f^2(t,\tau;T)}n(d).$$

Since the forward $F(t,T_1,T_2)$ can be derived from $f(t,T)$ by the equation (1.4), we can similarly price vanilla options on the forward under the risk neutral probability measure $\mathbb{Q}$, noting that the forward is normally distributed with variance:

$$\sigma_F^2(t,\tau;T_1,T_2) := Var[F(\tau,T_1,T_2)|\mathcal{F}_t] = \int_t^\tau \big(\psi_0^2(s,T_1,T_2) + 2\psi_0(s,T_1,T_2)\sum_{i=1}^n \psi_i(s,T_1,T_2)\rho_{0i} + \sum_{i=1}^n\sum_{j=1}^n \psi_i(s,T_1,T_2)\psi_j(s,T_1,T_2)\rho_{ij}\big)ds.$$

Where $\psi_0(s,T_1,T_2) = \int_{T_1}^{T_2} \psi_0(s,u)du$ and $\psi_i(s,T_1,T_2) = \int_{T_1}^{T_2} \psi_i(s,u)du$. Thus, the call and the put prices can be obtained as before,by replacing $\sigma_f^2(t,\tau;T)$ with $\sigma_F^2(t,\tau;T_1,T_2)$ and $f(t,T)$ with $F(t,T_1,T_2)$. The Gaussian structure of the forward dynamics therefore ensures analytical tractability of European option prices despite the presence of fractional components in the spot model.

Remark 8.2.1. *Even though the market generated by the multi-factor fractional structure may not be complete, the pricing formula derived above does not depend on the particular equivalent martingale measure $\mathbb{Q}$ chosen.*

Indeed, under any equivalent martingale measure, the instantaneous forward admits a Gaussian martingale representation with deterministic volatility. As a consequence, the conditional distribution of $f(\tau,T)$ given $\mathcal{F}_t$ is fully determined by its mean $f(t,T)$ and the deterministic variance $\sigma_f^2(t,\tau;T)$, which do not depend on the specific choice of $\mathbb{Q}$.

Therefore, European option prices on forward contracts are invariant with respect to the equivalent martingale measure and depend only on the volatility kernel entering the forward representation.

Conclusions

In this thesis, we exploit the distinctive features of electricity markets together with the main properties of fractional Brownian motion, with the aim of capturing long-range dependence and non-Markovian effects observed in energy price dynamics. The analysis of fractional processes, including the normalized integrated fractional Brownian motion, is developed as part of the theoretical background. Although this process is not directly employed in the proposed model, it represents a natural candidate for future research. Indeed, if the elementary price dynamics are assumed to follow a fractional Brownian motion, then daily prices—being time averages of the underlying process—cannot themselves be modeled as an fBm, but should instead be described through suitable time-averaged versions of it.

Our model for electricity forward prices relies on fundamental martingales associated with fractional Brownian motion, which allow us to preserve analytical tractability while incorporating fractional features into the dynamics. In particular, the stochastic components are driven by fundamental martingales rather than by fractional processes directly. This modeling choice provides a flexible and realistic representation of forward price dynamics across different time scales, while maintaining a martingale structure that is especially suitable for calibration and empirical analysis.

Despite these encouraging results, several directions for future research naturally arise. A first extension concerns the development of a multi-factor specifications, in which both the number and the nature of the stochastic components could be selected, allowing the model to adapt to different market conditions and contract structures.

Finally, from an applied perspective, the proposed framework could be tested on different electricity markets or on more recent datasets characterized by a higher penetration of renewable energy sources, in order to assess the robustness of the results and to investigate the impact of evolving market dynamics on forward price formation.

In conclusion, the results presented in this thesis provide a solid theoretical and empirical framework for electricity forward price modeling, laying the groundwork for further developments both from a mathematical and an applied standpoint.

Appendix A

Proof of chapter 5

Proof of Lemma 5.1.1. Let $s \geq t$. Then

$$\begin{aligned}
\mathbb{E}[X_t^h X_s^h] &= \mathbb{E}\left[\left(\frac{1}{h}\int_t^{t+h} W_u^H du\right)\left(\frac{1}{h}\int_s^{s+h} W_v^H dv\right)\right] \\
&= \frac{1}{h^2}\int_0^h \int_0^h \mathbb{E}[W_{u+t}^H W_{v+s}^H] du\, dv = \\
&= \frac{1}{2h^2}\int_0^h \int_0^h ((u+t)^{2H} + (v+s)^{2H} - |v-u+s-t|^{2H}) du\, dv \\
&= \frac{1}{2h^2}\left(\int_0^h \int_0^h (u+t)^{2H} du\, dv + \int_0^h \int_0^h (v+s)^{2H} du\, dv - \int_0^h \int_0^h |v-u+s-t|^{2H} du\, dv\right) \\
&=: \frac{1}{2h^2}\left(J_1 + J_2 - J_3\right).
\end{aligned}$$

Obviously,

$$J_1 = \frac{h}{2H+1}\big((t+h)^{2H+1} - t^{2H+1}\big),$$
$$J_2 = \frac{h}{2H+1}\big((s+h)^{2H+1} - s^{2H+1}\big).$$

To calculate J_3, denote for simplicity $\rho = s - t \geq 0$. Then

$$J_3 = J(\rho, h) = \int_0^h \int_0^h |v-u+\rho|^{2H} du\, dv.$$

Consider two cases. If $\rho \geq h$, then

$$\begin{aligned}
J(\rho,h) = \int_0^h \int_0^h (v-u+\rho)^{2H} du\, dv &= \frac{1}{2H+1}\int_0^h [(h+\rho-u)^{2H+1} - (\rho-u)^{2H+1}] du \\
&= \frac{1}{2H+1}[(h+\rho)^{2H+2} + (\rho-h)^{2H+2} - 2\rho^{2H+2}].
\end{aligned} \tag{A.1}$$

If $\rho \leq h$, then

$$\begin{aligned} J(\rho,h) &= \int_0^\rho \int_0^h (v-u+\rho)^{2H} dv\, du + \int_\rho^h \int_0^{u-\rho} (u-v-\rho)^{2H} dv\, du \\ &\quad + \int_\rho^h \int_{u-\rho}^h (v-u+\rho)^{2H} dv\, du \\ &= \frac{1}{2H+1}\Bigg[\int_0^\rho [(h+\rho-u)^{2H+1} - (\rho-u)^{2H+1}] du \\ &\quad + \int_\rho^h (u-\rho)^{2H+1} du + \int_\rho^h (h-u+\rho)^{2H+1} du \Bigg] \\ &= \frac{1}{(2H+1)(2H+2)} \left[(h+\rho)^{2H+2} + (h-\rho)^{2H+2} - 2\rho^{2H+2} \right], \end{aligned} \tag{A.2}$$

and the proof follows.

Proof of Lemma 5.1.2. (i) Of course, it is enough to analyze the sign of the numerator, that is, of the function $f(H) := 7 - 2^{2H+4} + 3^{2H+2}$. Note that $f(0) = 0$ and $f'(H) = -2\log 2 \cdot 2^{2H+4} + 2\log 3 \cdot 3^{2H+2}$, which is positive for

$$H > \bar{H} := \frac{\log \frac{4\log 2}{\log 3}}{2\log \frac{3}{2}} - 1 = \frac{\log \frac{16\log 2}{9\log 3}}{2\log \frac{3}{2}} \simeq 0.14157$$

and negative for $H < \bar{H}$. Thus, f is decreasing and negative in $(0, \bar{H}]$, and increasing in $[\bar{H}, 1]$. Since $f(\bar{H}) < 0$ and $f(1) = 7 - 64 + 81 > 0$, it follows that there exists a unique $H_0 \in [\bar{H}, 1]$ such that $f(H_0) = 0$, consequently $\gamma(H_0, 1) = 0$.

(ii) In this case

$$\begin{aligned} &\mathbb{E}[(X^h_{t+h} - X^h_t)(X^h_{t+(n+1)h} - X^h_{t+nh})] \\ &= \int_0^h \int_0^h \mathbb{E}[(W^H_{u+t+h} - W^H_{u+t})(W^H_{v+t+(n+1)h} - W^H_{v+t+nh})] du\, dv, \end{aligned}$$

and for $n \geq 2$ $(u+t, u+t+h) \cap (v+t+nh, v+t+(n+1)h) = \emptyset$. Therefore the sign of $\mathbb{E}[(X^h_{t+h} - X^h_t)(X^h_{t+(n+1)h} - X^h_{t+nh})]$ follows the sign of incremental covariance of fBm for non-overlapping intervals.

Proof of Lemma 5.1.3. The claim follows because

$$\begin{aligned} \{X^{ch}_{ct}, t \geq 0\} &= \left\{ \frac{1}{ch} \int_{ct}^{c(t+h)} W^H_u du, t \geq 0 \right\} \\ &= \left\{ \frac{1}{ch} \int_t^{t+h} W^H_{cs} c ds, t \geq 0 \right\} \overset{\mathrm{d}}{=} \left\{ \frac{1}{h} \int_t^{t+h} c^H W^H_s ds, t \geq 0 \right\} \\ &= \left\{ c^H X^h_t, t \geq 0 \right\}. \end{aligned} \tag{A.3}$$

Appendix B

Tools for asymptotic normality

This appendix collects a number of auxiliary results, definitions, and theoretical tools that are used throughout the thesis but are omitted from the main text for the sake of brevity. They are included here to provide a complete and self-contained mathematical background, ensuring that all the statements and proofs presented in the main chapters can be properly understood and verified.

Theorem B.0.1. *(Cramér–Wold theorem)*
Let

$$X_n = (X_{n1}, \dots, X_{nk}), \qquad X = (X_1, \dots, X_k)$$

be random vectors of dimension k. Then X_n converges in distribution to X if and only if

$$\sum_{i=1}^{k} t_i X_{ni} \xrightarrow{d} \sum_{i=1}^{k} t_i X_i,$$

for each $(t_1, \dots, t_k) \in \mathbb{R}^k$, that is, if every fixed linear combination of the coordinates of X_n converges in distribution to the corresponding linear combination of the coordinates of X.

Moreover, if X_n takes values in $\mathbb{R}^k_+$, then the statement also holds with $(t_1, \dots, t_k) \in \mathbb{R}^k_+$.

Theorem B.0.2. *(The Delta Method)*
Let $g : \mathbb{R}^d \to \mathbb{R}^k$ be a function continuously differentiable in a neighborhood of $\theta \in \mathbb{R}^d$. If T_n is a sequence of d-dimensional random vectors such that

$$\sqrt{n}(T_n - \theta) \xrightarrow{d} T,$$

then

$$\sqrt{n}\big(g(T_n) - g(\theta)\big) \xrightarrow{d} g'(\theta)T.$$

In particular, if

$$\sqrt{n}(T_n - \theta) \xrightarrow{d} T \sim \mathcal{N}(0, \Sigma),$$

then

$$\sqrt{n}\big(g(T_n) - g(\theta)\big) \xrightarrow{d} Y \sim \mathcal{N}\Big(0, g'(\theta)\Sigma\big(g'(\theta)\big)^T\Big),$$

where $(g'(\theta))^T$ *is the transpose of the matrix* $g'(\theta)$.

Further details on this result can be found in [43].

Theorem B.0.3. *(Breuer–Major theorem for stationary vectors)[5, Theorem 4]*
Let $d \geq 1$*, and let* $X = \{X_k, k \in \mathbb{Z}\}$ *be a* d*-dimensional centered stationary Gaussian process,* $X_k = (X_k^{(1)}, \ldots, X_k^{(d)})$*. For* $1 \leq i, l \leq d$ *and* $j \in \mathbb{Z}$*, define*

$$r^{(i,l)}(j) = \mathbb{E}\big[X_1^{(i)} X_{1+j}^{(l)}\big].$$

Let $f\colon \mathbb{R}^d \to \mathbb{R}$ *be a measurable function such that* $\mathbb{E}[f^2(X_1)] < \infty$*, and assume that* f *has Hermite rank* $q \geq 1$*. Suppose further that*

$$\sum_{j\in\mathbb{Z}} \big|r^{(i,l)}(j)\big|^q < \infty, \quad \textit{for all } i, l \in \{1, \ldots, d\}. \tag{B.1}$$

Then

$$\sigma^2 := \mathbb{V}ar\big(f(X_1)\big) + 2\sum_{k=1}^{\infty} \mathbb{C}ov\big(f(X_1), f(X_{1+k})\big)$$

is finite and nonnegative. Moreover,

$$\frac{1}{\sqrt{n}} \sum_{k=1}^{n} \big(f(X_k) - \mathbb{E}[f(X_k)]\big) \xrightarrow{d} \mathcal{N}(0, \sigma^2), \quad \textit{as } n \to \infty.$$

Theorem B.0.4. *(Isserlis' theorem) [36]:*
If (X_1, X_2, X_3, X_4) *is a zero-mean multivariate normal random vector, then*

$$\mathbb{E}(X_1X_2X_3X_4) = \mathbb{E}[X_1X_2]\,\mathbb{E}[X_3X_4] + \mathbb{E}[X_1X_3]\,\mathbb{E}[X_2X_4] + \mathbb{E}[X_1X_4]\,\mathbb{E}[X_2X_3].$$

In particular,

$$\mathbb{C}ov(X_1^2, X_2^2) = 2\left(\mathbb{C}ov(X_1, X_2)\right)^2. \tag{B.2}$$

For the direct proof of (B.2) *see [79, Lemma 2.2].*

Appendix C

Spot price process

In this appendix, we present some characteristic properties of the spot price model introduced in Section 6.1. In particular, we derive its variance both in the case $d = 1$ and in the multifactor case $d > 1$.

In contrast to the approach adopted in the computation of the closed-form solution for the forward price, we now allow the Brownian motions driving the diffusive components to be correlated. The simpler case of independent drivers can be recovered by setting the cross-variation terms equal to zero. Under the above assumptions, the spot price process remains Gaussian. Indeed, it is defined as a linear combination of deterministic functions and stochastic integrals with respect to Brownian motions. As a consequence, for each fixed time t, the random variable $S(t)$ is normally distributed and fully characterized by its mean and variance.

In particular, assuming $\mu = 0$, the spot price is given by the equation (6.6) with $\mu = 0$:

$$\begin{aligned} S(t) =& \phi(t) + X_0(0)\mathrm{e}^{-kt} + \sigma_0 \int_0^t \mathrm{e}^{-k(t-s)} dW_0^{\mathbb{Q}}(s) \\ &+ \sum_{i=1}^{d} g_i(t) \left[X_i(0) + \sigma_i \int_0^t \frac{c_{H_i}}{2H_i} s^{\frac{1}{2}-H_i} \, dW_i^{\mathbb{Q}}(s) \right], \end{aligned} \tag{C.1}$$

Then the expectation is given by

$$\mathbb{E}[S(t)] = \phi(t) + e^{-kt} X_0(0) + \sum_{i=1}^{d} g_i(t) X_i(0),$$

The Gaussian nature of the process plays a crucial role in the subsequent analysis, as it allows for explicit computation of the variance.

C.0.1 Variance of the spot price

We first consider a simplified case of the spot model (6.6), obtained by setting $d = 1$ and $\mu = 0$. Under these assumptions, the spot price dynamics reduces to

$$S(t) = \phi(t) + e^{-kt}X_0(0) + \int_0^t e^{-k(t-s)}\sigma_0\, dW_0^{\mathbb{Q}}(s) + X_1(0) + \sigma_1 g_1(t) \int_0^t \frac{c_{H_1}}{2H_1} s^{\frac{1}{2}-H_1}\, dW_1^{\mathbb{Q}}(s).$$

The variance of $S(t)$ can then be computed explicitly, using the power series expansion (6.19) of the exponential function,

$$\begin{aligned}\mathrm{Var}(S(t)) = \frac{\sigma_0^2}{2k}\left(1 - e^{-2kt}\right) + \frac{\sigma_1^2 g_1^2(t) c_{H_1}^2}{4H_1^2(2-2H_1)}\, t^{2-2H_1} \\ + \rho_{01}\frac{\sigma_0\sigma_1 c_{H_1}}{2H_1} g_1(t) e^{-kt} \sum_{n=0}^{\infty} \frac{k^n}{n!} \frac{t^{\frac{3}{2}-H_1+n}}{\frac{3}{2}-H_1+n}.\end{aligned}$$

We now extend the result to the general case $d > 1$. Assuming that the spot dynamics is driven by d fractional components with seasonal indicators $g_i(t)$ equation (C.1), the variance takes the form

$$\begin{aligned}\mathrm{Var}(S(t)) = \frac{\sigma_0^2}{2k}\left(1 - e^{-2kt}\right) + 2\sigma_0 e^{-kt} \sum_{i=1}^{d} g_i(t)\rho_{0i}\sigma_i \frac{c_{H_i}}{2H_i} \sum_{n=0}^{\infty} \frac{k^n}{n!} \frac{t^{\frac{3}{2}-H_i+n}}{\frac{3}{2}-H_i+n} \\ + \sum_{i=1}^{d} \sigma_i^2 g_i^2(t) \frac{c_{H_i}^2}{4H_i^2(2-2H_i)}\, t^{2-2H_i} + 2\sum_{i<j} g_i(t) g_j(t) \rho_{ij}\sigma_i\sigma_j \frac{c_{H_i} c_{H_j}}{4H_i H_j} \frac{t^{2-H_i-H_j}}{2-H_i-H_j}.\end{aligned}$$

The explicit expressions for the variance highlight the different roles played by the mean-reverting and the fractional components in the spot price dynamics. While the Ornstein–Uhlenbeck factor contributes a bounded and exponentially decaying term, the fractional components generate polynomial growth driven by the Hurst parameters H_i.

This decomposition clarifies how rough dynamics affect the spot price variability and provides analytical insight into the behavior observed in energy markets. Moreover, when uncertainty is transferred from the spot to the forward market, the mean-reverting Ornstein–Uhlenbeck structure selectively attenuates long-term fluctuations, while emphasizing short-term fluctuations as maturity approaches. As a consequence, forward contracts with shorter maturities exhibit higher volatility, giving rise to the Samuelson effect, a well-documented feature of electricity and commodity markets (see, e.g., [12, 48]).

Finally, the explicit form of the spot variance is fully consistent with the closed-form solution derived in the previous section and constitutes a key ingredient for the analytical characterization of forward prices, providing a solid foundation for model calibration. In the next section, these results are exploited to estimate the model parameters from market data, linking the theoretical structure of the model to its empirical performance.

Appendix D

Quadratic Covariation of the forward prices

In this appendix, we report the explicit computations of the quadratic covariation associated with the forward contract dynamics given in (6.16).

In the main body of the thesis, we restrict our attention to the quadratic variation only. This choice allows us to significantly reduce the numerical complexity of the calibration procedure and avoids the introduction of unnecessary equations, since the number of parameters to be estimated remains limited.

Throughout the estimation procedure, we assume that the Brownian motions driving the forward dynamics are mutually independent. Under this assumption, all cross–variation terms vanish, and the quadratic variation fully characterizes the diffusive contribution of the model.

Nevertheless, in order to provide a complete and general treatment, in this appendix we relax the independence assumption and derive the quadratic covariation in the general case. This allows us to explicitly identify all cross–terms arising from correlated Brownian drivers and to better understand the structure of the covariance induced by the model.

Let us assume that we observe N forward prices with delivery periods $[T_{i,1}, T_{i,2}],\ i = 1, \cdots, N$ during an observation period $[t_0, t]$ with $t_0 \leq T_{i,1}$ for all $i = 1, ..., N$. Let also $[\tau_{i,1}, \tau_{i,2}]$ be the trading period of forward F_i in the interval $[t_0, t]$. Then, if $[\tau_{i,1}, \tau_{i,2}] \cap [\tau_{j,1}, \tau_{j,2}] \neq \emptyset$, the maximum interval contained in our observation period where we can define the quadratic covariation between the forwards F_i and F_j is $[max(\tau_{i,1}, \tau_{j,1}), min(\tau_{i,2}, \tau_{j,2})]$. In the following we call $\tau_1 := max(\tau_{i,1}, \tau_{j,1})$ and $\tau_2 := min(\tau_{i,2}, \tau_{j,2})$.

Then the (predictable) quadratic covariation between F_i and F_j can be defined on $[\tau_1, \tau_2]$.

Let $W = (W_0, W_1, \ldots, W_d)$ be a $(d+1)$–dimensional Brownian motion with instantaneous covariation

$$d[W_a, W_b]_s = \rho_{ab}\, ds, \qquad a, b \in \{0, 1, \ldots, d\},$$

where $\rho = (\rho_{ab})$ is a symmetric positive semidefinite matrix with $\rho_{aa} = 1$.

For notational convenience, let us recall that

$$G_{i,r} := \frac{1}{T_{i,2} - T_{i,1}} \int_{T_{i,1}}^{T_{i,2}} g_r(u)\, du, \qquad r = 1, \ldots, m_i.$$

the quadratic covariation on $[\tau_1, \tau_2]$ admits the decomposition

$$\langle F_i, F_j \rangle_{\tau_1}^{\tau_2} = A_{ij} + B_{ij} + C_{ij} + D_{ij},$$

where the four terms correspond respectively to: (1) the W_0–W_0 contribution, (2) the fractional–fractional contribution, (3) the W_0–fractional cross term, (4) the fractional–W_0 cross term.

Term A_{ij}.

$$A_{ij} := \int_{\tau_1}^{\tau_2} \Sigma_i \Sigma_j e^{2ks}\, ds = \frac{\Sigma_i \Sigma_j}{2k}\Big(e^{2k\tau_2} - e^{2k\tau_1}\Big).$$

Term B_{ij}.

$$\begin{aligned} B_{ij} &:= \sum_{r=1}^{m_i}\sum_{v=1}^{m_j} \rho_{rv} \left(\sigma_1 \frac{c_{H_r}}{2H_r} G_{i,r}\right)\left(\sigma_1 \frac{c_{H_v}}{2H_v} G_{j,v}\right) \int_{\tau_1}^{\tau_2} s^{1-H_r-H_v}\, ds \\ &= \sum_{r=1}^{m_i}\sum_{v=1}^{m_j} \rho_{rv}\, G_{i,r}\, G_{j,v}\, \frac{\sigma_1^2 c_{H_r} c_{H_v}}{4H_r H_v}\, \frac{\tau_2^{2-H_r-H_v} - \tau_1^{2-H_r-H_v}}{2 - H_r - H_v}, \end{aligned}$$

Term C_{ij}.

$$C_{ij} := \sum_{v=1}^{m_j} \rho_{0v}\, \Sigma_i \Big(\sigma_1 \frac{c_{H_v}}{2H_v} G_{j,v}\Big) \int_{\tau_1}^{\tau_2} e^{ks} s^{\frac{1}{2}-H_v}\, ds.$$

Term D_{ij}.

$$D_{ij} := \sum_{r=1}^{m_i} \rho_{r0} \left(\sigma_1 \frac{c_{H_r}}{2H_r} G_{i,r}\right) \Sigma_j \int_{\tau_1}^{\tau_2} e^{ks} s^{\frac{1}{2}-H_r}\, ds.$$

The integrals in C_{ij} and D_{ij} can be left in integral form, or expanded as a convergent power series:

$$\begin{aligned} \int_{\tau_1}^{\tau_2} e^{ks} s^{\frac{1}{2}-H}\, ds &= \sum_{n=0}^{\infty} \frac{k^n}{n!} \int_{\tau_1}^{\tau_2} s^{\frac{1}{2}-H+n}\, ds \\ &= \sum_{n=0}^{\infty} \frac{k^n}{n!}\, \frac{\tau_2^{\frac{3}{2}-H+n} - \tau_1^{\frac{3}{2}-H+n}}{\frac{3}{2} - H + n}, \qquad H \in (0,1). \end{aligned}$$

This decomposition makes explicit the role of each stochastic component in the covariation structure.

Bibliography

[1] P. Abry and F. Sellan. The Wavelet-Based Synthesis for Fractional Brownian Motion proposed by F. Sellan and Y. Meyer: Remarks and Fast Implementation. *Applied and Computational Harmonic Analysis*, 3:377–383, 1996.

[2] M. Abundo and E. Pirozzi. On the integral of the fractional brownian motion and some pseudo-fractional gaussian processes. *Mathematics*, 7(10):991, 2019.

[3] M. Abundo and E. Pirozzi. On the estimation of the persistence exponent for a fractionally integrated Brownian motion by numerical simulations. *Fractal and Fractional*, 7(2), 2023.

[4] E. Alòs and D. García Lorite. *Malliavin Calculus in Finance*. Taylor & Francis Group, 2021.

[5] M. A. Arcones. Limit theorems for nonlinear functionals of a stationary gaussian sequence of vectors. *The Annals of Probability*, 22(4):2242–2274, 1994.

[6] F. Aurzada and M. Kilian. Asymptotics of the persistence exponent of integrated fractional Brownian motion and fractionally integrated Brownian motion. *Theory Probab. Appl.*, 67(1): 77–88, 2022.

[7] R. Baviera. The Additive Bachelier Model with an Application to Oil Futures. *arXiv preprint arXiv:2506.09760*, 2025.

[8] M Bennedsen. A rough multi-factor model of electricity spot prices. *Energy Economics*, 63: 301–313, 2017.

[9] F. E. Benth and P. Krühner. Representation of infinite-dimensional forward price models in commodity markets. *Communications in Mathematics and Statistics*, 2:47–106, 2014.

[10] F. E. Benth, Š. J. Benth, and S. Koekebakker. *Stochastic Modelling of Electricity and Related Markets*, volume 11 of *Advanced Series on Statistical Science & Applied Probability*. World Scientific Publishing Co. Pte. Ltd., 2008.

[11] F.E. Benth and S. Koekebakker. Stochastic modeling of financial electricity contracts. *Energy Economics*, 30(3):1116–1157, 2008.

[12] F.E. Benth, M. Piccirilli, and T. Vargiolu. Additive energy forward curves in a Heath-Jarrow-Morton framework. *Mathematics and Financial Economics*, 13:543–577, 2019.

[13] J. Beran. *Statistics for Long-Memory Processes*. Chapman & Hall/CRC, 1994.

[14] J. Beran, Y. Feng, S. Ghosh, and R.ł Kulik. *Long-Memory Processes: Probabilistic Properties and Statistical Methods*. Springer, Berlin Heidelberg, 2013.

[15] R. Bhar, D. B. Colwell, and Y. Xiao. A jump-diffusion model for spot electricity prices and market price of risk. *Physica A: Statistical Mechanics and its Applications*, 392(15): 3213–3222, 2013.

[16] F. Biagini, Y. Hu, B. Øksendal, and T. Zhang. *Stochastic Calculus for Fractional Brownian Motion and Applications*. Springer, 2008.

[17] T. Björk. *Arbitrage Theory in Continuous Time*. Oxford University Press, 3 edition, 2009.

[18] T. Björk and C. Landén. On the construction of forward price curves in electricity markets. *Quantitative Finance*, 2:329–336, 2002.

[19] P. J. Brockwell and R. A. Davis. *Time Series: Theory and Methods*. Springer, New York, 2nd edition, 1991.

[20] Á. Cartea and M. G. Figueroa. Pricing in electricity markets: a mean reverting jump diffusion model with seasonality. *Applied Mathematical Finance*, 12(4):313–335, 2005.

[21] P. Cheridito. Arbitrage in fractional Brownian motion models. *Finance and Stochastics*, 7 (4):533–553, 2003.

[22] J. Choi, M. Kwak, C. W. Tee, and Y. Wang. A Black–Scholes user's guide to the Bachelier model. *Journal of Futures Markets*, 42(6):959–980, 2022.

[23] A. Cicone and H. Zhou. Numerical analysis for iterative filtering with new efficient implementations based on fft. *Numerische Mathematik*, 2020.

[24] J.-F. Coeurjolly. Simulation and identification of the fractional Brownian motion: a bibliographical and comparative study. *Journal of Statistical Software*, 5(7):1–53, 2000.

[25] T. Deschatre, O. Féron, and P. Gruet. A survey of electricity spot and futures price models for risk management applications. *Energy Economics*, 102:105504, 2021.

[26] H. Erzgräber, F. Strozzi, J.-M. Zaldívar, H. Touchette, E. Gutiérrez, and D. K. Arrowsmith. Time series analysis and long range correlations of Nordic spot electricity market data. *Physica A: Statistical Mechanics and its Applications*, 387(26):6567–6574, 2008.

[27] S.-E. Fleten and J. K. Lemming. Constructing forward price curves in electricity markets. *Energy Economics*, 25(5):409–424, 2003.

[28] J. Gatheral, T. Jaisson, and M. Rosenbaum. Volatility is rough. *Quantitative Finance*, 18(6): 933–949, 2014.

[29] H. Geman. *Commodities and Commodity Derivatives: Modeling and Pricing for Agriculturals, Metals and Energy*. Wiley Finance. John Wiley & Sons, Chichester, 2005.

[30] R. Gibson and E. S. Schwartz. Stochastic convenience yield and the pricing of oil contingent claims. *Journal of Finance*, 45(3):959–976, July 1990.

[31] Skorokhod A.V.. Gikhman I.I. *The theory of stochastic processses I*. Springer Berlin, Heidelberg, 2004.

[32] L. Giordano and Morale D. A fractional Brownian–Hawkes model for the Italian electricity spot market: estimation and forecasting. *Quantitative Finance*, 14(3):65–109, 2021.

[33] Clive W.J. Granger and Zhuanxin Ding. Varieties of long memory models. *Journal of Econometrics*, 73(1):61–77, 1996.

[34] D. Heath, R. Jarrow, and A. Morton. Bond pricing and the term structure of interest rates: A new methodology for contingent claims valuation. *Econometrica*, 60(1):77–105, 1992.

[35] H. E. Hurst. Long-term storage capacity of reservoirs. *Transactions of the American Society of Civil Engineers*, 116:770–808, 1951.

[36] L. Isserlis. On a formula for the product-moment coefficient of any order of a normal frequency distribution in any number of variables. *Biometrika*, 12(1/2):134–139, 1918.

[37] C. Jost. *Integral Transformations of Volterra Gaussian Processes*. Helsingin yliopisto, 2007.

[38] C. Jost. On the connection between Molchan–Golosov and Mandelbrot–Van Ness representations of fractional Brownian motion. *Journal of Integral Equations and Applications*, 20 (1):93–107, 2008.

[39] Ioannis K. and Steven E. S. *Brownian Motion and Stochastic Calculus*, volume 113 of *Graduate Texts in Mathematics*. Springer New York, 1991.

[40] J. W. Kantelhardt, E. Koscielny-Bunde, H. H. A. Rego, S. Havlin, and A. Bunde. Detecting long-range correlations with detrended fluctuation analysis. *Physica A*, 295:441–454, 2001.

[41] A.N. Kolmogorov. Wienersche spiralen und einige andere interessante kurven im hilbertschen raum. *C.R. (Doklady) Acad. Sci. URSS(N.S.)*, 26:115–118, 1940.

[42] D. P. Kroese and Z. I. Botev. *Spatial Process Simulation*, pages 369–404. Springer International Publishing, 2015.

[43] K. Kubilius, Y. Mishura, and K. Ralchenko. *Parameter Estimation in Fractional Diffusion Models*. Springer, 2017.

[44] J. W. Lamperti. Semi-stable stochastic processes. *Transactions of the American Mathematical Society*, 104(1):62–78, 1962.

[45] L. Latini, M. Piccirilli, and T. Vargiolu. Mean-reverting no-arbitrage additive models for forward curves in energy markets. *Energy Economics*, 79:157–170, 2019.

[46] W. V. Li and Q.-M. Shao. Gaussian processes: inequalities, small ball probabilities and applications. In *Stochastic processes: theory and methods*, volume 19 of *Handbook of Statist.*, pages 533–597. North-Holland, Amsterdam, 2001.

[47] R. S. Liptser and A. N. Shiryaev. *Theory of Martingales*, volume 49 of *Mathematics and Its Applications (Soviet Series)*. Kluwer Academic Publishers, Dordrecht, 1986.

[48] J.J. Lucia and E.S. Schwartz. Electricity prices and power derivatives: Evidence from the nordic power exchange. *Review of Derivatives Research*, 5(1):5–50, 2000.

[49] B. Mandelbrot. *Gaussian Self-Affinity and Fractals: Globality, the Earth, 1/f Noise, and R/S*. Springer, New York, New York, NY, 2002.

[50] B. Mandelbrot and J.W. van Ness. Fractional brownian motions, fractional noises and applications. *SIAM Review*, 10:422–437, 1968.

[51] Y. Mishura. *Stochastic Calculus for Fractional Brownian Motion and Related Processes*. Springer, 2008.

[52] Y. Mishura, K. Ralchenko, and S. Shklyar. Maximum likelihood estimation for gaussian process with nonlinear drift. *Nonlinear Analysis: Modelling and Control*, 23(1):120–140, 2018.

[53] Y. Mishura, K. Ralchenko, and S. Shklyar. Parameter estimation for Gaussian processes with application to the model with two independent fractional Brownian motions. In *Stochastic processes and applications*, volume 271 of *Springer Proc. Math. Stat.*, pages 123–146. Springer, Cham, 2018.

[54] Y. Mishura, S. Ottaviano, and T. Vargiolu. Gaussian volterra processes as models of electricity markets. *SIAM Journal on Financial Mathematics*, 15(4):989–1019, 2024.

[55] G. Molchan. Integrated fractional Brownian motion: Persistence probabilities and their estimates, 2018. arXiv:1806.04949.

[56] G. Molchan and A. Khokhlov. Small values of the maximum for the integral of fractional Brownian motion. *J. Statist. Phys.*, 114(3-4):923–946, 2004.

[57] G. M. Molchan and J. Golosov. Gaussian stationary processes with asymptotic power spectrum. *Soviet Mathematics Doklady*, 10:134–137, 1969.

[58] M. Musiela and M. Rutkowski. *Martingale Methods in Financial Modeling*. Springer-Verlag, 1998.

[59] P. Norouzzadeh, W. Dullaert, and B. Rahmani. Anti-correlation and multifractal features of spain electricity spot market. *Physica A: Statistical Mechanics and its Applications*, 380 (1–2):333–342, 2007.

[60] I. Norros, E. Valkeila, and J. Virtamo. An elementary approach to a Girsanov formula and other analytical results on fractional Brownian motions, 1999.

[61] I. Nourdin, G. Peccati, and M. Podolskij. Quantitative Breuer–Major theorems. *Stochastic Processes and their Applications*, 121(4):793–812, 2011.

[62] D. Nualart. *The Malliavin Calculus and Related Topics*. Springer, 2006.

[63] A. Palipana, S. Song, N. Gupta, and R. Szczesniak. Bayesian two-stage modeling of longitudinal and time-to-event data with an integrated fractional Brownian motion covariance structure. *Biometrics*, 80(1), 2024.

[64] C.-K. Peng, S. V. Buldyrev, S. Havlin, M. Simons, H. E. Stanley, and A. L. Goldberger. Mosaic organization of dna nucleotides. *Physical Review E*, 49(2):1685–1689, 1994.

[65] V. Pipiras and M. S. Taqqu. *Long-Range Dependence and Self-Similarity*, volume 45 of *Cambridge Series in Statistical and Probabilistic Mathematics*. Cambridge University Press, 2017.

[66] M. B. Priestley. *Spectral Analysis and Time Series*. Academic Press, London, 1981.

[67] B. Qian and K. Rasheed. Hurst exponent and financial market predictability. *Proceedings of the Second IASTED International Conference on Financial Engineering and Applications*, 01 2004.

[68] K. Ralchenko and M. Yakovliev. Parameter estimation for fractional mixed fractional Brownian motion based on discrete observations. *Modern Stoch. Theory Appl.*, 11(1):1–29, 2023.

[69] L. C. G. Rogers. Arbitrage with fractional Brownian motion. *Mathematical Finance*, 7(1): 95–105, 1997.

[70] M. Rypdal and O. Løvsletten. Modeling electricity spot prices using mean-reverting multifractal processes. *Physica A: Statistical Mechanics and its Applications*, 392(1):194–207, 2013.

[71] E. S. Schwartz. The stochastic behavior of commodity prices: Implications for valuation and hedging. *The Journal of Finance*, 52(3):923–973, 1997.

[72] A. Serletis, editor. *Quantitative and Empirical Analysis of Energy Markets*. World Scientific Publishing Company, Singapore, 2013. ISBN 978-9814434818.

[73] I. Shaikh. On the relation between the crude oil market and pandemic covid-19. *International Review of Applied Economics*, 35(3-4):416–439, 2021.

[74] I. Simonsen. Measuring anti-correlations in the nordic electricity spot market by wavelets. *Physica A*, 322:597, 2003.

[75] M. S. Taqqu, V. Teverovsky, and W. Willinger. Estimators for long-range dependence: an empirical study. *Fractals*, 3(4):785–798, 1995.

[76] Satoshi Terakado. On the option pricing formula based on the Bachelier model. *SSRN Electronic Journal*, 2019. Available at SSRN: https://ssrn.com.

[77] R. Weron. Measuring long-range dependence in electricity prices. In Hideki Takayasu, editor, *Empirical Science of Financial Fluctuations*, pages 110–119. Springer, Tokyo, 2002.

[78] R. Weron and B. Przybylowicz. Hurst analysis of electricity price dynamics. *Physica A: Statistical Mechanics and its Applications*, 2000.

[79] L. Wu and Y. Ding. Wavelet-based estimator for the Hurst parameters of fractional Brownian sheet. *Acta Math. Sci. Ser. B (Engl. Ed.)*, 37(1):205–222, 2017.

[80] H.F. Zhang, Y.T. Shu, and O. Yangt. Estimation of Hurst parameter by variance-time plots. *IEEE*, 1997.

Acknowledgements

I would like to express my sincere gratitude for the support, encouragement, and guidance I have received throughout my PhD journey. This experience has been long and demanding, yet at the same time it has been a wonderful adventure and a stimulating challenge that allowed me to grow both academically and personally.

First and foremost, I would like to thank Professor Fabio Antonelli. Despite the difficulties I faced at the beginning, coming from a background outside the academic world, he placed his trust in me and gave me the opportunity to undertake this path. Through his guidance, patience, and constant availability, I was able to overcome many of the challenges encountered along the way. He has always been willing to provide valuable advice, and continuous support for my academic and personal development. I am deeply grateful for his generosity, dedication, and commitment to my education and to the completion of this work.

I would also like to thank Professor Marco Castellani, who has always been available to offer valuable advice and guidance on academic life throughout these years.

My sincere thanks go to the two referees, Maria Elvira Mancino and Alessandro Ramponi, whose comments, suggestions, and careful revisions have significantly contributed to improving the quality of this dissertation.

A special thanks goes to Tiziano Vargiolu, Stefania Ottaviani, and Yuliya Mishura, who welcomed me at the University of Padova during a particularly important stage of my research journey. Their expertise, generosity, and scientific enthusiasm provided me with an invaluable opportunity for both academic and personal growth. Through numerous discussions and exchanges of ideas, I was able to deepen my knowledge, explore new research directions, and broaden my scientific perspective. Beyond their professional contribution, I will always remember their kindness, humanity, and the pleasant company that made my time in Padova both productive and enjoyable.

I would also like to thank my fellow PhD colleague, Ivan Gallo. Throughout these years, our discussions, exchanges of ideas, and mutual support have been a constant source of motivation. It has always been a pleasure to share both the challenges and the achievements of this journey with him, and I am grateful for the friendship that accompanied our doctoral experience.

Finally, I cannot forget my family and Alessia. They have constantly encouraged me to pursue my goals and never give up, even when the road seemed particularly difficult. Although they could not always fully understand the challenges behind a proof that would not work or a problem that refused to yield a solution, they were always there for me. In their own unique way, they reminded me that there is a world beyond mathematics. Their love, patience, and support have been my greatest source of strength throughout this journey. For this, and for so much more, I am profoundly grateful.